12-2006

# Development of a Cellular Fiber Spinning Technology for Regenerative Medicine

Willie Jones
*Clemson University*, williejwilliej@gmail.com

Recommended Citation

DEVELOPMENT OF A CELLULAR FIBER SPINNING TECHNOLOGY
FOR REGENERATIVE MEDICINE


_____


A Thesis
Presented to
the Graduate School of
Clemson University


_____


In Partial Fulfillment
of the Requirements for the Degree
Master of Science
Bioengineering


_____


by
Willie Franklin Jones Jr.
December 2006


_____


Accepted by:
Dr. Karen JL Burg, Committee Chair
Dr. Martine LaBerge
Dr. Phillip J Brown

ABSTRACT

The prolonged success of cellular encapsulation in delivering insulin to treat Type I Diabetes has encouraged researchers to conceptualize ways in which cellular encapsulation can be implemented in an array of other clinical applications. This thesis investigated the development of a novel in-house textile hollow fiber spinning process in order to encapsulate cells. After development of the cellular encapsulation methods, a 21 day *in vitro* macroscopic evaluation was employed to confirm cellular viability and quantify the metabolic activity response of green fluorescent protein (GFP) labeled bovine mammary epithelial cells (MAC-Ts) that were either suspended in a low viscosity sodium alginate based solution, manually injected into the lumen of the hollow fiber (MI method), and later immobilized through a gelation process; or pre-mixed and co-extruded with a medium viscosity sodium alginate based solution (CO-X method), and immobilized inside the walls of the hollow fiber. No decrease in fluorescence was observed, and it was found that the CO-X and MI methods provided total lactic acid productions of 1.6 and 1.5 g/L glucose consumptions of 6.1 and 4.0 g/L, respectively, after 21 days of culturing. Histomorphological analyses revealed that the average cell area of MAC-Ts increased 25 and 88% after 21 days of encapsulation under the CO-X and MI methods, respectively. There was little to no evidence of cell clusters, and oval, cobblestone morphologies. Based on our findings, it is concluded that our novel in-house textile hollow fiber

spinning process can be used to encapsulate cells using the CO-X and MI methods.

DEDICATION

Completing this thesis has been an act of faith and persistent effort. I would like to dedicate this thesis to my family and friends, who have been patient mentors to me throughout my graduate school experience. Their prayers and proverbs have given me the ability and courage to laugh at adversity, discover opportunities in failure, and desire tranquility above emulation, wealth and prestige. Most importantly, they have helped me to stay rooted in the Bible and its teachings. I am the beneficiary of God's grace and mercy.

I would also like to dedicate this thesis to patients who suffer from skin ulcers and severe burns. They are constant reminders that my work is not in vain.

ACKNOWLEDGEMENTS

spinning equipment and were willing to modify the equipment in order to streamline the technology.  I would also like to thank Cassie Gregory for going above and beyond her normal responsibilities by modifying the spinning hood power cord so that it would fit a standard outlet.

A great working environment is made by kind and intelligent people. Therefore, I would like to thank the Tissue Engineering Laboratory (TEL) members for their technical support and friendship.

TABLE OF CONTENTS

Page

Table of Contents (Continued)                                    Page

Table of Contents (Continued)                                    Page

Table of Contents (Continued)                                    Page

# LIST OF TABLES

LIST OF FIGURES

List of Figures (Continued)

List of Figures (Continued)

# LIST OF EQUATIONS

PREFACE


Cellular encapsulation is a branch of tissue engineering that seeks to repair, restore, and maintain normal tissue function by implanting immunoisolated cells to deliver therapeutic agents. The prolonged success of cellular encapsulation to deliver insulin in the treatment of Type I Diabetes has encouraged researchers to conceptualize ways in which cellular encapsulation can be employed in an array of clinical applications. These efforts include the development of cellular encapsulation technologies that can be modified to meet the requirements posed by specific applications.

It is our contention is that we can encapsulate cells in a 3D-matrix by using an in-house novel textile hollow fiber spinning process. This thesis investigates our hypothesis in three parts. The first part of the study characterizes key properties of sodium alginate, our initial encapsulation material of choice. The second part of the study involves the development of two cellular encapsulation methods, one in which green fluorescent protein (GFP) labeled bovine mammary epithelial cells (MAC-Ts) are co-extruded (CO-X) with the sodium alginate. The second encapsulation method involved manually injecting (MI) an alginate-based cell suspension into the lumen of a pre-fabricated hollow fiber. The third part of the study is an *in vitro* 21 day macroscopic evaluation of the cellular response to these two encapsulation methods in which the cell

viability was confirmed, the cell respiration was quantified, and the cell morphology was characterized.

**CHAPTER ONE**

**INTRODUCTION**

## 1.1 Rationale for tissue engineering

According to the United States Department of Health and Human

Services, nearly 27,000 organs were transplanted in the year 2004, which was

an 11% increase from the previous year.  However, despite the increase in

transplantations, there were more than 87,000 patients waiting to receive organ

transplants in the year 2004[1]. Although new health technologies have been

developed, the need for replacement of living tissues and organs from donors

remains.  Tissue engineering is a field that has the potential to yield readily

available functioning organs.  The goal of tissue engineering is to decrease the

number of needed transplants by repairing, improving and maintaining damaged

tissues through the development of biologically based devices.

## 1.2 Rationale for cellular encapsulation

One tissue engineering application is the repair of diseased tissue through

the delivery of drugs from encapsulated living cells.  Cellular encapsulation

describes the capture of living cells in a suitable immunoprotective capsule.  The

capsule allows the diffusion of oxygen and nutrients to the cells and the secretion

of wastes and therapeutic drugs produced by the cells into the body across a

highly selective membrane.  Ideally, the membrane prevents the intrusion of cells

and cytokines or regulatory proteins that induce apoptosis (programmed cell

death) of cells within the encapsulated environment.  Thus, cellular encapsulation allows the transplantation of cells without the adverse long-term effects of using immunosuppressant drugs. In order to achieve high selectivity, the membrane's thickness, pore size, and surface chemistry must be well controlled.

## 1.3 Previous applications of cellular encapsulation

The literature mentions a number of diseases that have been treated using cellular encapsulation.  These ailments include anemia and hemophilia[2], chronic pain[3-5] and Parkinson's disease[6-8], pituitary and central nervous system insufficiencies[5,9], liver failure[10-18], and Type 1 diabetes[19,20].

Extensive research has been conducted on the encapsulation of pancreatic islets for treating insulin dependent (Type 1) diabetes, after transplanted pancreatic islets successfully delivered insulin in immunosuppressed patients[21].  Thus, cellular encapsulation was initiated to circumvent the need for immunosuppressants.  Studies with diabetic primates in which porcine (pig) islets were encapsulated also suggest the potential of the technology[22].  Despite promising results in small and large animal models[23]; however, human trials that have attempted to establish prolonged normoglycemia have had limited success.  Only 11% of all allotransplants performed before 1993 in diabetes mellitus patients resulted in normoglycemia and insulin independence post surgery[6].  The limited success in these clinical trials is attributed to: variability in the encapsulation processes that expose cells to the host rejection and promote enhanced scar tissue formation around the encapsulation device[6,7]; low islet seeding densities[2]; and restricted waste

transport out of the encapsulation device due to strict pore size limitations[2].

Soon-Shiong and coworkers have been able to address these variabilities by

improving the encapsulation process to allow higher islet seeding densities under

relatively low doses of immunosuppressants[24,25].  Other researchers have

suggested that cell viability can be enhanced by implanting the encapsulation

device months prior to adding cells[26].  The cell viability is enhanced because at

the time of cell transplantation, the exchange across the membrane of the

encapsulation device has increased.

**1.4 Potential uses of cellular encapsulation**

One of the main goals of tissue engineering is to provide cellular devices

and synthetic components that restore, maintain, or improve tissue function.

Specifically, tissue engineers seek to better understand drug delivery,

biocompatibility, and cell function in order to improve the success rate of medical

devices.  The human body naturally responds to an implanted device (or "foreign

body") by surrounding the implant with cells that will form a collagen capsule

around the matrix over time.  The transfer of vital nutrients to implanted living

tissue and the movement of mechanical components can be prohibited by the

deposition of a thick, fibrous capsule around an implant.

Over 13 million textile medical devices that are implanted annually in the

United States are affected by this naturally-occurring process.  These implants

range from simple fixation devices and lens implants to more complex devices

such as ear vent tubes and artificial heart valves[10].

Although these devices have improved the quality of life for patients, they often do not emulate the multitude of dynamic biologic and reparative processes that occur in normal tissue. Accordingly, the demand for medical devices with bioactive surfaces must be met with materials whose compatibility is tuned to a particular medical application. Cellular encapsulation may be useful in tuning textile based devices such as arterial or skin grafts, where the constituent fibers serve as the drug delivery vehicles.

## 1.4.1 Arterial grafts

Tissue is categorized as either soft or hard; replacement tissue must maintain the appropriate structural and mechanical properties in order to remain functional within the body. One specific type of soft tissue implant is the arterial graft. In 2005, the potential annual market for small-diameter arterial graft market was estimated to be more than $1.5 billion[27]. One of the major problems with transplanting human arterial homografts is their rapid degeneration, leading to decreased patency of the grafts. Tran and coworkers chemically stabilized autologous saphenous vein segments to enhance graft stability[28]; however, since the saphenous vein has a small wall thickness, it is limited in application to coronary artery bypass.

To avoid these complications as well as donor site morbidity issues, surgeons have attempted to use grafts constructed from synthetic and natural textile materials as to develop vascular conduits. The most prominent examples of early surgical use of synthetic textile materials to replace damaged vasculature were the implantation of an artificial heart valve comprised of a methyl

methacrylate shell and silicone-coated hollow nylon poppet by Hufnagel[29,30] and the clinical application of Vinyon N in the form of an arterial graft by Blakemore and Vorhees[9,30,31]. Although the Vinyon N graft developed septums or partitions within the graft, the possibility of developing artificial systems was realized. Thus, one of the first key initiatives of tissue engineering was to improve vessel patency by providing a more biocompatible interface between the graft material and the host by enlarging the selection of compatible medical materials and the incorporation of autologous endothelial cells onto these polymeric scaffolds.

Polyurethane (PU) prostheses have been shown to be instable after long-term use because of patency issues[32]. The main material in use for arterial grafts is expanded polytetrafluoroethylene (ePTFE). Comparatively, ePTFE grafts are more costly to manufacture, difficult to attach, and do not provide an appropriate interface with the body that allow cellular infiltration. Another commonly used material type is polyethylene terepthalate, which includes polyester or Dacron. Woven Dacron fabrics have been found to prevent liquid leakage, and their high modulus and low wear resistance make them easier to sew in place and handle. Knitted Dacron prostheses however, are flexible and porous, which allow the body tissue to grow inside the graft to form a distinctive intima-like layer. Surgeons have been able to prevent blood leaks in the knitted Dacron prostheses by allowing the patient's blood to clot on the graft's outer surface[21]. However, using blood clots to seal these prostheses is associated with increased blockage downstream of the graft. To avoid these additional complications, pre-existing knitted Dacron grafts have been sealed by

incorporating PU with functionalized carboxyl groups that allow covalent protein bonding[33]. Also, sealed hybrid grafts containing both a synthetic and biological component have been manufactured. Biological components, such as collagen, albumin, and gelatin, have been used to fill surface voids on the prostheses to prevent the initial bleeding of the grafts[21]. By preventing grafts from leakage, hybrid grafts are beneficial because they decrease the need of blood replacement during surgery. As the tissue surrounding the grafts grows and infiltrates the scaffold, these biological components simultaneously disappear and allow tissue ingrowth to occur. Therefore, an effective hybrid prosthesis would be one with an appropriate interface in which the disappearing rate of its biological component is highly predictable.

**1.4.2 Skin grafts**

Another soft tissue application in which tissue engineering technology has been used to meet increased harvesting demands is skin replacement. The largest drawback to the traditional use of autologous skin is donor site morbidity. Although allografts harvested from cadavers have been used, graft rejection persists. Even more peculiar are the materials that can be used as skin wound dressings. Typically, skin grafts are used to expedite the healing process of burn victims. They may diminish the need for foot amputations and may serve as a remedy to the chronic foot ulcers of many diabetic patients. These topical grafts must be pliable, antimicrobial, and selectively permeable to exudate or wound discharge without allowing the loss of fluids and electrolytes from the wound[34]. The surface characteristics of skin grafts should be such that the graft peels

away from the wound easily, without disrupting the growth of the underlying new skin. For these reasons, few materials meet the performance criteria that are desired for skin grafts. Amongst the possible candidates are absorbable or degradable polymers which include a combination of collagen, chitin, polyglycolide (PGA) and poly-L-lactide (PLL)[35], or extracellular matrices (ECM) such as hyaluronic acid[36] that encourage tissue ingrowth. These materials can incorporate fibroblasts (dermal cells) and keratinocytes (epidermal cells) into porous sheets or woven fabrics known as split-thickness grafts. The first commercially available living skin equivalent was Apligraf®, which features a bovine collagen dermis seeded with allogeneic fibroblasts and keratinocytes[37]. Along with Apligraf®, the uses, advantages and disadvantages of numerous other commercially available skin grafts are shown below in Table 1.

Kirsner suggested, in 1993, that autologous skin grafts can not only replace tissue, but also provide stimulating growth factors to promote tissue growth[38]. Also of note was the observation that increasing the time to wound closure changes the biochemistry of the wound and increases the likelihood of scar formation[39]. More recent clinical trials substantiate similar pharmacological effects in skin grafts that incorporate allogeneic or donor cells[40]. Because the autologous cell retrieval, cell population, and graft preparation process may extend from three to five weeks, thereby increasing a patient's susceptibility to infection[41], novel approaches to decrease culturing time are being investigated[42]. Despite the new developments in skin graft technology, there have been few to no reports of the currently available skin grafts promoting new tissue growth

without the formation of scars in severe burn victims. Therefore, an opportunity exists for the development of a cost-effective skin graft that promotes scarless wound healing and reduced inflammation with comparable re-epithelization times to existing commercial grafts.

Table 1: Alphabetical listing of commercial skin substitutes, adapted from Eisenbud et al.[43]

| Product | Company | FDA-Approved Indications (PMA, HDE, 510K, or other)* | Other Published Uses | Competitive Advantages | Disadvantages |
|---|---|---|---|---|---|
| Alloderm® | LifeCell Inc. | Burns/full-thickness wounds (allograft) | Other formulations (Cymetra™, Repliform™) used to fill soft tissue defects in plastic, gynecological, dental and urologic surgery | Not rejected; no cases of viral transmission after >100,000 product applications; 2 year shelf life | Lacks cellular components |
| Apligraf® | Organogenesis Inc. | Venous/diabetic ulcers (PMA) | Epidermolysis bullosa; anecdotal reports, case studies and pilot trials in many other skin conditions | Mimics function of dermis; cryopreserved product | 5 day shelf life; awkward logistics of ordering and use |
| Biobrane®, Biobrane-L® | Bertek Pharmaceuticals | Partial-thickness burns/meshed autografts/donor sites (510K) | | Three year shelf life; good barrier function and water exchange | No antimicrobial properties/temporary replacement requires removal in 7-10 days |
| Celaderm™ | Celadon Science LLC | (None) | Partial and full thickness burns, venous wounds | >6 month shelf life; relatively inexpensive; good results in many pilot studies | Not FDA approved |
| Dermagraft® | Smith & Nephew Inc. | Diabetic foot ulcers (PMA); ulcers secondary to epidermolysis bullosa (HDE) | | Mimics function of dermis; cryopreserved product | Difficult logistics of ordering and application; short shelf life (unless stored cryopreserved) |
| Epicel® | Genzyme Biosurgery | Deep partial-thickness and full-thickness burns (HDE); congenital nevi (HDE) | | Autologous cells; no rejection, high incidence of permanent take | Fragile; custom preparation; one day shelf life; inferior cosmesis in many patients |

*PMA, pre-market approval; HDE, humanitarian device exemption; 510K substantial equivalence to predicate (previously approved) device

Table 1 (Continued): Alphabetical listing of commercial skin substitutes, adapted from Eisenbud et al.[43]

| Product | Company | FDA-Approved Indications (PMA, HDE, 510K, or other)* | Other Published Uses | Competitive Advantages | Disadvantages |
|---|---|---|---|---|---|
| EZ DermTM | Brennen Medical Inc. | Partial-thickness burns/venous, diabetic, pressure ulcers; porcine xenograft (510K) | | Relatively long shelf life | Potential immune response and/or disease transmission |
| Integra® | Integra LifeSciences Corp. | Deep partial-thickness and full-thickness burns (PMA) | | Two layers; good barrier function; used in over 10,000 patients; moderate shelf life | Operative removal of silicone layer and autograft required |
| Laserskin® | Fidia Advanced Biopolymers | (None) | Partial thickness burns, chronic venous, pressure ulcers, vitiligo | Autologous cells; no rejection; high incidence of permanent take | Two day shelf life; custom preparation; fragile |
| Oasis® | Healthpoint | Partial/full-thickness pressure, venous and diabetic wounds/partial-thickness burns (510K) | | 1.5 year shelf life | Potential immune response |
| OrCel® | Ortec International Inc. | Split-thickness donor sites (PMA); mitten hand deformity surgery of epidermolysis bullosa (HDE) | Venous and diabetic wounds | Mimics cytokine expression of healing skin; 9 month shelf life cryopreserved | Requires cryopreserved storage |
| TransCyte® | Smith & Nephew Inc. | Full- and partial-thickness burns (PMA) | | 1.5 year shelf life frozen | Silicone membrane must be removed |

*PMA, pre-market approval; HDE, humanitarian device exemption; 510K substantial equivalence to predicate (previously approved) device

**1.5. Controlling the inflammatory response through cellular encapsulation**

In order to formulate new materials that incorporate cells that deliver growth factors, one must address the role of the inflammatory response in wound healing. Based on correlations developed between porosity, material surface chemistry and host response of thirty-seven types of synthetic vascular grafts, Wesolowski concluded that the inflammatory response is controlled by material chemistry and other material factors that can stimulate biochemical changes in necrotic scar tissue[44]. Today, it is known that in regulating wound healing, it is necessary to control the molecules produced by activated macrophages. Namely, activated macrophages secrete matrix metalloproteases which degrade the surrounding collagenous tissue and release chemokines that promote the migration of fibroblasts from the adventitia layer of the surrounding blood vessels to secrete a new matrix of fibronectin and collagen[45]. Depending upon the composition and condition of the existing tissue, these new constituents will form acellular, nonfunctional fibrotic granular tissue, or scar tissue, that will isolate the implant from the physiological environment.

**1.5.1 Preventing the activation of macrophages**

Therefore, it is important to address the molecules that are known to have a key role in activating macrophages. These molecules do not act alone, but as part of an intricate system of synergistic pairs. Amongst these factors are interferon gamma (IFN-γ), tumor necrosis factor alpha and beta (TNF-α and TNF-β), interleukin 10 (IL-10), IL-4, and transforming growth factor beta (TGF-β). IFN-γ and TNF-β are lymphokines that are predominantly produced by IL-12

stimulated Th-1 type T cells. These lymphokines encourage macrophages to release nitrous oxide and other toxins that kill and degrade bacteria and other foreign material they have engulfed. The TNF-α molecule acts as the macrophages' signaling device, upregulating the inflammatory response by recruiting, activating, and promoting the maturation of inflammatory cells. IL-4 and IL-10 both inhibit macrophage production of cytokines by suppressing the formation of Th-1 type T cells[46].
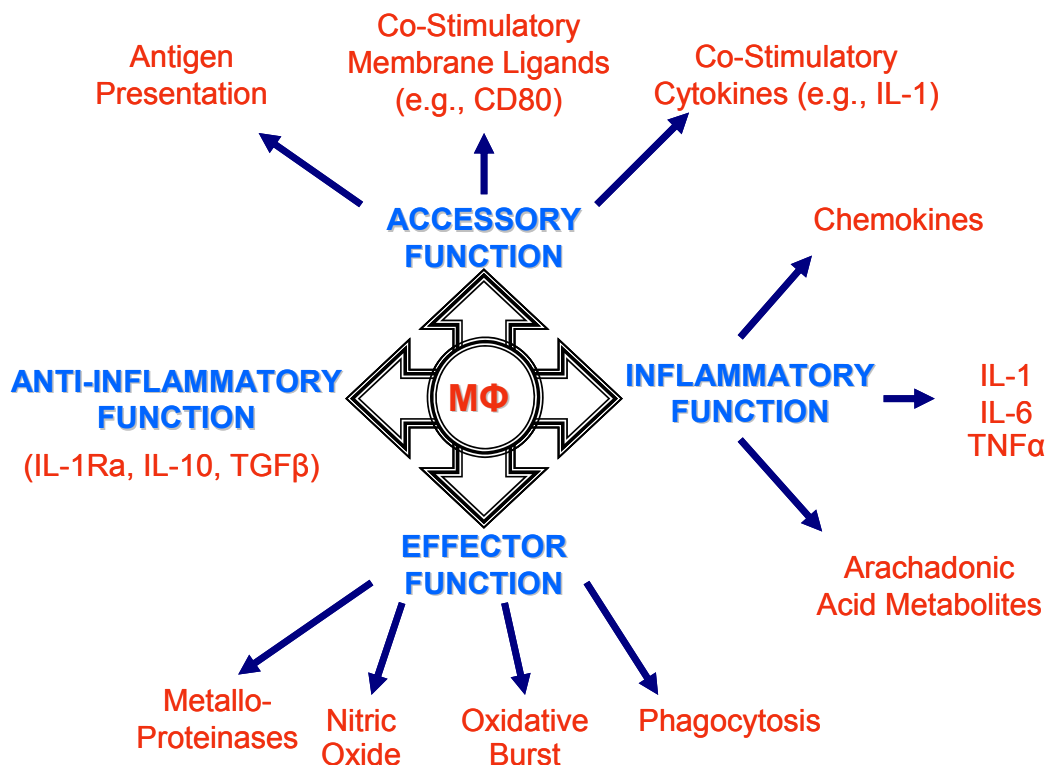


Figure 1.1: The role of macrophages in inflammatory responses. During an inflammatory response, macrophages can display both inflammatory and anti-inflammatory functions. Through the regulation of transforming growth factor beta (TGF- β), however, macrophages can be induced to inhibit their effector functions, allowing for a more directed wound healing response[47].

Of particular interest is TGF-β because it can be used to control the inflammatory cytokine production from macrophages[47]. Also, the ratios and

regulation of its isoforms have been shown to play key roles in promoting scarless wound healing[48-50]. In mammals, TGF-β (25kDa) exists in three unique homodimers (TGFβ1-3)[51]. It is important to note that these isoforms not only differ in conformation, but also in their potency and functionality. TGF-β1 and TGF-β2 are derived from platelets and macrophages, whereas the primary cell source of TGF-β3 is fibroblasts[52]. These factors function as chemotactic agents to recruit inflammatory cells and fibroblasts. Although inappropriate amounts of these growth factors promote the deposition of fibrous epithelial layers in diseases such as glomerulonephritis and proliferative vitreoretinopathy[50], their proper regulation has an unlimited arena for therapeutic use. The introduction of exogenous TGF-β3 at cutaneous wound sites in rats has been shown to prevent scarring in cutaneous wounds[50]. Prevention occurs by decreasing the wounded tissue density of macrophages and monocytes, increasing blood vessel density in the healing wound, and decreasing the deposition of fibronectin and collagen Types I and III by fibroblasts. Respectively, these events promote healing in which there is a less severe inflammatory response, less likelihood for infection and necrosis, and a less contracted and a more organized skin architecture. Moulin and coworkers' *in vitro* studies suggest that the addition of TGF- β3 (most potent) decreases the contraction of adult wounds by increasing the expression of α-smooth muscle (SM) actin and the α3 and β1 integrin subsets of fibroblasts, while not affecting the fibroblasts' growth or contractile capacity and their expression of α1 and α2 integrin subsets. However, the studies suggest that in fetal fibroblasts, in which wounds heal without contractions and scars, the

addition of TGF- β3 would inhibit cellular growth and contractile capacity and decrease the expression of α1, α2 and β1 integrin subsets, while not affecting the expression of α-SM actin and the α3 integrin subset[49]. Collectively, the differences in the ratios of TGF- β isoforms that are present during wound healing and the intrinsic cellular responses to TGF- β may account for the differences in healing quality between fetal and adult wounds.

**1.5.2 The role of endothelial cells in wound healing**

Although macrophages are responsible for secondary phases of inflammation and fibroblasts are responsible for extracellular matrix deposition, endothelial cells play a major role in inflammation resolution[53]. Endothelial cells secrete soluble factors that promote wound closure and neovascularization. Neovascularization is promoted by the activation of quiescent endothelial cells by angiogenic factors such as VEGF, bFGF, IL-8, PDGF, and hematopoeietic growth factors derived from tumors or inflammatory cells. Activated endothelial cells cause basement membrane proteolysis and endothelial cell proliferation, migration, and alignment to form rope-like structures, followed by vessel maturation[54,55]. Implanting autologous tissue causes donor site morbidity. Implanting allogeneic and xenogeneic cells into the body causes an immune response that may result in lysis of implanted cells. However, if these cells were placed into an immunoprotective, semi-permeable cocoon that allowed nutrients and waste transport, but denied host's antibodies, this type of implantation might be successful. Ideally, one would expect the endothelial cells to be activated by

the appropriate factors and to begin directing wound healing from their location inside the encapsulation device.

The incorporation of endothelial cells into small diameter artificial arterial grafts will promote the regulation of thrombotic activity in the lining of natural blood vessels[56]. It has been proposed that surrounding endothelial cells with porous, hollow fiber components might allow allogeneic or xenogeneic transplantation with minimal immune response. These hollow fibers would be constructed in either woven or nonwoven forms to create a bioactive surface for medical devices and soft tissue transplants or to introduce a clinically applicable arterial substitute. The novel bioactive surface would incorporate genetically modified endothelial cells that would direct wound healing at the implant site by delivering healing agents such as TGF-β3. The use of these devices as arterial grafts and living skin replacements would promote specific and complete wound healing, which would increase the functionality of new tissues and improve the patient's outcome.

## 1.6 Alginate: a classic encapsulation material

Material selection of the immunoisolation membrane has enormous influence on the success of cellular encapsulation devices. Prakash and Soe-Lin have reviewed the strengths and weaknesses of various materials used to encapsulate living cells[57]. The biomaterials reviewed include alginate and alginate variants. Alginates are linear unbranched polymers (carbohydrates) that are found in various sources of brown seaweed and which contain randomly arranged blocks of α-(1→4)-linked D-mannuronic acid (**M**) and α-(1→4)-linked L-

guluronic acid (**G**) residues of high molecular weight (Figure 1.2)[58]. Although the M and G blocks are epimers and are chiral at the C4 carbon, the conformation of the G block allows its carboxylic acid groups to be more readily available for prosthetic modification and crosslinking by positive divalent metal ions such as calcium.



α-(1→4)-linked L-guluronic acid (**G**)     β-(1→4)-linked D-mannuronic acid
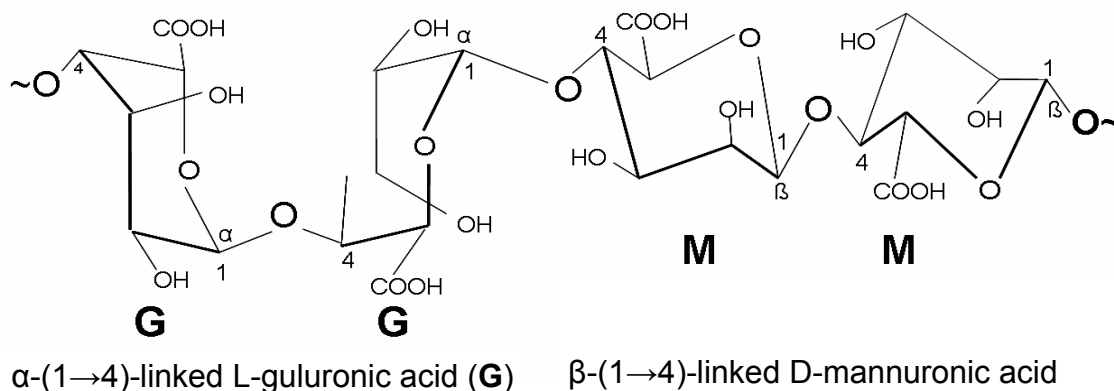
Figure 1.2:  A common GGMM block found in alginate.

The degradation of alginate can occur in calcium alginate when the calcium diffuses into a lesser concentrated physiological environment. Degradation of alginate can be retarded through the esterification of carboxylic acids groups on the G blocks[57].  Alginate and alginate variants are promising polymers for live cell encapsulation because they can provide short/medium-term mechanical stability, flexible permselectivity, and low immunogenicity.

## 1.6.1 Apparent viscosity of sodium alginate

Viscosity is the limiting factor in determining sodium alginate concentration and spinnability, as well as the membrane's immunoprotective permeability and the diffusion capability.  Moreover, cell viability is highly dependent upon maintaining low alginate viscosity.  Kong and coworkers demonstrated that mixing suspended osteoblasts in a highly viscous sodium alginate matrix resulted

in a substantial loss of cell viability[59]; however, use of low molecular weight alginates increased the brittleness of the hydrogels. The prescribed method of circumventing or minimizing these issues is to combine low molecular weight alginates with a small fraction of high molecular weight alginates[60].

## 1.6.2 M/G ratio of alginates

M/G ratio is an important characteristic in the design of an alginate encapsulation device. The %G in the alginate hydrogel determines the rigidity of the gel. Mooney and colleagues suggest that a higher %G promotes cell proliferation whereas a lower %G causes cells to differentiate[61]. Since cells are more likely to adhere to and proliferate on more rigid gels, the %G not only influences gel rigidity, but also influences cell function by guiding cell-matrix interactions. Kong and coworkers showed that irradiation methods can decrease the viscosity of the sodium alginate matrix without affecting the % G content or the gelling capability of the gel[59].

## 1.6.3 Sterilization of alginates

It was once theorized that the high M content of some alginates induced an immune response. However, recent data suggest that contaminants are the more likely cause of the response, and novel purification methods have been developed that render alginates of various contents eligible for implantation[62]. Other techniques have been suggested for sterilization, including sonochemical and ultraviolet light methods[63]. Autoclave sterilization of alginate also effectively decreases the molecular weight by polymer chain degradation[64,65].

### 1.6.4 Importance of alginate processing parameters

The potential use of alginate in cellular encapsulation applications is determined by the processing parameters used to construct a specific form. Research conducted by Burg and coworkers indicated that porous calcium alginate beads facilitated cell adhesion when compared with other specific alginate forms such as nonporous beads, tubes, and solid masses[66] (Table 1.2). Porous calcium alginate beads are indeed noteworthy for their high surface to volume ratio.

Table 1.2: The influence of alginate processing parameters on cell viability / tissue ingrowth

| Construct | Diffusion | Cell Friendly | Even Distribution of Calcium Ions Throughout Mass | Porosity | Cell Viability/ Tissue Ingrowth |
|---|---|---|---|---|---|
| Solid Mass | - | - | + | - | - |
| Tube / Disc | - | - | - | - | - |
| Solid Bead | - | - | - | - | - |
| Porous Bead | + | + | - | + | + |

### 1.6.5 Incorporation of cells into alginate

The technology of fabricating hollow fiber membranes for filtering applications already exists[67,68] and might readily be transferred to process alginate. Clinically, islet cells have been incorporated into poly (acrylonitrile-co-vinyl chloride) hollow fibers by Lacy and coworkers[2]. Emerich and colleagues compared the delivery of dopamine from cells encapsulated into the lumen and wall of polyacrylonitrile-vinyl chloride copolymer (PAN/PVC) hollow fiber

membranes[69].  Li suggests that suspending cells in a 1% alginate hydrogel matrix for cells prevents necrotic cluster formation caused by cell – cell adhesion[70].

**1.6.6 Pore diameter**

The importance of pore diameter throughout the alginate hydrogel fibers arises due to the target biological application.  Too large a pore diameter may allow the influx of complements that could mark the cells within the alginate matrix as foreign, causing the activation of an immune response.  If the pore diameter is too small, then there could be a delay or burst effect of the healing agents released from the cells.

Pore introduction techniques have been reviewed that will allow proper diffusion of nutrients and oxygen without initiating an immune response in the alginate hollow fiber matrix.  Mooney and collegues have shown that pores can be incorporated into poly-lactide-co-glycolide scaffolds through a gas foaming technique without the use of organic solvents[71]; however, this technique is limited to semi-crystalline polymers and does not lend well to hydrogels.  Lyophilization[72] and swelling techniques[54] have also been evaluated and allow more widespread treatments of materials; however, both methods are applied post processing.

**1.7 Project goals**

Given the potential clinical benefit of producing a cellular alginate with permselectivity using minimal processing steps, the goal of this research was to demonstrate cellular encapsulation in hollow alginate fibers using two innovative spinning methodologies and a newly designed benchtop fiber spinning

apparatus. Long-term, this technology could lead to the development of cellular fiber based products that include biosynthetic skin grafts and arterial graft replacements.

## References

1.  Shmerling, R.H. News review from Harvard Medical School -- transplants at record levels: Aetna InteliHealth Inc. March 31, 2005.

2.  Lacy, P.E., Hegre, O.D., Gerasimidivazeou, A., Gentile, F.T., and Dionne, K.E. Maintenance of normoglycemia in diabetic mice by subcutaneous xenografts of encapsulated islets. Science 1991;254(5039):1782-1784.

3.  Bes, J.C., Lazorthes, Y., Sol, J.C., Tkaczuk, J., and Sallerin, B. Clinical perspectives of xenografts: Encapsuled chromaffin cells and pain. Pathologie Biologie 2000;48(4):365-367.

4.  Czech, K.A. and Sagen, J. Update on cellular transplantation into the CNS as a novel therapy for chronic pain. Progress in Neurobiology 1995;46(5):507-529.

5.  Kim, Y.M., Jeon, Y.H., Jin, G.C., Lim, J.O., and Baek, W.Y. Immunoisolated chromaffin cells implanted into the subarachnoid space of rats reduce cold allodynia in a model of neuropathic pain: A novel application of microencapsulation technology. Artificial Organs 2004;28(12):1059-1066.

6. Date, I., Shingo, T., Yoshida, H., Fujiwara, K., Kobayashi, K., and Ohmoto, T. Grafting of encapsulated dopamine-secreting cells in Parkinson's disease: Long-term primate study. Cell Transplantation 2000;9(5):705-709.

7. Kim, Y.T., Hitchcock, R., Broadhead, K.W., Messina, D.J., and Tresco, P.A. A cell encapsulation device for studying soluble factor release from cells transplanted in the rat brain. Journal of Controlled Release 2005;102(1):101-111.

8. Li, R.H., White, M., Williams, S., and Hazlett, T. Poly(vinyl alcohol) synthetic polymer foams as scaffolds for cell encapsulation. Journal of Biomaterials Science-Polymer Edition 1998;9(3):239-258.

9. Shalaby, S. and Burg, K.J.L. Absorbable and biodegradable polymers. New York: CRC Press; 2004.

10. Aoki, T., Koizumi, T., Kobayashi, Y., Yasuda, D., Izumida, Y., Jin, Z.H., Nishino, N., Shimizu, Y., Kato, H., Murai, N., Niiya, T., Enami, Y., Mitamura, K., Yamamoto, T., and Kusano, M. A novel method of cryopreservation of rat and human hepatocytes by using encapsulation technique and possible use for cell transplantation. Cell Transplantation 2005;14(9):609-620.

11. Balladur, P., Crema, E., Honiger, J., Calmus, Y., Baudrimont, M., Delelo, R., Capeau, J., and Nordlinger, B. Transplantation of allogeneic hepatocytes without immunosuppression - long-term survival. Surgery 1995;117(2):189-194.

12.  Chia, S.M., Leong, K.W., Li, J., Xu, X., Zeng, K.Y., Er, P.N., Gao, S.J., and Yu, H. Hepatocyte encapsulation for enhanced cellular functions. Tissue Engineering 2000;6(5):481-495.

13.  Haque, T., Chen, H., Ouyang, W., Martoni, C., Lawuyi, B., Urbanska, A.M., and Prakash, S. *In vitro* study of alginate-chitosan microcapsules: An alternative to liver cell transplants for the treatment of liver failure. Biotechnology Letters 2005;27(5):317-322.

14.  Mai, G., Huy, N.T., Morel, P., Mei, J., Bosco, D., Berney, T., Majno, P., Mentha, G., Trono, D., and Buhler, L.H. Treatment of fulminant liver failure by transplantation of microencapsulated primary or immortalized xenogeneic hepatocytes. Transplantation Proceedings 2005;37(1):527-529.

15.  Nicoluzzi, J.E., Barbu, V., Baudrimont, M., Lakehal, F., Becquemont, L., Chafai, N., Delelo, R., Sarkis, R., Honiger, J., Housset, C., and Balladur, P. Viability and differentiation of human hepatocytes immunoprotected by macroencapsulation and transplanted in rats. Gastroenterologie Clinique Et Biologique 2000;24(3):342-348.

16.  Rahman, T.M., Selden, C., Khalil, M., Diakanov, I., and Hodgson, H.J.F. Alginate-encapsulated human hepatoblastoma cells in an extracorporeal perfusion system improve some systemic parameters of liver failure in a xenogeneic model. Artificial Organs 2004;28(5):476-482.

17. Ringel, M., Von Mach, M.A., Santos, R., Feilen, P.J., Brulport, M., Hermes, M., Bauer, A.W., Schormann, W., Tanner, B., Schon, M.R., Oesch, F., and Hengstler, J.G. Hepatocytes cultured in alginate microspheres: An optimized technique to study enzyme induction. Toxicology 2005;206(1):153-167.

18. Stange, J. and Mitzner, S. Hepatocyte encapsulation - initial intentions and new aspects for its use in bioartificial liver support. International Journal of Artificial Organs 1996;19(1):45-48.

19. Gentile, F.T., Doherty, E.J., Rein, D.H., Shoichet, M.S., and Winn, S.R. Polymer science for macroencapsulation of cells for central-nervous-system transplantation. Reactive Polymers 1995;25(2-3):207-227.

20. Lembert, N., Wesche, J., Petersen, P., Doser, M., Zschocke, P., Becker, H.D., and Ammon, H.P.T. Encapsulation of islets in rough surface, hydroxymethylated polysulfone capillaries stimulates VEGF release and promotes vascularization after transplantation. Cell Transplantation 2005;14(2-3):97-108.

21. Paton, D. Materials used for arterial replacement. Sulzer technical review 1991;73(2):5-10.

22. Sun, Y.L., Ma, X.J., Zhou, D.B., Vacek, I., and Sun, A.M. Normalization of diabetes in spontaneously diabetic cynomologus monkeys by xenografts of microencapsulated porcine islets without immunosuppression. Journal of Clinical Investigation 1996;98(6):1417-1422.

23. Sambanis, A. Encapsulated islets in diabetes treatment. Diabetes Technology & Therapeutics 2003;5(4):665-668.

24. Soon-Shiong, P. Treatment of Type I diabetes using encapsulated islets. Advanced Drug Delivery Reviews 1999;35(2-3):259-270.

25. Soon-Shiong, P., Heintz, R.E., Merideth, N., Yao, Q.X., Yao, Z.W., Zheng, T.L., Murphy, M., Moloney, M.K., Schmehl, M., Harris, M., Mendez, R., Mendez, R., and Sandford, P.A. Insulin independence in a Type-1 diabetic patient after encapsulated islet transplantation. Lancet 1994;343(8903):950-951.

26. Rafael, E., Wu, G.S., Hultenby, K., Tibell, A., and Wernerson, A. Improved survival of macroencapsulated islets of langerhans by preimplantation of the immunoisolating device: A morphometric study. Cell Transplantation 2003;12(4):407-412.

27. Lavallee, D. Textiles researcher teams up to invent small-diameter artificial arteries. The University Pacer (University of Rhode Island). Online ed. Volume 2005. Kingston, RI; 2005.

28. Tran, H.M., Paterson, H.S., Meldrum-Hanna, W., and Chard, R.B. Tunnelling versus open harvest technique in obtaining venous conduits for coronary bypass surgery. European Journal of Cardio-Thoracic Surgery 1998;14(6):602-606.

29. Butany, J., Ahluwalia, M.S., Fayet, C., Munroe, C., Blit, P., and Ahn, C. Hufnagel valve - the first prosthetic mechanical valve. Cardiovascular Pathology 2002;11(6):351-353.

30. Schmidt, C.E. and Baier, J.M. Acellular vascular tissues: Natural biomaterials for tissue repair and tissue engineering. Biomaterials 2000;21(22):2215-2231.

31. Reis, R.L. and Cohn, D. Polymer based systems on tissue engineering, replacement and regeneration. Netherlands: Kluwer Academic Publishers; 2002. 371-390 p.

32. Zhang, Z., Marois, Y., Guidoin, R.G., Bull, P., Marois, M., How, T., Laroche, G., and King, M.W. Vascugraft(r) polyurethane arterial prosthesis as femoro-popliteal and femoro-peroneal bypasses in humans: Pathological, structural and chemical analyses of four excised grafts. Biomaterials 1997;18(2):113-124.

33. Phaneuf, M.D., Dempsey, D.J., Bide, M.J., Quist, W.C., and Logerfo, F.W. Coating of Dacron vascular grafts with an ionic polyurethane: A novel sealant with protein binding properties. Biomaterials 2001;22(5):463-469.

34. Ramakrishna, S., Mayer, J., Wintermantel, E., and Leong, K.W. Biomedical applications of polymer-composite materials: a review. Composites Science and Technology 2001;61(9):1189-1224.

35. Santos, A.R., Jr., Barbanti, S.H., Duek, E.A., Dolder, H., Wada, R.S., and Wada, M.L. Vero cell growth and differentiation on poly(l-lactic acid) membranes of different pore diameters. Artif Organs 2001;25(1):7-13.

36. Campoccia, D., Doherty, P., Radice, M., Brun, P., Abatangelo, G., and Williams, D.F. Semisynthetic resorbable materials from hyaluronan esterification. Biomaterials 1998;19(23):2101-2127.

37.     Griffiths, M., Livingstone, R., Price, R., and Navsaria, H. Survival of Apligraf in acute human wounds. Tissue Engineering 2004;10(7-8):1180-1195.

38.     Kirsner, R.S., Falanga, V., and Eaglstein, W.H. The biology of skin-grafts - skin-grafts as pharmacological agents. Archives of Dermatology 1993;129(4):481-483.

39.     Demling, R.H., Orgill, D.P., Desanti, L., and Mclaughlin, D.A. Section 9: Burn scar and its complications. May 3, 2006.

        http://www.burnsurgery.com/Modules/BurnWound%201/sect_IX.htm

40.     L  P  M  Lloyd-Evans  &  Biobridge  Associates.  Development  of biodegradable scaffold for dermo-epidermal skin grafts 2005.

41.     Harris, P.A., Leigh, I.M., and Navsaria, H.A. Pre-confluent keratinocyte grafting: The future for cultured skin replacements. Burns 1998;24(7):591-593.

42.     Rennekampff, H.O., Kiessig, V., and Hansbrough, J.F. Current concepts in the development of cultured skin replacements. Journal of Surgical Research 1996;62(2):288-295.

43.     Eisenbud, D., Huang, N.F., Luke, S., and Silberklang, M. Skin substitutes and wound healing: Current status and challenges. Wounds-a Compendium of Clinical Research and Practice 2004;16(1):2-17.

44.     Wesoloski, S.A., Fries, C.C, Karlson, K.E., Bakey, M.D, and Sawyer, P.N.. Porosity: Primary determinant of ultimate fate of synthetic vascular grafts. Surgery 1961;50(1):91-96.

45. Bizios, R., Dee, K. C., and Puleo, D. A. An introduction to tissue biomaterial interactions. Hoboken: John Wiley & Sons Inc.; 2002.

46. Kimball, J.W. Kimball's biology pages. http://users.rcn.com/jkimball.ma.ultranet/BiologyPages/T/Th1_Th2.html January 14, 2006.

47. Stout, R.D. and Suttles, J. T-cell signaling of macrophage function in inflammatory disease. Frontiers in Bioscience 1997;2(d):197-206.

48. Kohama, K., Nonaka, K. Hosokawa, R., Shum, L., and Ohishi, M. TGF-beta 3 promotes scarless repair of cleft lip in mouse fetuses. Journal of Dental Research 2002;81(10):688-694.

49. Moulin, V., Tam, B.Y.Y, Castillouz, G., Auger, F.A., O'conner-Mccourt, M.D., Philip, A., and Germain, L. Fetal and adult human skin fibroblasts display intrinsic differences in contractile capacity. Journal of Cellular Physiology 2001;188:211-222.

50. Shah, M., Foreman, D.M., and Ferguson, M.W. Neutralisation of TGF-beta 1 and TGF-beta 2 or exogenous addition of TGF-beta 3 to cutaneous rat wounds reduces scarring. J Cell Sci 1995;108 ( Pt 3):985-1002.

51. Clark, D.A. and Coker, R. Transforming growth factor-beta (TGF-beta). Int J Biochem Cell Biol 1998;30(3):293-8.

52. Miller, M.C. and Nanchahal, J. Advances in the modulation of cutaneous wound healing and scarring. BioDrugs 2005;19(6):363-81.

53. Kadl, A. and Leitinger, N. The role of endothelial cells in the resolution of acute inflammation. Antioxid Redox Signal 2005;7(11-12):1744-54.

54. Bocci, G., Fasciani, A., Danesi, R., Viacava, P., Genazzani, A.R., and Del Tacca, M. *In vitro* evidence of autocrine secretion of vascular endothelial growth factor by endothelial cells from human placental blood vessels. Mol Hum Reprod 2001;7(8):771-7.

55. Hartlapp, I., Abe, R., Saeed, R.W., Peng, T., Voelter, W., Bucala, R., and Metz, C.N. Fibrocytes induce an angiogenic phenotype in cultured endothelial cells and promote angiogenesis *in vivo*. Faseb J 2001;15(12):2215-24.

56. Xu, C., Yang, F., Wang,S., and Ramakrishna, S. *In vitro* study of human vascular endothelial cell function on materials with various surface roughness. Journal of Biomedical Materials Research 2004;71(A):154-161.

57. Arlon Materials for Electronics Inc. Focus on rheology. November 30, 2006. http://www.arlon-med.com/Focus%20on%20Rheology.PDF

58. Drury, J.L. and Mooney, D.J. Hydrogels for tissue engineering: Scaffold design variables and applications. Biomaterials 2003;24:4337-4351.

59. Kong, H.J., Smith, M.K., and Mooney, D.J. Designing alginate hydrogels to maintain viability of immobilized cells. Biomaterials 2003;24(22):4023-9.

60. Kong, H.J., Kaigler, D., Kim, K., and Mooney, D.J. Controlling rigidity and degradation of alginate hydrogels via molecular weight distribution. Biomacromolecules 2004;5(5):1720-7.

61. Mooney, D.J. Clemson University Department of Bioengineering: Hunter Lecture Series. Charleston, SC; 2004.

62. Zhang, W.J., Laue, C., Hyder, A., and Schrezenmeir, J. Purity of alginate affects the viability and fibrotic overgrowth of encapsulated porcine islet xenografts. Transplantation Proceedings 2001;33(7-8):3517-3519.

63. Wasikiewicz, J.M., Yoshii, F., Nagasawa, N., Wach, R.A., and Mitomo, H. Degradation of chitosan and sodium alginate by gamma radiation, sonochemical and ultraviolet methods. Radiation Physics and Chemistry 2005;73(5):287-295.

64. Leo, W.J., Mcloughlin, A.J., and Malone, D.M. Effects of sterilization treatments on some properties of alginate solutions and gels. Biotechnology Progress 1990;6(1):51-53.

65. Srinivasulu, B., Adinarayana, K., and Ellaiah, P. Investigations on neomycin production with immobolized cells of streptomyces marinensis NUV-5 in calcium alginate matrix. AAPS PharmSciTech 2003;4(4):E57.

66. Burg, K.J.L., Holder Jr, W.D., Culberson, C.R., Beiler, R.J., Greene, K.G., Loesack, A., Roland, W.D., Wyatt, S., and Halberstadt, C.R. Alginate processing parameters and influence on cellular attachment. Transactions of the Biomedical Engineering Society Conference (1998).

67. He, T., Mulder, M.H.V., and Wessling, M. Preparation of porous hollow fiber membranes with a triple-orifice spinneret. Journal of Applied Polymer Science 2003;87(13):2151-2157.

68. Wang, D., Li, K., and Teo, W.K. Preparation of annular hollow fibre membranes. Journal of Membrane Science 2000;166:31-39.

69. Emerich, D.F., Flanagan, T.R., Frydel, B.R., Gentile, F.T., Palmatier, M.A., and Winn, S.R. Transplantation of encapsulated dopamine-secreting cells as a treatment for Parkinson's disease. Jounal of Neural Transplantation & Plasticity 1992;3(4):267-268.

70. Li, R.H. Materials for immunoisolated cell transplantation. Advanced Drug Delivery Reviews 1998;33 87-109.

71. Mooney, D.J., Baldwin, D.F., Suh, N.P., Vacanti, L.P., and Langer, R. Novel approach to fabricate porous sponges of poly(d,l-lactic-co-glycolic acid) without the use of organic solvents. Biomaterials 1996;17(14):1417-1422.

72. Kang, H.W., Tabata, Y., and Ikada, Y. Fabrication of porous gelatin scaffolds for tissue engineering. Biomaterials 1999;20(14):1339-1344.

# CHAPTER TWO

# MATERIALS AND METHODS

## 2.1 Investigative approach

Our approach to achieving optimized cellular encapsulation in the long term includes four crucial topics, as shown in Figure 2.1. In order to first demonstrate that this spinning technology can be used to encapsulate cells, Topics I and IV will be discussed extensively within this thesis, while Topics II and III remain topics of future interest and investigation.
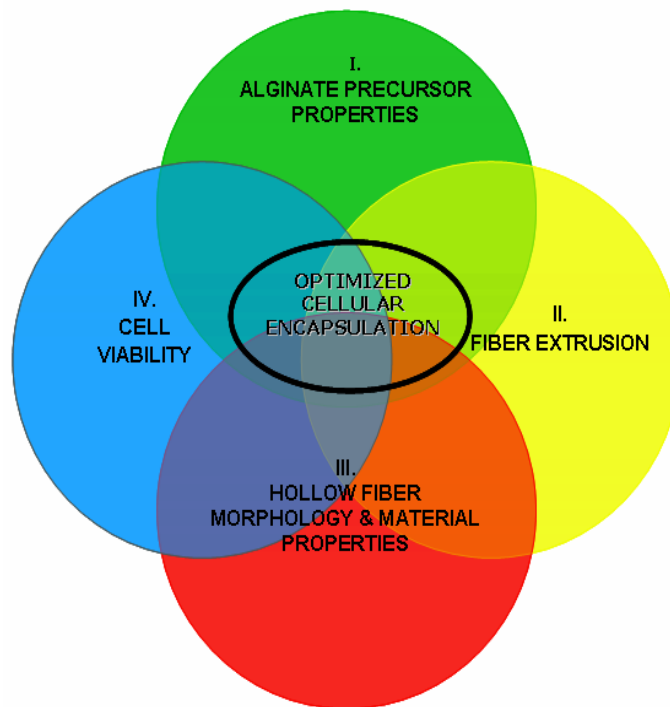


Figure 2.1: Venn diagram displaying the research topics required to optimize cellular encapsulation includes evaluating the effects of the solution properties of alginate (Topic I), fiber spinning parameters (Topic II), and hollow fiber morphology and material (construct) properties (Topic III) on cell viability (Topic IV).

In Topic 1, we characterize the solution properties of several types of alginate in order to determine which alginate type is best for spinning fibers and incorporating cells.  These alginate solution properties have been characterized previously in the literature; and, although the equipment used in the literature is not readily available in our lab, our contention is that we have successfully developed comparable characterization methods that yielded the selection of an alginate type with which we pursued further encapsulation studies.

In Topic 4, we investigate the hypothesis that our spinning apparatus can be used to incorporate green fluorescent protein labeled, bovine mammary epithelial cells (MAC-Ts) into the walls and lumen of our hollow fibers, and we demonstrate that the MAC-Ts remain viable throughout the hollow fibers during our 21 day *in vitro* study.

## 2.2 Solution properties of sodium alginate
## 2.2.1 Rheological properties of alginate

100 mL solutions of sodium alginate were prepared at concentrations from 0 – 8 wt% (wt alginate/wt $H_2O$), at increments of 1% by using an overhead stirrer (Eurostar digital, IKA®-WERKE, Wilmington, NC).  The distilled water was stirred as the alginate powder was dispersed into the water to prevent clumping.

## 2.2.2 The effect of alginate concentration on apparent viscosity

The viscosity behavior of low and medium viscosity (LV and MV) grade sodium alginate (Sigma-Aldrich, St. Louis, Missouri) and Acros Organics (AO) sodium alginate (Acros Organics, Geel, Belgium) was investigated using a plate and cone rheometer (Physica MCR 300 Rheometer; Anton Paar Physica Co., Graz, Austria).  Volumes in the amount of 2 mL of the sodium alginate samples

were pipetted onto the test plate, which allowed the surface of the disk to touch the surface of the sample. The rheometer applied torque to the cone (PP-25: diameter = 24.96 mm and contact angle = 1°; Anton Paar Physica Co., Graz, Austria) to achieve the specified shear rates. The US200® software (Anton Paar Physica Co., Graz, Austria) automatically calculated the viscosity by multiplying the shear stress times the shear rate. The cone height was adjusted appropriately from 1 to 1.5 mm to obtained accurate measurements prior to each viscosity measurement, as the height of the bubble was dependent upon concentration. The temperature of the measuring plate was maintained at 25°C using the water pump connected to the rheometer. A constant shear rate (CSR) test was used to measure the viscosity profile of these alginates at a shear rates up to 100 s$^{-1}$.

Additionally, 100 mL solutions of AO alginate were made at 0 – 2 wt%, at 0.5 wt% increments to provide additional technical knowledge about the response of the alginate to changing shear rates (i.e flow rates through the syringe) when making alginate beads. To determine this viscosity profile, a CSR test was used to measure the viscosity profile of these alginates at a shear rates up to 100 s$^{-1}$. The cone type, test sample volume, cone height, and test temperature stated for the 2-8 wt% concentrations were held constant throughout this study.

## 2.2.3 The effect of autoclaving and adding Dulbecco's Modified Eagle's Medium (DMEM) on apparent viscosity

To determine an optimal viscosity for spinning cellular fibers using the co-extrusion process, it was necessary to determine how the viscosity of alginate changes after each processing step. The alginate is prepared, sterilized, cooled to room temperature, and then an additive is mixed with the alginate. For this study, the additive was DMEM, whereas future studies could include biomaterials such as gelatin, fibrin or chitosan.

A 500 mL solution of 6 wt% medium viscosity grade (MV) alginate was prepared using an overhead stirrer (Eurostar digital, IKA®-WERKE, Wilmington, NC). To prevent aggregation, the appropriate amount of distilled water was stirred in a 1 L glass beaker as the alginate powder was dispersed into the water. After 30 minutes of mixing at a shear rate of 2000 min$^{-1}$, an intermediate sample, sample A, was gathered by pouring 20 mL of the alginate into a 100 mL plastic specimen cup. Aluminum foil was loosely placed over the beaker. The beaker was secured in an autoclave oven (Model 3870M; Brinkmann Instruments, Inc., Westbury, New York), where it was heated to 121°C using a 45 - minute cycle for liquids. After autoclaving, the beaker was placed in a -20°C freezer for 1 hour of cooling. A 20 mL sample of the cooled alginate was pipetted into a 100 mL specimen cup and labeled as sample B. Cooled alginate in aliquots of 10 mL was pipetted into each of two 100 mL plastic specimen cups, samples C and D, using a sterilized 10 mL pipette and electric pipetter. 1 mL of DMEM was pipetted into the cup containing sample C, and 10 mL of DMEM were pipetted into the cup

containing sample D.  A spoon was used to thoroughly mix the contents of each cup.

Using a plate and cone rheometer, the apparent viscosity of the samples A-D was evaluated using a constant shear rate (CSR) test at a shear rate of 100 $s^{-1}$ for 60 seconds.  The cone height was 0.5 mm and the measuring plate was held at a constant temperature of 22.5°C, the average co-extrusion spinning temperature.  The apparent viscosities of samples A-C were related and used to predict the intermediate behavior of the spinning solution during preparation.

### 2.2.4 Determination of molecular weight

Solutions of low (LV) and medium (MV)viscosity grade sodium alginate (Sigma Aldrich, St. Louis, Missouri) and Acros Organics (AO) sodium alginate (Acros Organics, Morris Plains, New Jersey) were prepared at concentrations of 0 – 2 % (wt/vol) at increments of 0.5 %.  A 0.1M sodium chloride solution was used as the solvent to minimize molecular coiling.  A rheometer (MCR 300; Anton-Paar, Ashland, Virginia) was used to measure the "apparent" viscosity of these alginate solutions from shear rates of 0.1 to 100 $s^{-1}$.  The apparent viscosity is highly dependent upon concentration of alginate and shear rate.  The relative viscosity of each alginate concentration was calculated by dividing the apparent viscosities measured for the solutions by the apparent viscosity of the solvent.  The relative viscosity shows changes in viscosity on a solvent basis.  A plot was made of the inherent viscosity versus concentration using Microsoft Excel®, as shown in Figure 3.1.  It was from these plots that an intrinsic viscosity

was interpolated. A Mark-Houwink plot was then used to correlate the intrinsic viscosity and molecular weight, according to methods found in the literature[1,2].

A box and whisker plot was made by using Microsoft Excel© (Microsoft Corporation, Redmond, Washington)[3-5]. In addition to the plot, the coefficient of variation ($C_v$) and the interquartile mean (IQM) were calculated to determine the degree of dispersion for the viscosity average molecular weight results[6]. $C_v$ is the ratio of the standard deviation to the mean. Since the IQM excludes the lowest and highest 25% of the values in a given data set, it is insensitive to outliers and typically preferred over the arithmetic mean or average in measuring the data set's central tendency. Therefore, the IQM is a more precise calculation of the molecular weight.

## 2.2.5 Evaluating the M/G ratio of sodium alginate

A total of three methods were used to calculate the G block percentage of each alginate type. Methods 1 and 2 involved calculating P/T ratios from CD spectra. Method 1 used an empirical equation (Eq. 2.1) to estimate the M/G block ratio, and a second equation (Eq. 2.2) to calculate the G block percentage contained in each alginate type. Method 2 applied the P/T ratios determined from the CD spectra to a correlation chart to estimate the M/G block ratio (Figure 3.6), and an equation (Eq. 2.3) was fitted to the linear portion of the correlation graph to calculate the G block percentage. The M/G ratio was back calculated by using an additional equation (Eq. 2.4). Method 3 did not involve the use of CD spectra but instead equated the M/G block ratio to the ratio of the normalized characteristic absorbance peaks at 1028 and 1100 $cm^{-1}$, that were observed by

using Fourier Transform Infrared, Attenuated Total Reflectance (FTIR-ATR) spectroscopy (Figure 3.7).

The following equations were employed to determine the %G block:

*Method 1: Empirical method*

Eq. 2.1  $\dfrac{M}{G} = 2.0 \times \left(\dfrac{P}{T}\right)$

Eq. 2.2  $\%G = \dfrac{1}{\left[\left(\dfrac{M}{G}\right) + 1\right]} \times 100\%$

*Method 2: Correlation chart*

Eq. 2.3  $\%G = 100\% - \left(\dfrac{\left(\dfrac{P}{T}\right) - 1.172}{3.364 \times 10^{-2}}\right)$  The linear correlation of P/T Ratio and G%.

Eq. 2.4  $\dfrac{M}{G} = \dfrac{100\%}{\%G} - 1$  Solving for the M/G Ratio.

*Method 3: Ratio of characteristic absorbance peaks.*

Eq. 2.5  $\dfrac{M}{G} = \dfrac{Absorbance_{@1100cm^{-1}}}{Absorbance_{@1028cm^{-1}}}$

Eq. 2.6  (Same as Eq. 2 from *Method 1*)

## 2.2.5.1 Circular Dichroism (CD) spectroscopy

Low viscosity (LV) and medium viscosity (MV) alginate (Sigma-Aldrich, St. Louis, Missouri) and Acros Organics (Acros-Organics; Fairlawn, New Jersey) alginate samples were prepared at 0.04% (weight of alginate/volume of distilled water). The alginate sodium salt granules were dissolved and thoroughly mixed

for 5 hours on a magnetic stir plate (Stirrer/Hot Plate; Corning, Corning, New York).

A standard rectangular measurement cuvette with a 20.00 mm pathlength (QS -20.00 mm; Starna Cells. Inc., Atascadero, California) was thoroughly rinsed with distilled water, dried, and filled to the measurement line with 3.5 mL of the prepared solutions. The cuvette was placed in the cuvette chamber of the circular dichroism spectrophotometer (J-810 Circular Dichroism System; JASCO, Easton, Maryland). The three alginate types were analyzed at scanning speeds of 20 nm/min and 100 nm/min from 250 nm to 195 nm (the spectrophotometer initiates at higher wavelengths and terminates at lower wavelengths). The data was exported from the Spectra Analysis® software to a Microsoft® Office Excel 2003 (Microsoft Corporation, Redmond, Washington) spreadsheet. The M/G block ratio was calculated as a ratio of the resulting height of the peak (P) to that of the trough depth (T), as shown below in Figure 2.2. The percentage of guluronic acid block (%G) was determined through a chart found in the literature[7] that correlated P/T ratios to %G ratios for common sources of alginates.
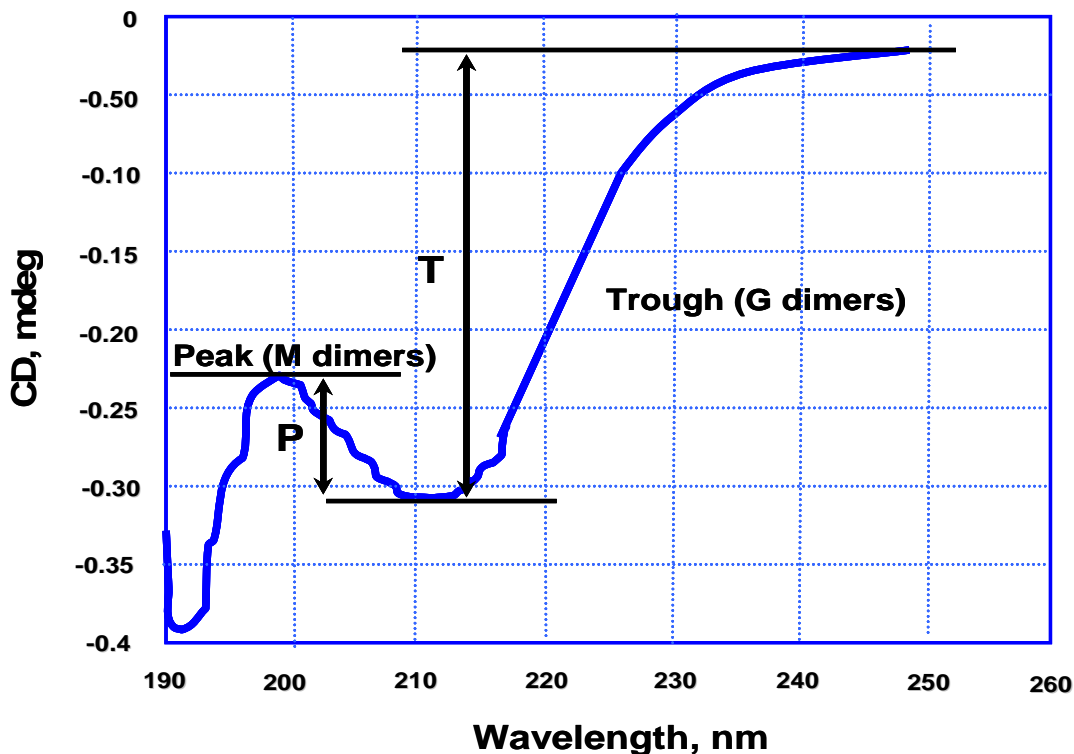
Figure 2.2: Typical CD spectra for Macrocystis pyrifera sodium alginate[8].

### 2.2.5.2 Fourier Transform Infrared Attenuated Total Reflectance (FTIR-ATR) spectroscopy

The FTIR-ATR technique has been used to analysis the chemical composition of polymers that are used in a wide variety of applications. ATR works by passing infrared radiation through an ATR crystal. The ATR crystal has a totally reflective surface and refines the infrared radiation into an evanescent wave of energy. When a sample is brought in contact with the surface of the ATR crystal, the wave attenuates in regions of the infrared spectrum where the sample absorbs energy. In the ATR spectra analysis, the energy absorption may appear as a combination of sharp or broad peaks, or as a combination of the two. There are a number of factors that affect the ATR analysis of a given sample. Amongst the these factors are the wavelength of the infrared radiation, refractive index of the ATR crystal material, depth of penetration of the evanescent wave

into the sample, thickness of the sample, and sample coverage on the ATR crystal.

The FTIR-ATR spectra were recorded using a Nicolet Magna 550 FTIR-spectrometer equipped with a single reflection diamond ATR system (Spectra-Tech Inc., Oak Ridge, Tennessee).  In order to minimize the potential combined effect of these factors, a sample was loaded to a glass region and pressed down to promote small sample thickness and even distribution over the entire surface of the ATR crystal.  All spectra analyses were performed twice, with a total of 32 scans each at a resolution of 4 cm$^{-1}$.

## 2.3 Cell culture

A mammary gland epithelial cell line labeled with green fluorescent protein (GFP), designated MAC-T-R was to study the cellular response to fibers developed by the two encapsulation methods.  The cells were cultured at passages 19 and 23 in roller bottles (850 cm$^2$, vented cap; Corning, Acton, Massachusetts) for 28 days.  These roller bottle cultures were incubated at 37°C and 5% $CO_2$ in a $CO_2$ controlled environment (Forma Reach-In $CO_2$ Incubator, Thermo Electron Corporation, Waltham, Massachusetts).  Each roller bottle contained 35 mL of Dulbecco's Modified Eagle's Medium (DMEM), supplemented with 10% (v/v) Fetal Bovine Serum (BioWhittaker; Walkersville, Maryland), 1% Antibiotic-Antimycotic (Invitrogen, Grand Island, New York), and 0.2% Fungizone (Invitrogen, Grand Island, New York). The bottles were rotated at 0.33 rpm using a roller culture apparatus (Wheaton, Millville, New Jersey).  The DMEM was changed every 5-7 days over the total culturing time.  During medium changes,

the cells in each roller bottle were rinsed with 10 mL of Phosphate Buffer Solution

(PBS) to remove any remaining supplemented DMEM.

## 2.4 Co-extrusion encapsulation procedure
### 2.4.1 Preparation and sterilization of alginate and calcium chloride solutions

Solutions of 90 mL and 500 mL 6 wt% (wt alg/wt distilled $H_2O$) medium

viscosity (MV) grade sodium alginate (Sigma, St. Louis, Missouri) were prepared

by using an overhead stirrer (IKA®-WERKE; Eurostar Digital, Wilmington, NC).

The distilled water was contained in Kimax® 200 mL and 1 L glass beakers

(Kimble Kontes, Vineland, New Jersey) and stirred at a speed of 1000 $min^{-1}$; the

sodium alginate powder was gently added to minimize aggregation. Once the

powder was added, the solution was stirred at a speed of 2000 $min^{-1}$ for 30

minutes at room temperature. The glass beakers containing the 6 wt% alginate

solution were loosely covered with aluminum foil and placed inside of an

autoclave-steam sterilizer (3870M Tuttnauer Autoclave-Steam Sterilizer;

Tuttnauer Co. Ltd, Islip, New York). The liquid sterilization cycle, which included

a 15 minute depressurizing cycle, was conducted at 121°C for 1 hour. The

beakers were tightly covered with aluminum foil before transferring the beakers

to a -20°C freezer for 1 hour to cool the solutions to room temperature. A sterile

spoon was used to stir 3 drops of water/propylene glycol based green food

coloring (Assorted Food Colors & Egg Dye; McCormick & Co. Inc., Hunt Valley,

Maryland) and 20 mL of supplemented DMEM into the 200 mL solution of MV

alginate so that the acellular control fibers would be easily identifiable after the

spinning process.

A 7 L solution of 15 wt% (wt CaCl2/wt distilled $H_2O$) $CaCl_2$ (Mallinckrodt & Baker Inc., Paris, Kentucky) was prepared by using an overhead stirrer (IKA®-WERKE; Eurostar Digital, Wilmington, NC). The distilled water was contained in a high density polyethylene 18.9L (5 gallons) bucket. The solution was stirred at a speed of 2000 $min^{-1}$ for 1 hour.

Three – 1000 mL glass media bottles were sterilized using a steam autoclave. The media bottles were attached to 1L, 0.22µm polyethersulfone (PES) bottle top-filters (Corning, Corning, New York) and used to collect the vacuum filtered 15 wt% $CaCl_2$. As per product manual, specifications an additional 0.22 µm filter mesh was added to the filter unit to extend the use of the unit. Three of the four units received an additional 0.22 µm filter mesh.

## 2.4.2 Preparation and sterilization of spinning equipment

A 16G injection needle (Becton Dickinson, Franklin Lakes, New Jersey) (EI#9) was modified by shortening the length of the needle to ¼ inches. As listed in Table 2.1, equipment items 2-9 were placed inside the 60 cm basin, as shown in Figure 2.3. The basin was sealed inside a 61 cm X 91.4 cm polyethylene autoclavable bag (VWR International, West Chester, Pennsylvania); and the equipment items were sterilized using an autoclave (3870M Tuttnauer Autoclave-Steam Sterilizer; Tuttnauer Co. Ltd, Islip (Hauppauge), New York) at 121°C for 30 minutes, followed by a 15 minute depressurization cycle. The 16G needles were washed with LYSOL® all purpose cleaner (Reckitt Benckiser Inc., Parsippany, New Jersey), rinsed with hot tap water, and disinfected with 70% ethanol (Table 2.1).

Table 2.1: Description of equipment items used during the co-extrusion experiment

| Equipment Item Number | Description of Equipment Item |
|---|---|
| 1 | 1-60 cm coagulation basin |
| 2 | 2-Teflon Rollers |
| 3 | 1-long handle gear key |
| 4 | 1- Assembled spinning apparatus |
| 5 | 1 spoon |
| 6 | 1-100 mL glass beaker |
| 7 | 2-500 mL glass beaker |
| 8 | Silicone tubing (0.062ID X 0.125OD X 0.032 WALL) |
| 9 | 1-16G injection needles (modified) |
| 10 | 2 - large metal stands with attachment grips |
| 11 | Chrome shaft air motor |
| 12 | Syringe pump |
| 13 | Wind-up roller |
| 14 | 2-1/2", 0-30psig pressure gauge |
| 15 | 2-1/2", 0-60psig pressure gauge |

Figure 2.3: Preparation for the sterilization of the equipment items. Equipment items used in the alginate fiber spinning process were cleaned with LYSOL® All Purpose Cleaner, dried, sprayed with 70% ethanol, and placed inside a pre-cleaned basin.

The modified lab cabinet (Class II Biological Safety Cabinet; The Baker Co., Sanford, Maine) was cleaned with Naval Jelly® rust dissolver/protector (Naval Jelly Co., Inc., Kansas City, Missouri). The lab cabinet was then sprayed with a solution of 70% ethanol. The lab bench was aligned with a double layer of white, cross-linked, polyethylene bench paper (Clean Sheets Bench and Shelf Liners; VWR International, West Chester, Pennsylvania). The plastic tubing modifications (VWR International, West Chester, Pennsylvania), pressure indicators (Cole-Palmer, Vernon Hills, Illinois), syringe pump (kdScientific, New Hope, Pennsylvania), and air motor (Series M-00X; Ingersoll-Rand, Southern

Pines, North Carolina) were cleaned with 70% ethanol and set up in the lab cabinet. The lab cabinet was then sterilized with ultraviolet (UV) light for 1 hour.

The autoclave bag that contained the 60 cm basin was placed inside the lab cabinet. The equipment items were removed from the basin and placed to the side in the lab cabinet. The polyethylene wind-up roller (Memorex Products, Inc., Cerritos, California) (E#12) was sterilized with 100 % ethanol and set up in the lab cabinet. The long handle gear key (EI#3) was used to tighten the wind-up roller onto the air motor. The sterilized pre-assembled spinning apparatus (Figure 2.4), was setup inside of the lab cabinet securing the silicon tubing (EI #8) to the coagulant injection pin and to the modified 16G injection needle with copper wire (VWR International, West Chester, Pennsylvania). The basin (EI#1) was filled with 6 L of sterile 15 wt% $CaCl_2$. The colored MV alginate solution was poured into the pot of the spinning apparatus and the top of the spinning apparatus was replaced and tightened. The nitrogen supply line was connected to the spinning apparatus. The air gap, or the height of the spinning apparatus from the surface of the $CaCl_2$ solution in the basin, was adjusted to 25 mm by using the adjustable clamp on the metal stands to reposition the spinning apparatus.
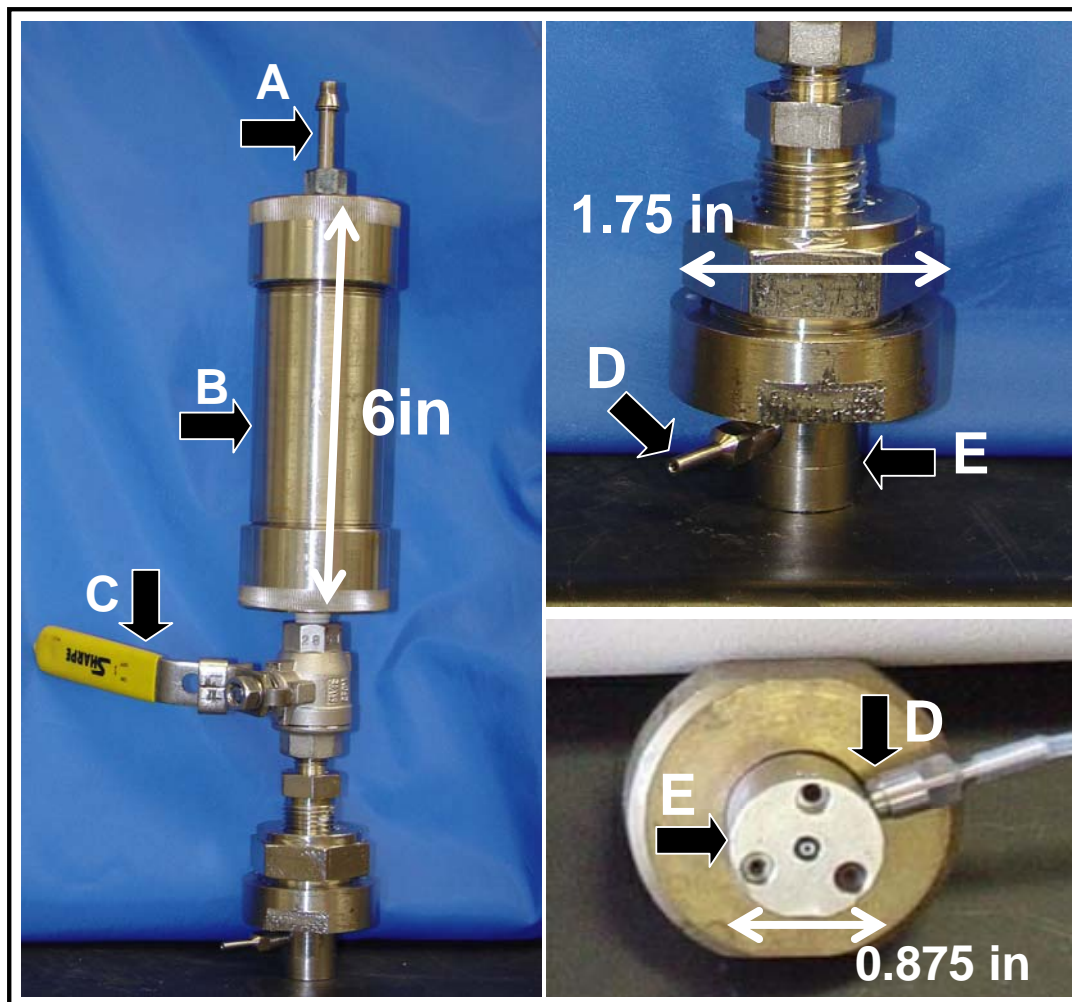
Figure 2.4: The fully assembled stainless steel (316) spinning apparatus. The spinning apparatus features a nitrogen inlet line (A), 200 mL polymer loading chamber (B), ball valve equipped (shown in the fully close position) with a safety pin (C), coagulant or additive injection pin (D), and spinneret pack (E).

### 2.4.3 Co-extrusion encapsulation procedure

The acellular hollow fibers (control) were spun under the constant conditions shown in Table 2.2. As the nascent filament was extruded, it was guided through the 15 wt% CaCl$_2$ coagulation bath to the wind-up roller. Once a steady alginate extrusion was established, the Telfon rollers were added to the bath to keep the fiber submerged in the bath as coagulant was pumped through the lumen of the fiber. One roller was placed so that the nascent filament would

be guided perpendicularly through the bath to the extrusion axis.  These acellular fibers served as the controls for the experiment.

To make the cellular fibers, 10 mL of supplemented Dulbecco's Modified Eagle's Medium (DMEM) solution (Gibco Invitrogen Corporation, Grand Island, New York) containing $3.2 \times 10^9$ MAC-T cells was prepared.  The cell suspension was pipetted (VWR International, West Chester, Pennsylvania) into the 90 mL solution of sterile MV alginate, decreasing the cell concentration to the desired density of $3.2 \times 10^6$ cells / mL of sodium alginate + supplemented DMEM.  A sterile spoon was used to thoroughly distribute the cells throughout the alginate.  The even distribution was confirmed by adding 2 mL of the cell/alginate precursor solution to a 6-well plate and viewing the distribution through a blue fluorescent filter and microscope at 25x total magnification.

A volume of 100 mL of the colored alginate solution was added to the spinning solution and used as a primer solution to establish the spinning conditions listed in Table 2.2.  A volume of 80 mL of the cell/alginate precursor solution was poured into the spinning pot.  The top of the spinning apparatus and the nitrogen supply line was replaced and tightened.  The air gap, or the height of the spinning apparatus from the surface of the $CaCl_2$ solution in the basin, was re-adjusted to 7.5 cm by using the adjustable clamp on the metal stands to reposition the spinning apparatus.  The hollow fibers were spun under the constant conditions shown in Table 2.2.

Table 2.2: Description of constant spinning parameters used in the co-extrusion encapsulation method

| Spinning Parameter | Description |
|---|---|
| * Spinneret Size | : 4 mm OD 1 mm ID, 2 mm OD capillary tube |
| * Extrusion Nitrogen Pressure | : 4.5 ±1 psig |
| * Air Gap between Spinneret and Coagulant Bath | : 25 mm |
| * Room Temperature | : 23°C, 30% humidity |
| * Coagulant Bath Length | : 60 cm |
| * Coagulant Concentration | : 15% CaCl2 |
| * Coagulant Injection Rate | : 15 mL/min |
| * Wind-up Roller Pressure | : 14 ±5 psig |
| * Fiber storage | : 15% CaCl2 |

The fibers were removed from the 15% $CaCl_2$ solution and cut into 1 - inch sections with a sterile razor blade (VWR International, West Chester, Pennsylvania). Each completed fiber was placed into a well of a labeled 6-well plate that contained 5 mL of supplemented DMEM, the composition of which is specified in section 2.3 of this thesis. The acellular and cellular fibers were incubated at 37°C and 5% $CO_2$.

A fiber section was cut in half and used for wet dimensional analysis. The wet ½ inch section was placed upright onto a microscope slide (Colorfrost microslide; VWR International, West Chester, Pennsylvania). A microphotograph was made using an inverted microscope and ProgRes CaptureBasic© software. Measurements of the fiber diameter and wall thickness were made with Image-Pro Plus© software (Media Cybernetics, Inc., Silver Spring, Maryland).

## 2.5 Manual injection encapsulation procedure
## 2.5.1 Preparation and sterilization of alginate and calcium chloride solutions

A 100 mL stock solution of 0.74 wt% (wt alg/wt distilled $H_2O$) LV alginate (Sigma, St. Louis, Missouri) was prepared using a stir bar (cylindrical, 1-inch length, Fisher, Fair Lawn, New Jersey) and magnetic stir plate (Corning, Acton, Massachusetts).  The distilled water was contained in a plastic 100 mL specimen cup and stir bar at a setting of 5 for 1 hour.  The 0.74 wt% alginate solution was sterilized by using a 0.2 µm sterile 100 mL polyethersulfone (PES) filter unit (Corning, Corning, New York).  The remainder of the alginate and calcium chloride solutions were prepared and sterilized as per section 2.4.1 of this thesis.

## 2.5.2 Preparation and sterilization of spinning equipment

The spinning equipment was prepared and sterilized as per section 2.4.2. The hollow fibers were spun under the constant conditions shown in Table 2.3.

Table 2.3: Description of constant spinning parameters used in the manual injection encapsulation method

| Spinning Parameter | Description |
|---|---|
| * Spinneret Size | : 4 mm OD 1 mm ID, 2 mm OD capillary tube |
| * Extrusion Nitrogen Pressure | : 5± 0.45 psi |
| * Air Gap between Spinneret and Coagulant Bath | : 25 mm |
| * Room Temperature | : 25 °C, 80% humidity |
| * Coagulant Bath Length | : 60 cm |
| * Coagulant Concentration | : 15% CaCl2 |
| * Coagulant Injection Rate | : 10 mL/min |
| * Fiber storage | : 15% CaCl2 |

## 2.5.3 Manual injection encapsulation procedure

The fibers were removed from the 15% $CaCl_2$ solution and cut into 1-inch sections.  Curved sections were excluded to minimize fiber puncturing by the tip

of the injection needle tip. The experiment setup for the manual injection encapsulation is shown in Figure 2.5. The excess solution found in the lumen of the hollow fiber was aspirated using a sterile glass pipette (Fisher Scientific, Pittsburg, Pennsylvania). The prepared 1-inch sections were placed in a sterile 200 mL storage container filled with 15% $CaCl_2$ solution.
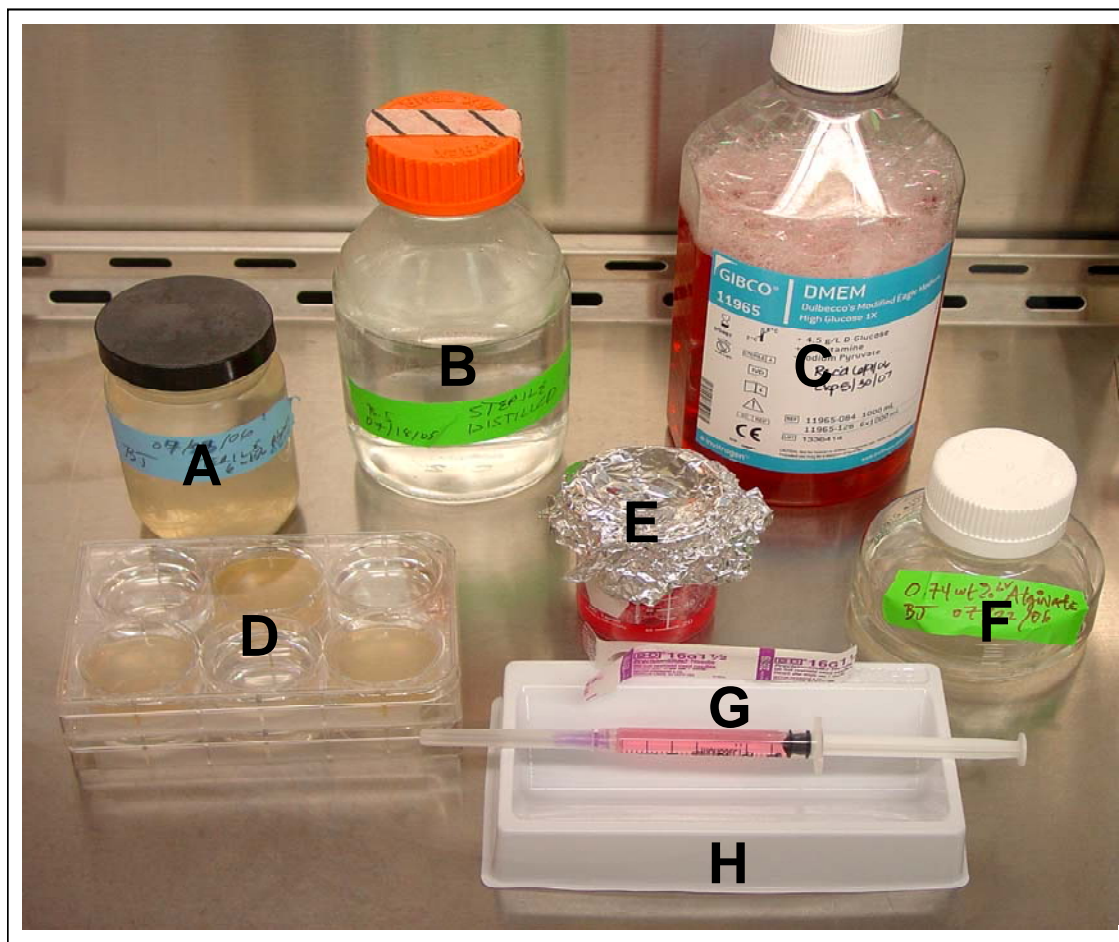


Figure 2.5: The experimental setup for the manual injection process. The items used in the manual injection process included 1-inch hollow fiber sections stored in 15 wt% $CaCl_2$ solution (A), sterile distilled water (B), supplemented DMEM (C), fiber end capping stations (D), a stock cell solution of 3.0 X $10^6$ cells/mL DMEM+0.74 wt% LV alginate (E), a stock solution of sterile 0.74 wt% LV alginate (F), a syringe loaded with the stock cell solution (G), an incubation tray (H), and a stock solution of 15 wt% $CaCl_2$ (not pictured).

Two 6-well plates (Corning, Corning, New York) were prepared by adding volumes 10 mL of filter sterilized 15 wt% $CaCl_2$ solution and autoclaved 0.74 wt% sodium alginate to alternating wells of the plates, as shown in Figure 2.6.
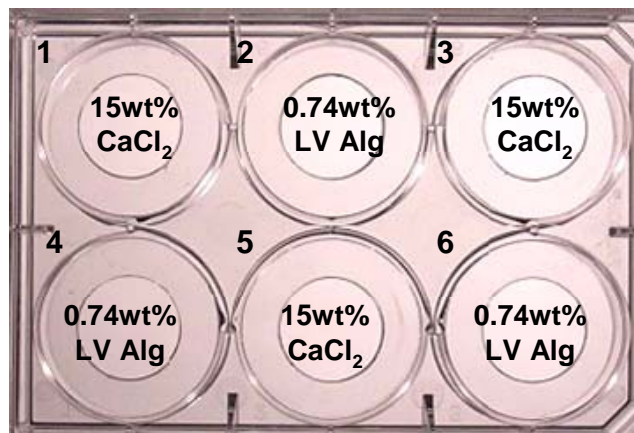


Figure 2.6: A 6-well plate served as the fiber capping station. The numbers indicted denote the order in which the fibers were dipped. Step 1 was repeated again for Step 7.

A 2 mL supplemented Dulbecco's Modified Eagle's Medium (DMEM) solution (Gibco Invitrogen Corporation, Grand Island, New York) containing 6.4 X $10^6$ MAC-T cells was prepared and pipetted (VWR International, West Chester, Pennsylvania) into an autoclaved Kimax® 10 mL beaker (Kimble Kontes, Vineland, New Jersey). A 2.1 mL aliquot of filter sterilized 0.74 wt% LV alginate was then added to the 10 mL beaker, decreasing the cell concentration to the desired density of 3.0 X $10^6$ cells / mL of sodium alginate + supplemented DMEM. The cell/alginate stock solution was thoroughly mixed using an autoclaved sterilized spoon (EI#5). The stock solution was drawn into a sterile Luer Lock 3 cc syringe (Tyco Healthcare, Mansfield, Massachusetts) and an unmodified 16G 1 ½ injection needle was attached to the syringe and capped.

A fiber was removed from the distilled water using sterile tweezers. The syringe unit was agitated manually to ensure the even distribution of the cells throughout the solution. When the cell/alginate stock solution was injected into the fiber, the needle was inserted to half the length of the fiber and, as the lumen was filled, the needle tip was slowly moved toward the entrance end of the hollow fiber. Each end of the fiber was hand-dipped three times into each well of the fiber capping 6-well plate at an approximate 45° angle, facilitating the production of a hollow fiber with bulbed ends. Each bulbed fiber was placed into a well of a second 6-well plate that contained 5 mL of 15 wt% $CaCl_2$ for 1 hour to gel the internal suspension matrix of LV alginate. Each fiber was gently rinsed with filter sterilized distilled water to remove trace amounts of $CaCl_2$ solution.

The controls for this study consisted of 10 acellular fibers that were made by injecting filter sterilized 0.74 wt% LV alginate into the lumens of the fibers, capping the fiber ends and gelling the fiber internal suspension matrices in the manner specified previously. Each completed fiber was placed into a well of a labeled 6-well plate that contained 5 mL of supplemented DMEM, the composition of which is specified in the Cell Culture section of the Methods section of this thesis. The acellular and cellular fibers were at 37°C and 5% $CO_2$. A fiber section was cut in half and used for wet dimensional analysis, as per section 2.4.3 of this thesis.

## 2.6 Cell response
### 2.6.1 Validating the expression of green fluorescent protein (GFP)

Green fluorescent protein (GFP) is a 27-kD monomer consisting of 238 amino acids. Labeling cells with GFP is a versatile tool for studying gene

expression in mammalian cells. GFP can be monitored in living cells[9-11]. It is superior to other biolumininiscent reporter assays, such as Live/Dead, that require the co-incubation of cells with substrates or co-factors to emit light.

GFP expression was examined using the blue fluorescent filter on an inverted fluorescent microscope (Carl Zeiss MicroImaging, Inc., Thornwood, New York) at 25X total magnification on days 1, 5, 7, 10, 14, 18, and 21 of the study.

## 2.6.2 Lactic acid and glucose measurement

Single aliquots of 1 mL were pipetted into micro-centrifuge tubes (VWR International, West Chester, Pennsylvania) and collected from six sample wells and three control wells. Also, a 1 mL aliquot was collected from a stock solution of supplemented DMEM at each time point before a media change occurred, in order to quantify the MAC-T production of lactic acid and consumption of glucose. From these measurements, the amount of alginate dissolution that occurred throughout the study was calculated. The measurements were completed using a bioanalyzer (YSI, Yellow Springs, Ohio). The bioanalyzer uses a three filter layer + platinum electrode system to quantify each of the analytes. The filter layers are comprised of a polycarbonate layer, immobilized enzyme layer, and cellulose acetate layer. The enzyme filter layer contains glucose oxidase and L-lactate oxidase. These enzymes oxidize glucose and lactic acid molecules into D-glucono-$\delta$-lactone + hydrogen peroxide ($H_2O_2$) and pyruvate + hydrogen peroxide ($H_2O_2$), respectively. The hydrogen peroxide is further oxidized and produces a stream of electrons. These electrons are

amplified and conditioned as a current.  The current is compared to the calibration current and a glucose and lactic acid concentration is assigned.

## 2.6.3 Alamar Blue reduction assay

Metabolic activity of the viable encapsulated cells was measured using alamarBlue™ Reduction Assay (Invitrogen, Carlsbad, California).  The assay reagent can be reduced intracellularly by accepting electrons from hydrogen molecules that are present in higher quantities during cellular respiration and glucose metabolism.  Upon reduction, alamarBlue changes from an oxidized indigio blue, non-fluorescing state, to a reduced pink fluorescent state.  The major difference between the MTT assay and alamarBlue™ is that alamarBlue™ does not lead to cell death[12].  The cell metabolic activity can be then be correlated and monitored spectrophotometrically either by color measurement or fluorescence.

A volume of 400μL of the alamarBlue assay was pipetted into one well that contained an acellular control fiber surrounded by 4 mL of supplemented DMEM and into three wells that each contained a cellular fiber for each time point.  The well plates containing the assay were incubated at 37°C and 5%$CO_2$ for 4 hours.  The assay/medium solution in each well was mixed by pipetting the solution from the well into a 3 mL sterile syringe (Tyco Healthcare Group, LP, Mansfield, Massachusetts) and back into the well three times.  A volume of 3 mL of the assay/medium solution was transferred to a well of a 24-well plate, where the mixing procedure was repeated.  After emptying the syringe into the well plate for the third time, the syringe was filled with 3 mL of the mixture.  A 0.2 μm,

25 mm Telfon syringe filter (Fisher, Fair Lawn, New Jersey) was attached to the syringe tip. Wetting the syringe filter required 0.4 mL of solution. A 1mL volume of the mixture was added at a slow and constant rate to another well of the 24-well plate. Aliquots of 100 µL of the filtered solution were pipetted into wells on a polystyrene 96-well plate (Corning, Corning, New York) in triplicate. This procedure was used for the assay/medium solution that surrounded the acellular and cellular fibers on days 1, 7, 10, 14, 18 and 21. The 96-well plate was inserted into the plate reader of a spectrophotometer (Fluoroskan Ascent FL; Thermo Electron Inc., Milford, Massachusetts) and the fluorescence from the alamarBlue reduction was measured using the Ascent© software version 2.4.2 (Fluoroskan Ascent FL; Thermo Electron Inc., Milford, Massachusetts) at a filter pair wavelength of 544 (excitation) and 590 nm (emission).

**2.6.4 Alginate cellular fiber dissolution/cell counting**

The feasibility of the two cell encapsulation methods was studied by observing the change in cell number during 21 days. At days 1, 7, 14, and 21, the alginate fiber was dissolved by removing the fibers from cell culture, removing excess DMEM remaining in the lumen of the fiber, and exposing the fibers to Dulbecco's Phosphate Buffered Saline (Sigma-Aldrich, St. Louis, MO) in washing wells for 10 minutes (co-extruded fibers) and 12 minutes (manual injected fibers), as shown in Figure 2.7. After swelling and softening, each fiber was transferred into a 1.5 mL micro centrifuge tube (VWR International, West Chester, PA). Volumes of 1.5 mL of 55 mM sodium citrate (Fisher Scientific Company, Fair Lawn, New Jersey) were pipetted into each centrifuge tube. The centrifuge tubes were placed in a preheated vacuum oven (National Appliance

Company, Winchester, Virginia) at 45°C ± 2°C for 45 minutes. This temperature was reached using an oven temperature setting of 1.3. After 45 minutes had passed, the tubes were checked for near total fiber dissolution. The tubes were replaced in the oven for additional dissolution time, as needed. A 101-1000 μL sized pipette tip (Fisher Scientific Company, Fair Lawn, New Jersey) and a pipetter (Eppendorf; VWR International, Wester Chester, PA) was used to mix the contents of the tube in 500 μL increments. Maintaining the pipette tip at the 0.5 mL marker, a 1-100 μL pipette tip (Fisher Scientific Company, Fair Lawn, New Jersey) and pipetter (Fisher Scientific Company, Fair Lawn, New Jersey) were used to pipette 20 μL of the mixed cell solution into a new 1.5 mL micro centrifuge tube. A 1-100 μL pipette tip was used to add 20 μL of Modified Trypan Blue cell viability assay solution (MP Biomedicals, Inc, Solon, Ohio) to the cell solution. The cell suspension and assay solution were mixed by triturating three times. Placing the pipette tip at the bottom of the centrifuge tube, 20 μL of mixture were transferred to a hemacytometer (Fisher Scientific Company, St. Louis, Missouri), and the cells were counted at a total magnification of 100 X on an inverted light microscope (Carl Zeiss MicroImaging, Inc., Thornwood, New York).

Top view of the fiber washing 6 – well plate

10mLs of PBS per well.

Side view of the fiber washing 6 – well plate
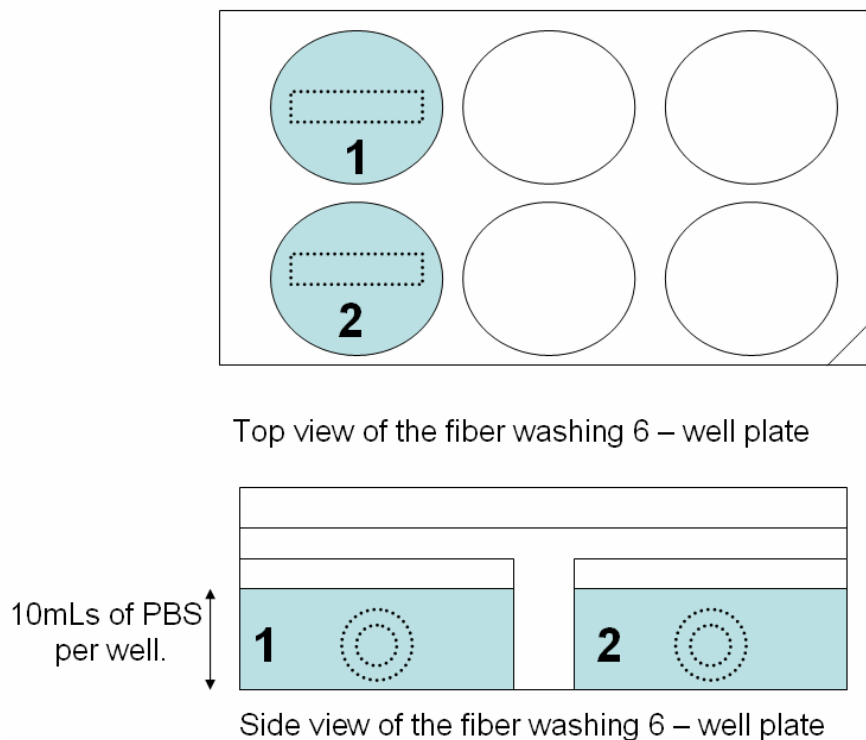
Figure 2.7: Fibers were soaked in a PBS bath to initialize the alginate dissolution process for 10 – 12 minutes. The PBS bath swelled the fibers and decreased their mechanical integrity by replacing the calcium crosslinking cations with sodium cations.

## 2.7 Histology
## 2.7.1 Hollow fiber embedding

A single hollow fiber was embedding into a glycol methacrylate (GMA) (Technovit 7100: GMA Embedding Agent; EB Sciences, East Granby, Connecticut) matrix using the experimental design and corresponding GMA embedding procedure, as shown in Figure 2.8 and Table 2.4, respectively. Steps 1 & 2 were conducted to fix the cells and preserve the fiber morphology. Steps 3 – 12 were implemented to infiltrate the fiber with GMA in a stepwise manner. Steps 13 & 14 were employed to embed the fiber into liquid GMA solution, which was allowed 48 hours to polymerize. Volumes of 10 mL volumes were used in Steps 1 - 12. Six well plates with ¼ -inch stir bars in each well served as

infiltration stations and were placed on a Corning Stirrer/Hot Plate as specified in Figure 2.8. The experiment was conducted at ambient temperature, 22°C, without vacuum.

The procedure was adapted from a previously described GMA embedding technique for alginate based beads[13].  The normal two hours fixation time was decreased to 5 minutes because it was noted that the 10% Neutral Buffered Formalin (NBF) caused the fiber to swell. An additional step (Step 2) was used to dehydrate and preserve the fiber morphology by removing the majority of water from the fiber. "Solution A" that was used in step 13 was twice the concentration found in previously described methods from our lab. The hardener concentration was increased to improve the durability of the fiber throughout the rigorous staining procedure.

Table 2.4: Glycol methacrylate embedding procedure

| Step | Time | |
|---|---|---|
| | min | Solution |
| 1 | 2 | 10% NBF |
| 2 | 5 | 100 % ethanol |
| 3 | 5 | 10% GMA |
| 4 | 5 | 20% GMA |
| 5 | 5 | 30% GMA |
| 6 | 5 | 40% GMA |
| 7 | 5 | 50% GMA |
| 8 | 5 | 60% GMA |
| 9 | 5 | 70% GMA |
| 10 | 5 | 80% GMA |
| 11 | 5 | 90% GMA |
| 12 | 15 | 100 % GMA |
| 13 | 15 | 0.02%(w/v) Solution A (0.06g of Hardener 1 + 3 mL of 100% GMA) |
| 14 | 5 | 15 to 1 solution of Solution A to Hardener II |
| Total time | 87 | |
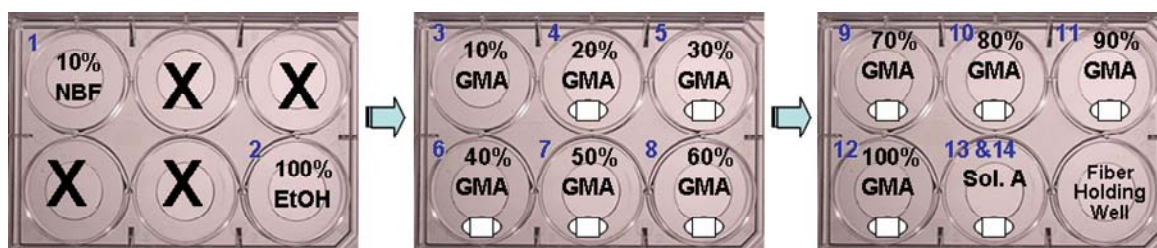


Figure 2.8: GMA embedding protocol.

## 2.7.2 Centrifuge tube sectioning

The GMA solution completely polymerized after 48 hours in a micro centrifuge tube. The centrifuge tube was cut into three cylindrical sections using an automatic band saw (Delta International Machinery Corporation, Pittsburgh, PA), which yielded a cylindrical block of interest for further histological analysis.

The plastic from the centrifuge tube was cut and removed using a single edge No. 12 industrial razor blade (VWR Scientific, Media, PA). A micrograph was taken of the cross section of one of the fiber sections.

### 2.7.3 Micro-sectioning

Using a microtome (Leica RM 2155, Leica Microsystems, Germany), 30 micron sections were obtained from the fiber block. To uncurl the sections, the sections were floated on the surface of a water bath at 35 - 37°C. The sections were retrieved from the water bath on glass microscope slides. The slides were transferred onto a flat plate dryer to remove excess water. After drying, a slide was selected for high magnification light microscopy. A drop of mineral oil and a coverslip was added to each slide in order to improve viewing quality.

### 2.7.4 Toluidine blue dying method

A volume of 0.5 – 1 mL 95% ethanol was pipetted onto the fiber cross section. Toluidine Blue was pipetted on the cross section on the glass microscope slide and left for 5 minutes. Excess dye was removed from the microscope after 2.5 minutes by gently tapping the side of the microscope slide on absorbent gauze. The slide was then rinsed in a gentle flow of distilled water to clarify the stain, as needed. Additional 95% ethanol was applied to the cross section to further distinguish the pink staining alginate from the blue staining cells. A temporary coverslip was added to one slide by using a non-sterile 1 mL pipetter to apply a drop of water after the cross section was dyed, clarified, and sprayed with ethanol.

### 2.7.5 Cell area and axial dimension analysis

Alginate fibers were embedded into glycol methacrylate (GMA) on Days 1, 7, 14 and 21. Sections of these fibers were stained using toludiene blue. An inverted microscope (Axioskop 2 Plus; Car Zeiss MicroImaging, Inc., Thornwood, New York) and software (SPOT© Version 3.5.9 for Windows; Diagnostic Instruments, Inc., Sterling Heights, Michigan) were used to create microphotographs of the stained sections at total magnifications of 100 and 200X. Axial measurements of 20 randomly selected encapsulated cells were measured on each micrograph using the Image-Pro© 5.1 software (MediaCybernetics, Silver Spring, Maryland). The x and y axis was assigned as the shortest and longest axis of the oval shaped cells. These axial measurements were converted into a Y/X ratio as an indication of diameter and implemented into the calculation of cell area using elliptical geometry (Cell Area = $\pi * 0.25 * x * y$).

### 2.8 Statistical analysis

Statistical analysis was conducted using a two-factor with replication ANOVA test in Microsoft Excel© for the C/A ratio and cell number data sets, whereas a one-factor ANOVA test was used to conduct statistical analyses on the Y/X ratio, cell area, and daily MAC-T lactic acid production and glucose consumption data sets. A Fisher's Least Significant Difference (LSD) calculation was made to supplement the ANOVA tests in which there was sufficient evidence (i.e $p < 0.05$ or F>Fcrit) to reject the null hypothesis of equal means with a 95% confidence level. Box and whisker plots were created in Microsoft Excel© to

show the dispersion and variability of those data sets in which there was sufficient evidence (i.e. $p > 0.05$ or $F < Fcrit$) to accept the null hypothesis of equal means with 95% confidence.

References

1.      Smidsrod, O. Solution properties of alginate. Carbohydrate Research 1970;13(3).

2.      Mancini, M., Moresi, M., and Sappino, F. Rheological behaviour of aqueous dispersions of algal sodium alginates. Journal of Food Engineering 1996;28(3-4):283-295.

3.      Banks, T. and Alcorn, D. Mathematics for AQA GCSE higher tier.: Causeway Press Ltd 2001.

4.      Mcclave, J.T. and Benson, P.G. A first course in business statistics. Prentice Hall International 1995.

5.      Oakshott, L. Essential elements of business statistics. DP Publications Ltd 1994.

6.      Ott, R.L. and Longnecker, M.T. An introduction to statistical methods and data analysis (hardcover). Duxbury Press 2001.

7.      Morris, E.R., Rees, D.A., Sanderson, G.R., and Thom, D. Conformation and circular dichroism of uronic acid residues in glycosides and polysaccharides. Journal of the Chemical Society-Perkin Transactions 2 1975:1418-1425.

8.    Joon, H. and Mooney, D.J. Typical CD spectra for macrocystis pyrifera sodium alginate. Jones W, editor; 2005.

9.    Baumstark-Khan, C., Palm, M., Wehner, J., Okabe, M., Ikawa, M., and Horneck, G. Green fluorescent protein (GFP) as a marker for cell viability after UV irradiation. Journal of Fluorescence 1999;9(1):37-43.

10.   Landry, S., Mcghee, P.L., Girardin, R.J., and Keeler, W.J. Monitoring live cell viability: Comparative study of fluorescence, oblique incidence reflection and phase contrast microscopy imaging techniques. Optics Express 2004;12(23):5754-5759.

11.   Yuk, I.H.Y., Wildt, S., Jolicoeur, M., Wang, D.I.C., and Stephanopoulos, G. A GFP-based screen for growth-arrested, recombinant protein-producing cells. Biotechnology and Bioengineering 2002;79(1):74-82.

12.   Gloeckner, H., Jonuleit, T., and Lemke, H.D. Monitoring of cell viability and cell growth in a hollow-fiber bioreactor by use of the dye alamar blue. Journal of Immunological Methods 2001;252(1-2):131-138.

13.   James, R. Thesis: Development of porous 3-D micro-bead scaffolds using alginate for tissue engineering applications. Clemson, SC: Clemson University; 2003.

# CHAPTER THREE

# RESULTS

## 3.1 Sodium alginate solution properties
## 3.1.1 Molecular weight distribution

A linear trend-line was fitted to the inherent viscosity plot for each alginate type.  It was observed that as the sodium alginate concentration approaches zero the AO and LV alginates approaches the same intrinsic viscosity value, as shown in Figure 3.1.  The MV alginate however has an intrinsic viscosity that is twice as much as the other two alginate types.  The inherent viscosity plot and intrinsic viscosities per alginate type obtained at a shear rate of 38.6 $sec^{-1}$ are given below in Figure 3.1 and Table 3.1, respectively.

Also, it was determined that the calculation of the viscosity average molecular weight is dependent upon the shear rate at which the apparent viscosity is assessed.  A median molecular weight was calculated from the molecular weight distribution (Figure 3.2 and Table 3.2).  It was determined that MV sodium alginate has the greatest median molecular weight value (284 kDa), followed by AO sodium alginate (212 kDa), and LV sodium alginate (187 kDa).

**Inherent Viscosity of Sodium Alginate at 38.6 s$^{-1}$**
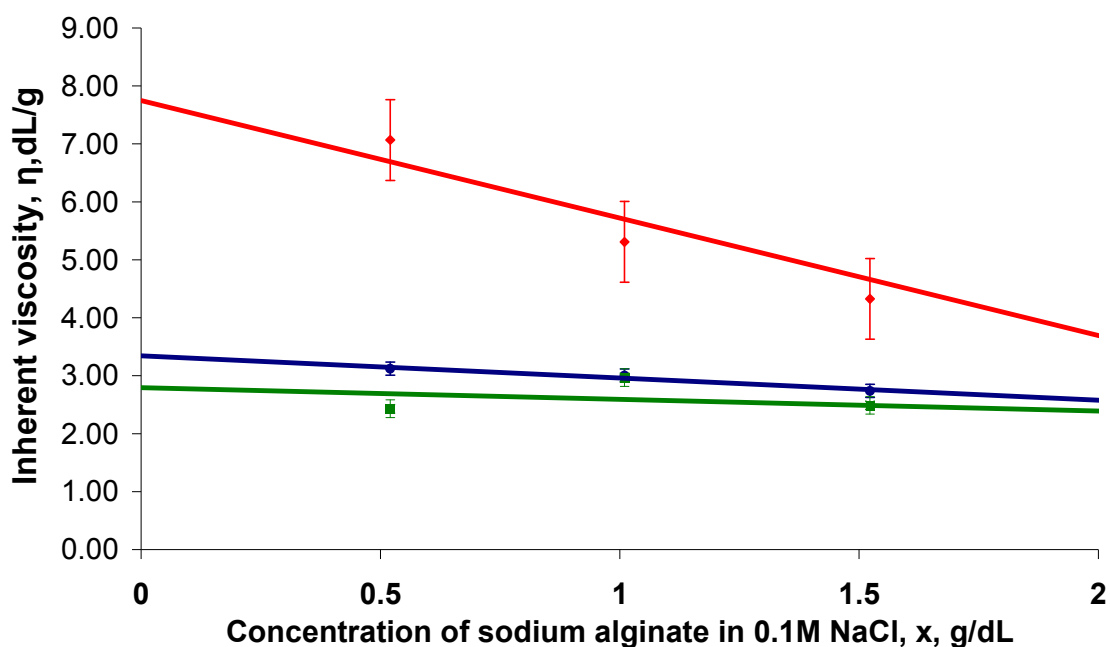


Figure 3.1: Inherent viscosity of sodium alginate at a shear rate of 38.6 sec$^{-1}$. This figure depicts the inherent viscosity results for the three alginate types: MV (▲), AO (●) and LV (■).  The error bars indicate the standard error.

Table 3.1: Intrinsic viscosity and viscosity average molecular weight data per alginate type at a shear rate of 38.6 sec$^{-1}$

|  | Intrinsic viscosity | Molecular weight |
|---|---|---|
|  | η | MW |
| **Alginate type** | **dL/g** | **kDa** |
| **MV** | 7.74 | 387 |
| **AO** | 3.34 | 167 |
| **LV** | 2.79 | 140 |

**Sodium Alginate Molecular Weight Distribution**
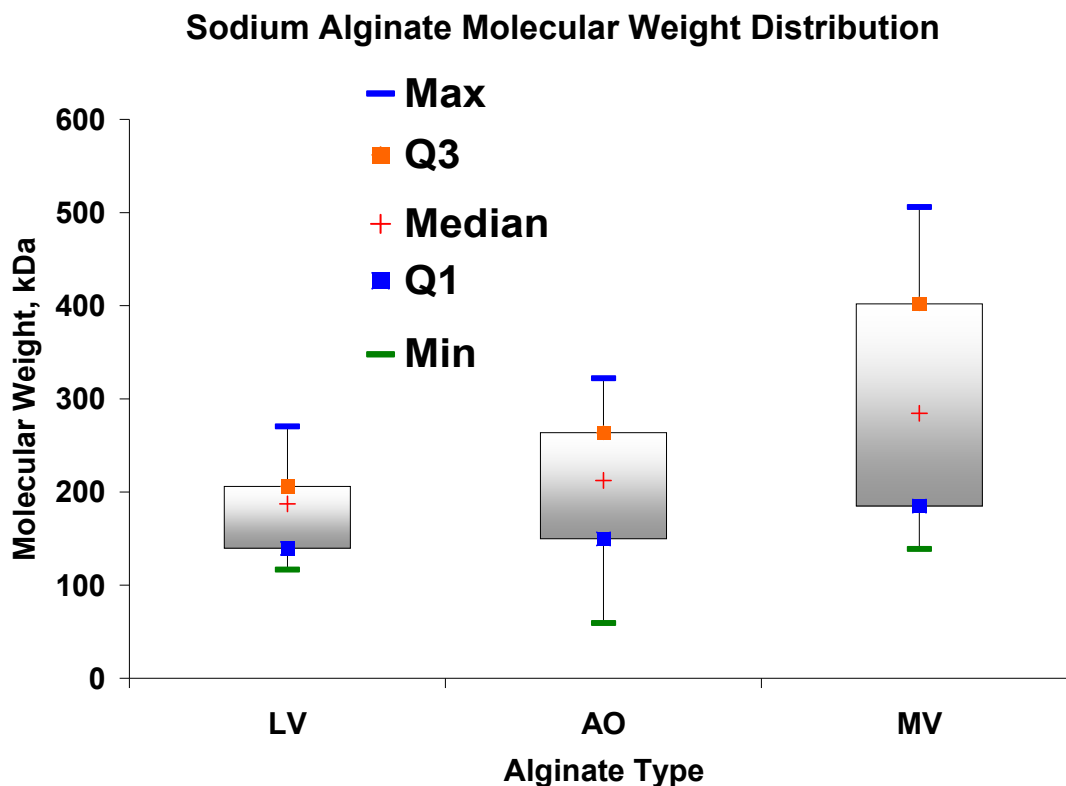


Figure 3.2: A box and whisker plot for the sodium alginate molecular weight distribution.

Table 3.2: Statistical analysis of sodium alginate molecular weight distribution

|  | LV | AO | MV |
|---|---|---|---|
|  | MW | MW | MW |
| **Statistic** | kDa | kDa | kDa |
| **Max** | 270 | 322 | 506 |
| **Q3** | 206 | 264 | 402 |
| **Median** | 187 | 212 | 284 |
| **Q1** | 140 | 150 | 185 |
| **Min** | 117 | 59 | 139 |
| **Coefficient of Variation, %** | 30 | 46 | 46 |

### 3.1.2 Viscosity profile of three alginate types

A viscosity – concentration profile of low (LV), medium (MV) and Acros Organics (AO) viscosity grades of sodium alginate was created by plotting the apparent viscosity as a function of the concentration of the sodium alginate at a

shear rate of 100 s$^{-1}$ (Figure 3.3). It was observed that the apparent viscosity of sodium alginate increases exponentially as the concentration of sodium alginate increases. The exponential behavior is typical for non-Newtonian, pseudo-plastic fluids and is best described as a power law function. The empirical equations that describe the relationship between apparent viscosity in centiPoise (y) and alginate concentration in weight percentages (for MV, AO, and LV viscosity grades are y = 152.66x$^{2.577}$, R$^2$ = 0.9874; y = 28.524x$^{3.0578}$, R$^2$ = 0.9974; and, y = 18.405x$^{2.6745}$, R$^2$ = 0.9901, respectively. It is important to note that these equations are simplified in that they do not include the apparent viscosity of DD water at 25 °C (0.89 cP), which is negligible in comparison to the viscosity of concentrated sodium alginate solutions. The viscosity profile of the three alginate types shows that at 6 wt% MV has an apparent viscosity of 15,000 cP. It was at this viscosity that the optimal fiber spinnability occurred using the motor powered extrusion system. Comparatively, the apparent viscosities of AO and low viscosity LV alginate at a concentration of 6 wt%, are approximately 6800 and 2200 cP, respectively. A summary of the measured apparent viscosity at 2 % has been noted and compared to literature value data (Table 3.3). Creating the viscosity profile facilitated the visualization of the dependency of sodium alginate on concentration and shear rate, as shown in Figure 3.4.
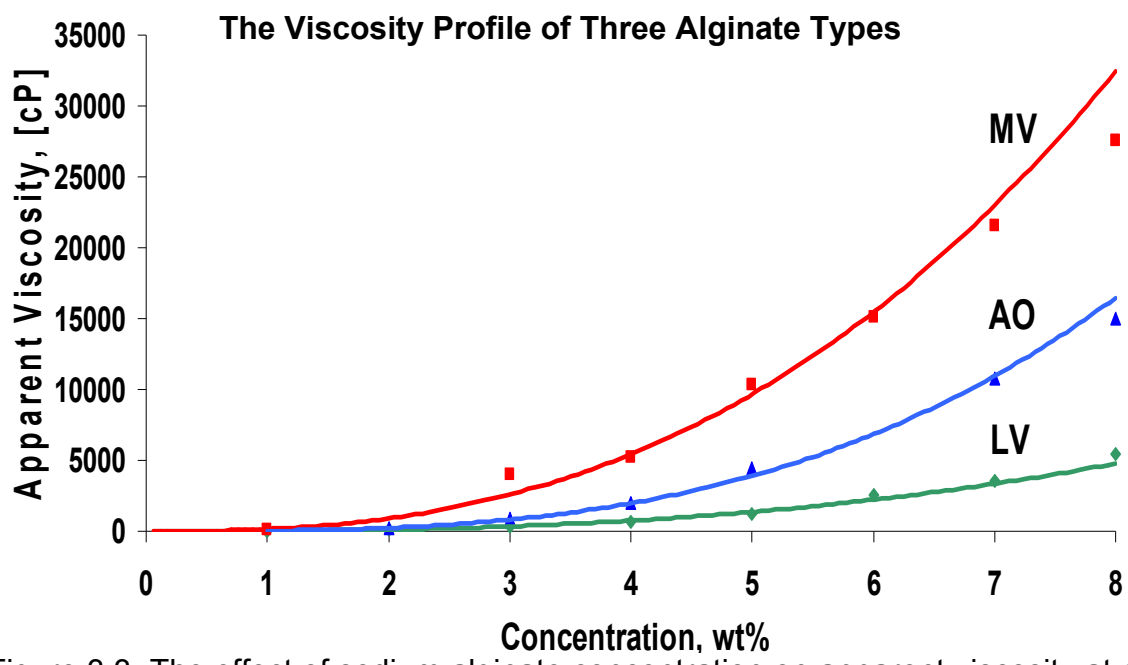
Figure 3.3: The effect of sodium alginate concentration on apparent viscosity at a shear rate of 100 $s^{-1}$.

**Effect of Concentration and Shear Rate on MV Sodium Alginate**
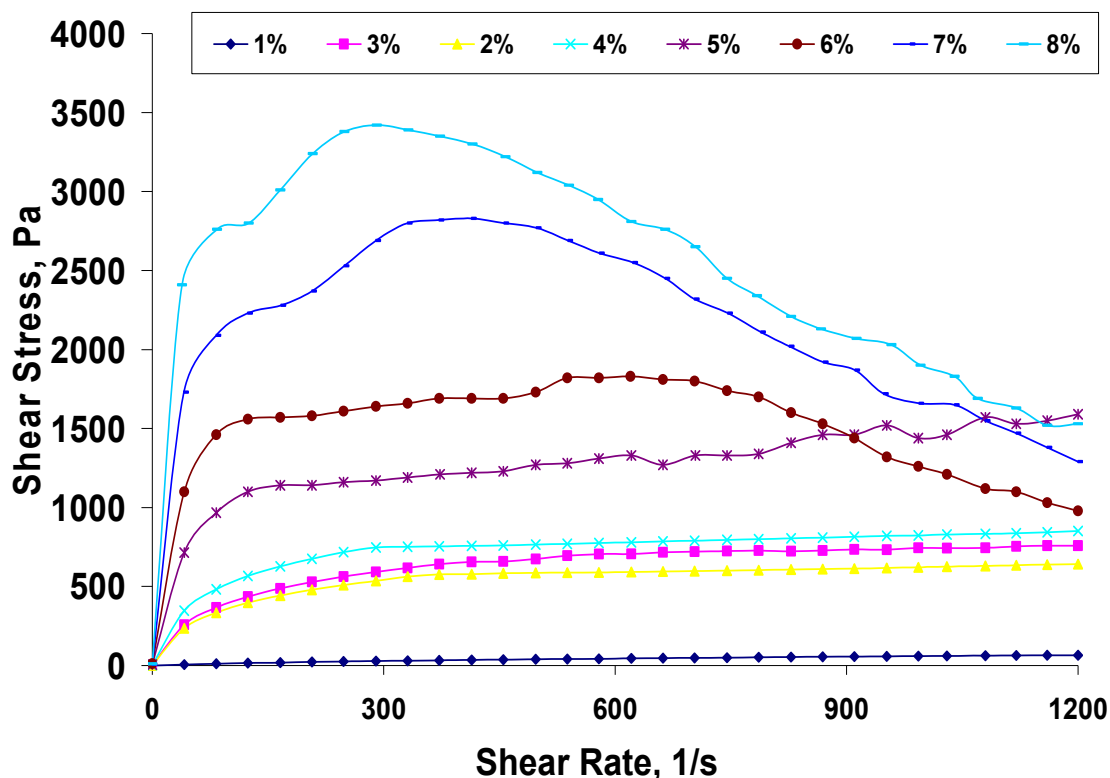


Figure 3.4: The effects of sodium alginate concentration and shear rate on medium viscosity sodium alginate's apparent viscosity. The apparent viscosity is shown as the slope of the concentration plots. MV alginate displays a viscosity behavior that decreases with respect to an increasing shear rate.

Table 3.3: Solution properties of sodium alginate

| Viscosity Grade | Viscosity Literature Values @ 2%, 25°C, (cP) | Measured Viscosity Values @ 2%, 25°C, (cP) | Molecular Weight Literature Values, (kDa) | Viscosity Average Molecular Weight Range, (kDa) |
|---|---|---|---|---|
| MV | 3500 | 910 | 120-180 | 153-382 |
| AO | 510 | 240 | 2000 | 185-254 |
| LV | 250 | 120 | 80-120 | 151-247 |

### 3.1.3  Autoclaving and DMEM addition on alginate's viscosity

In addition to determining the effects of concentration and molecular weight on the viscosity profiles of the three types of alginate, it was also desirable

to determine the effects of autoclaving and adding DMEM to provide nutritional value to alginate.  The intent of this characterization was to establish a viscosity range in which hollow fibers could be fabricated under the same coagulant bath concentration, extrusion pressure, and coagulant injection rate.

The results indicate that autoclaving 6 wt% MV sodium alginate at 121 °C for 1 hr and cooling to room temperature reduces its apparent viscosity by 50% from 11,000cP to 5,500 cP.  The outcome of this study also suggests that preparing a 1:1 solution of autoclaved 6 wt% MV alginate and DMEM decreases the viscosity even further to 250 cP.  However, if a 10:1:: autoclaved 6 wt% MV alginate and DMEM solution is prepared, the apparent viscosity of the autoclaved 6 wt% alginate is only reduced by to 3,600 cP, as shown in Figure 3.5.

**The Effects of Autoclaving and Adding Dulbecco's Modified Eagle's Medium (DMEM) on the Apparent Viscosity of Sodium Alginate @ 100 1/s.**
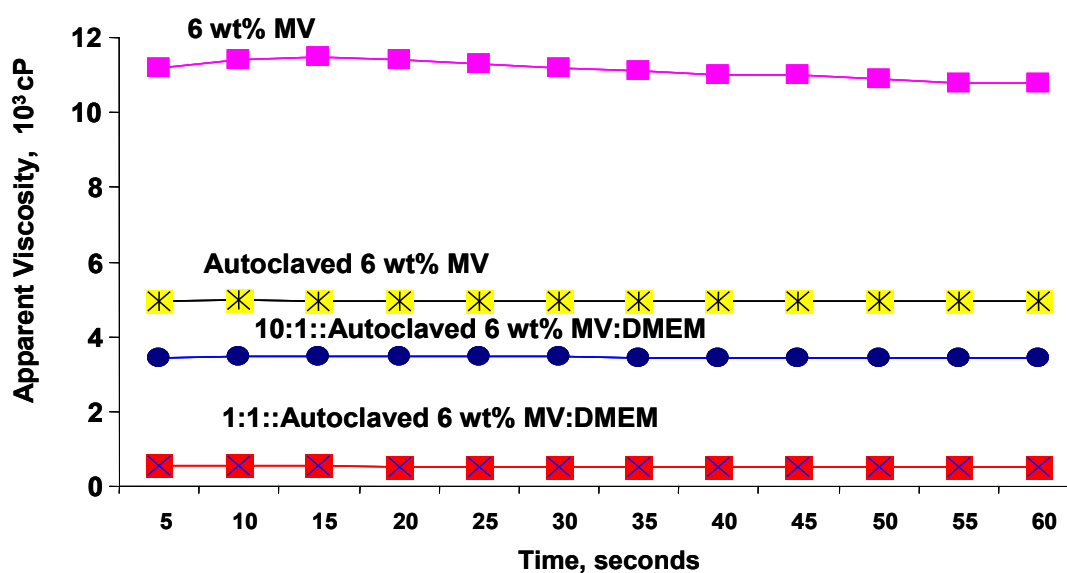


Figure 3.5: The effect of autoclaving and adding DMEM to 6 wt% MV sodium alginate.

### 3.1.4  M/G block ratio

There is an inverse relationship between P/T ratio and %G block (Figure 3.6). The G block percentages from Methods 1 and 2 indicate that the %G block from MV, AO, and LV alginate range from 45 and 47%, 38 and 41%, and 44 and 48%, respectively.  Method 3, however, suggests that the %G block is 70, 69, 70% for MV, AO, and LV alginate, respectively, as shown in Figure 3.7.  The vibration of several functional groups and bonds that are specific to alginate monomers are summarized in Table 3.4.  Analyses conducted by a One-way ANOVA test conclude with a 95% confidence level that there is no difference between the G block percentages generated by using Method 1 versus Methods 2.  However, an additional One-way ANOVA test suggests that there is a significant difference between the average M/G ratios calculated via Methods 1 and 2 and the M/G ratios that were determined using Method 3.
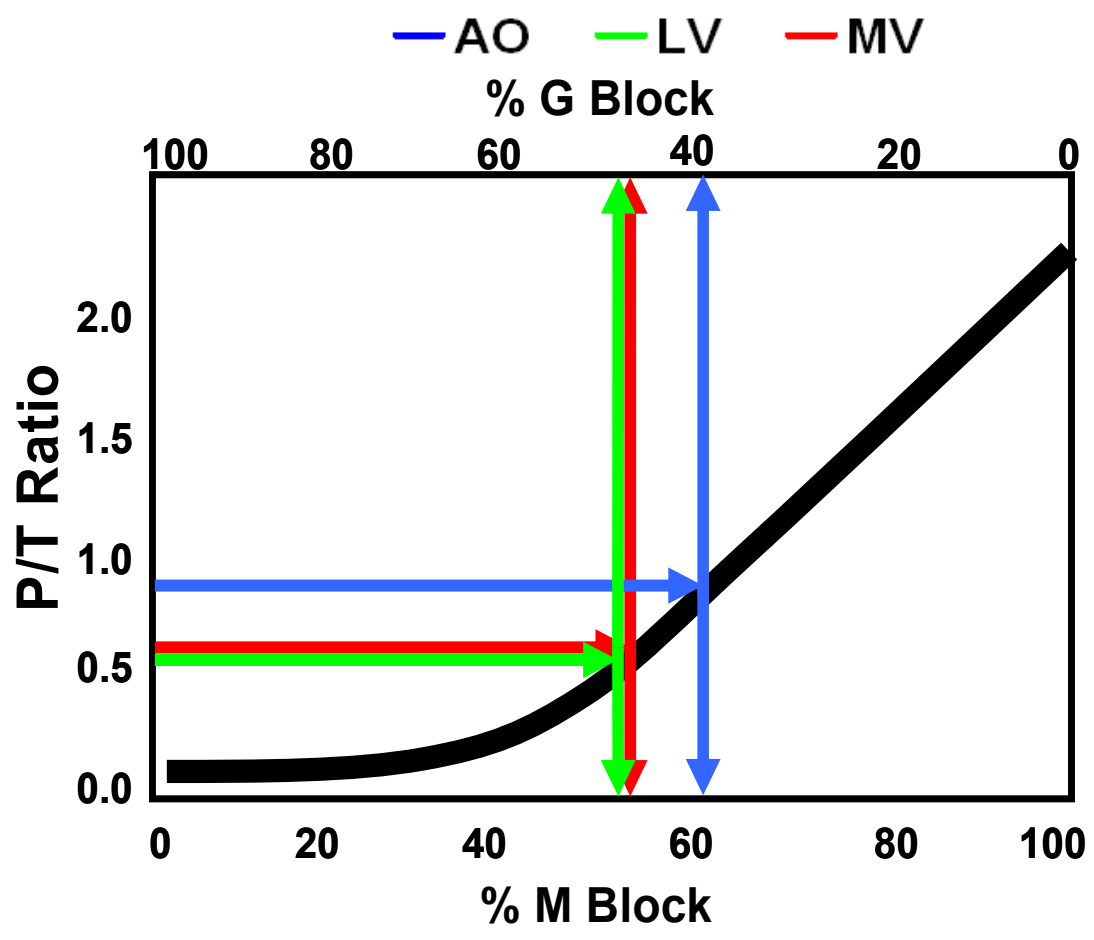
Figure 3.6: Determining the %G block of three alginate types. The linear portion of the P/T Ratio correlation chart (Eq. 2.5) was used to determine the % G block for AO (blue), MV (red) and LV (green) sodium alginate (Method 2).
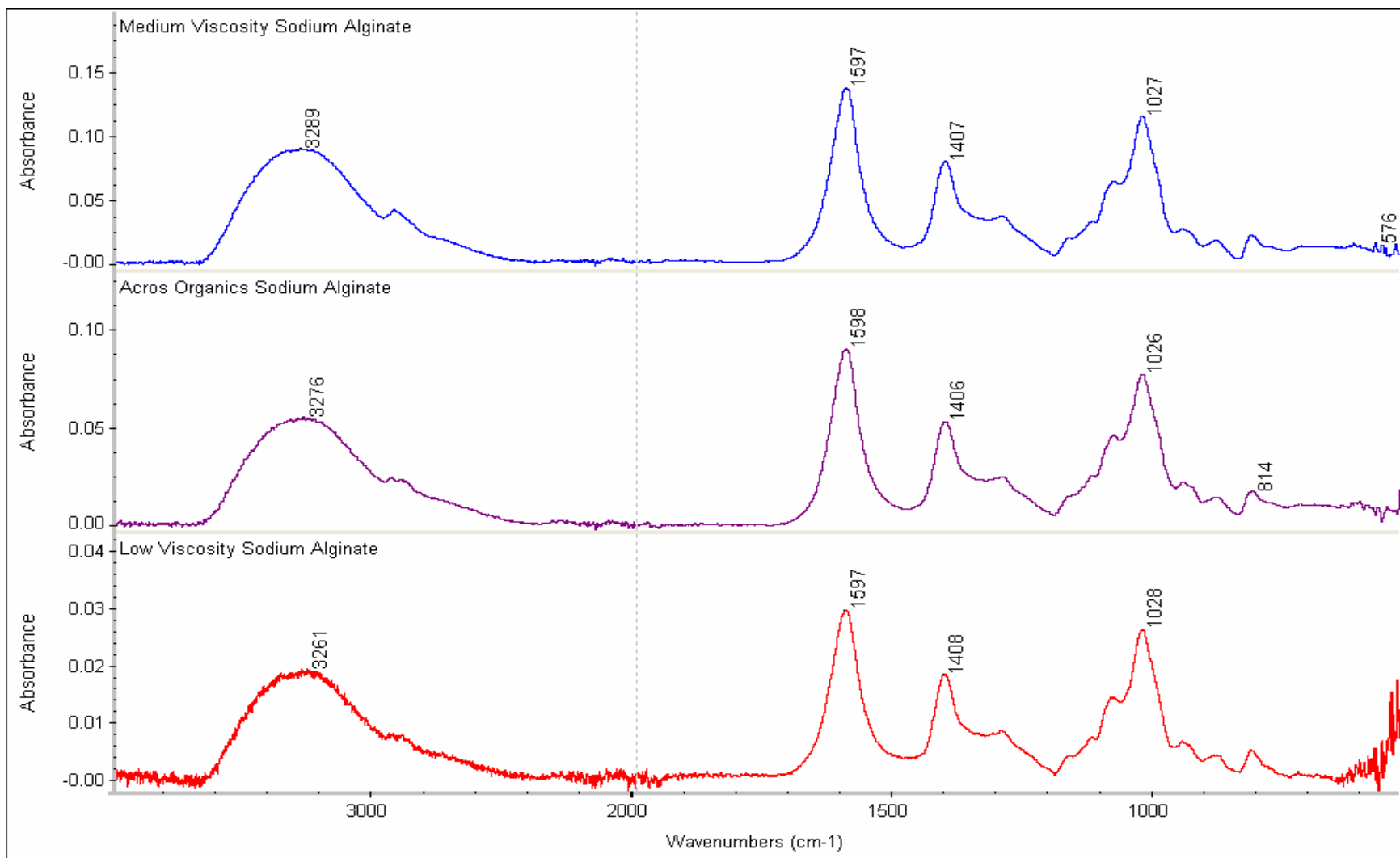
Figure 3.7: FTIR-ATR spectra showing similar functional groups and bond vibrations for three alginate types.

Table 3.4: Wavenumbers of key alginate functional groups and bonds, as cataloged in the literature[1-3]

| Wavenumbers at major absorbance peaks | Functional group(s) and bonds with associated vibration |
|---|---|
| cm$^{-1}$ | |
| 3300 | Hydroxyl (-OH) |
| 1600 | Carboxylic acid (COO-) |
| 1400 | Carboxylic acid (COO-) |
| 1297 | C-O bond |
| 1176 | C-O bond |
| 1122 | C-C or C-O bond |
| 1084 | C-O-C ester bond |
| 1028 | C-OH bond |
| 950 | (-OH) or C-C-H bond |

Table 3.5: Comparison of M/G ratio and % G block via three methods for three types of alginate

| Viscosity Grade | Method 1 | | | Method 2 | | Method 3 | |
|---|---|---|---|---|---|---|---|
| | P/T Ratio | M/G Ratio | %G | M/G Ratio | %G | M/G Ratio | %G |
| MV | 0.61 | 1.22 | 45 | 1.13 | 47 | 0.43 | 70 |
| AO | 0.81 | 1.62 | 38 | 1.44 | 41 | 0.45 | 69 |
| LV | 0.57 | 1.14 | 44 | 1.08 | 48 | 0.43 | 70 |

## 3.2 Cellular response
## 3.2.1 Lactic acid production

It was observed that the lactic acid produced by MAC-Ts encapsulated in CO-X type fibers (n=6 for Days 0-5, n=12 for Days 10-21) initiated at Day 5, whereas the production of lactic acid initiated at Day 1 in MI type fibers (n=6), as shown in Figure 3.8. The MAC-Ts within each fiber type produce similar amounts of lactic acid.

A One-Factor ANOVA test was employed to compare the average lactic acid productions on Days 1, 5, 10, 14, 18, and 21 for each encapsulation method. It was observed that there was no significant difference in the means of lactic acid production between time points within the MI (n=6) or CO-X (n=12) encapsulation study. These observations were confirmed by a corresponding p-value of 0.7142. Based on our sample size and procedure of measurement, it can be concluded with a 95% confidence level that there is no evidence to suggest that there is a difference in the average lactic acid production within each encapsulation method during Days 1, 5, 10, 14, 18, and 21.

One can observe that the distribution of daily MAC-T lactic acid production is skewed to the right for both methods. Although the skew of the lactic acid production in the MI method maintains as time progresses, the skew of the lactic acid production in the CO-X method increases with time (Figure 3.9 and Table 3.6). It is important to note that the skew of the lactic acid production values in the CO-X type fiber data set may have been influenced by an increased sample size.

**Cumulative MAC-T Lactic Acid Production**
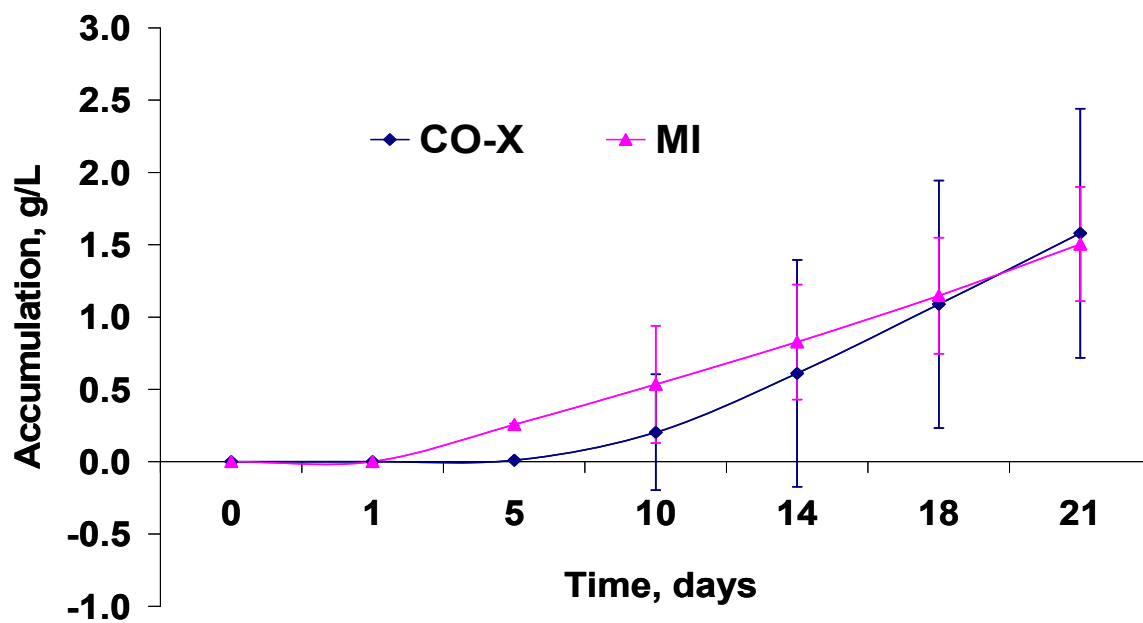


Figure 3.8: The accumulation of lactic acid produced by encapsulated MAC-Ts. Error bars express standard deviations.

**Daily MAC-T Lactic Acid Production**



Figure 3.9: Box and whisker plot of the MAC-Ts' daily production of lactic acid for the MI (n=6) and CO-X (n=6 for Days 0-5, n=12 for Days 10-21) encapsulation methods.

## 3.2.2 Glucose consumption

Overall, there were noticeable differences between the two encapsulation groups in the MAC-Ts' glucose consumption behavior (Figure 3.10 and Table 3.7). A greater lag time for MAC-Ts' consumption of glucose under the CO-X (n=6 for Days 0-5, n=12 for Days 10-21) encapsulation method; however, it appears that MAC-Ts encapsulated in the CO-X type fibers consumed more glucose than MAC-Ts encapsulated in the MI type fibers by Day 21 of the study. It was also observed that the glucose consumed by the MAC-Ts in the MI type

fibers (n=6) accumulates linearly, whereas the glucose consumed by the MAC-Ts in the CO-X fibers accumulates exponentially.

A One-Factor ANOVA test was performed to compare the average glucose consumption from days 1, 5, 10, 14, 18, and 21 for each encapsulation method (Figure 3.11).  There was no significant difference in the means of glucose consumption between time points within each encapsulation group, as confirmed by the p-value of 0.7532.  Based on our sample size and procedure of measurement, it can be concluded with a 95% confidence level that there is no evidence to suggest differences in the values for the average glucose consumption at each time point within each encapsulation method.

Notice that the values of the means of the daily consumption in the CO-X study are higher than the medians of the data, which indicates that the glucose consumption distribution is highly skewed to the right (Figure 3.11).  Although the distribution of MAC-T glucose consumption values within the MI type fibers is slightly skewed to the right, the distribution does not vary greatly from Days 5 to 21, which corresponds to the linear accumulation of the glucose consumed by MAC-Ts in the MI type fibers, as shown in Figure 3.10.

Figure 3.10: The accumulation of glucose consumed by encapsulated MAC-Ts. Error bars express standard deviations.
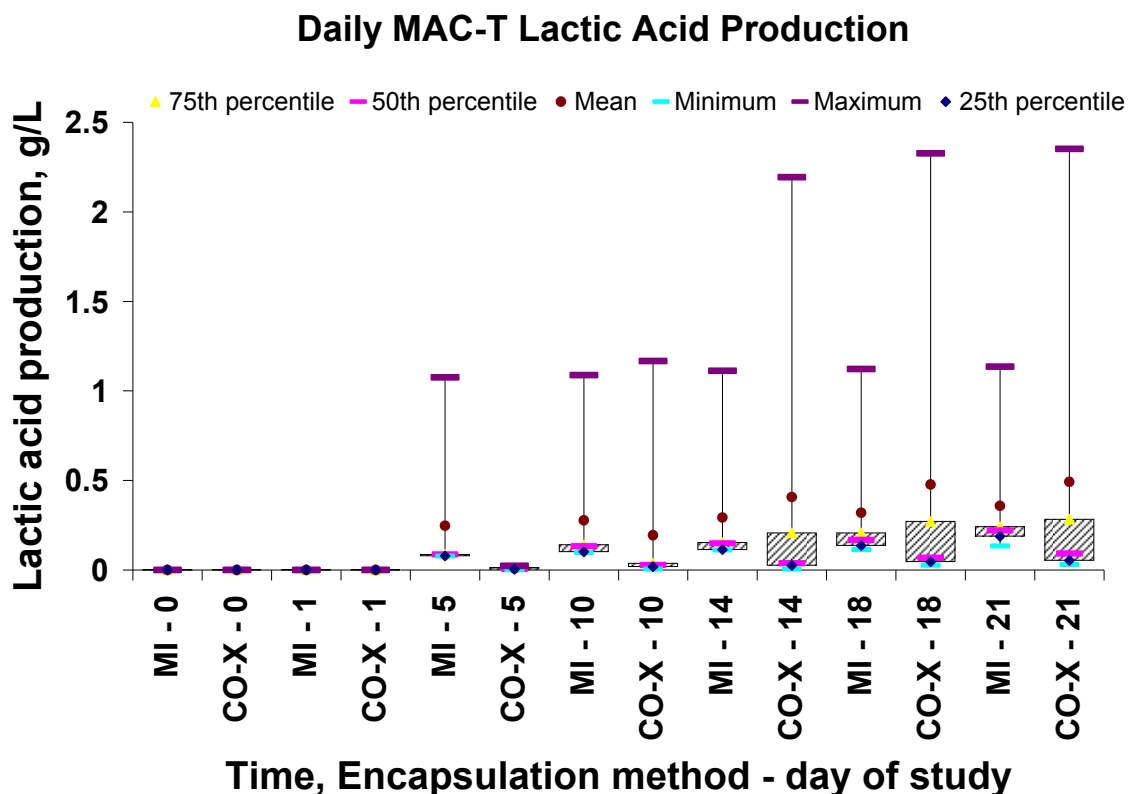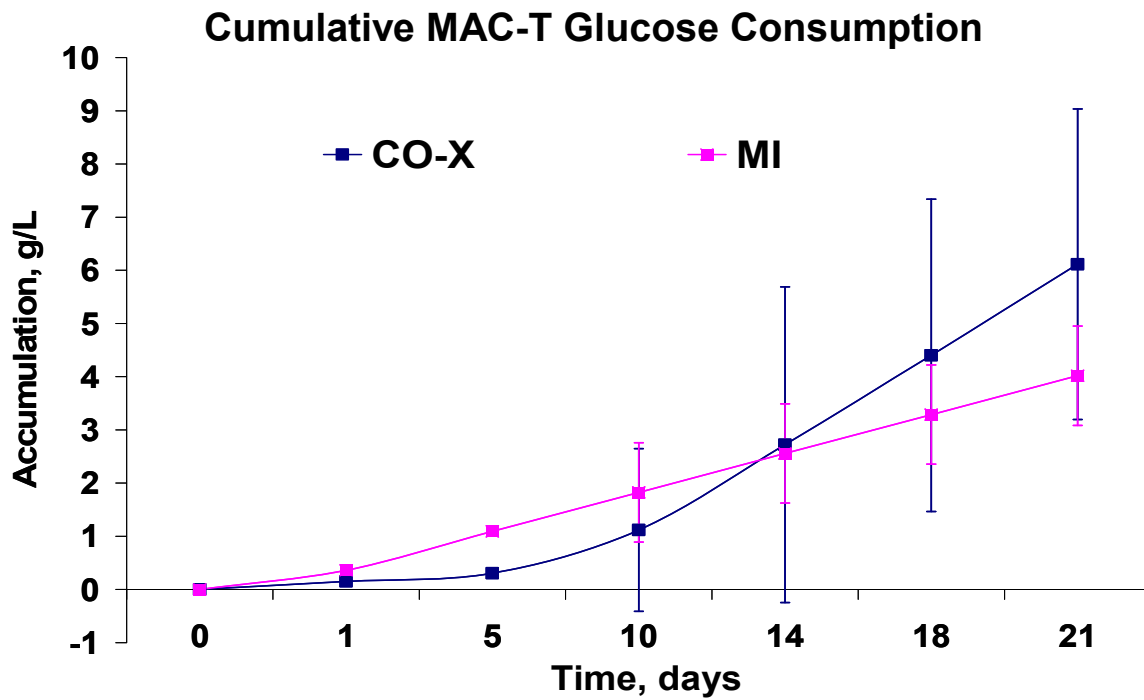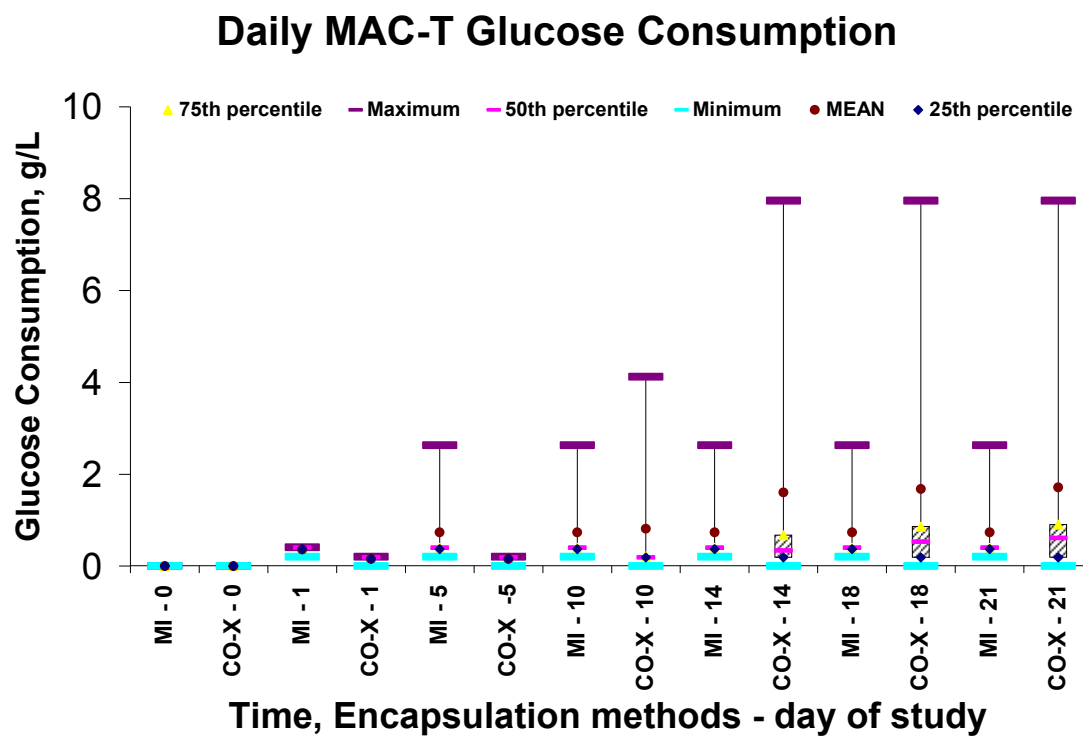
**Daily MAC-T Glucose Consumption**

Figure 3.11: Box and whisker plot of the MAC-Ts' daily consumption of glucose for the MI (n=6) and CO-X (n=6 for Days 0-5, n=12 for Days 10-21) encapsulation methods.

Table 3.6: Data summary of Figure 3.8: Daily MAC-T lactic acid production plot

| | Day 0 | | Day 1 | | Day 5 | | Day 10 | | Day 14 | | Day 18 | | Day 21 | |
|---|---|---|---|---|---|---|---|---|---|---|---|---|---|---|
| | MI | CO-X | MI | CO-X | MI | CO-X | MI | CO-X | MI | CO-X | MI | CO-X | MI | CO-X |
| | g/L | g/L | g/L | g/L | g/L | g/L | g/L | g/L | g/L | g/L | g/L | g/L | g/L | g/L |
| 25th percentile | 0 | 0 | 0 | 0 | 0.078 | 0.004 | 0.101 | 0.017 | 0.111 | 0.021 | 0.126 | 0.043 | 0.177 | 0.051 |
| 50th percentile | 0 | 0 | 0 | 0 | 0.079 | 0.006 | 0.102 | 0.020 | 0.115 | 0.031 | 0.147 | 0.055 | 0.199 | 0.064 |
| 75th percentile | 0 | 0 | 0 | 0 | 0.087 | 0.015 | 0.132 | 0.032 | 0.148 | 0.041 | 0.172 | 0.089 | 0.232 | 0.118 |
| Interquartile range | 0 | 0 | 0 | 0 | 0.009 | 0.011 | 0.031 | 0.015 | 0.037 | 0.020 | 0.046 | 0.046 | 0.055 | 0.067 |
| Interquartile mean | 0 | 0 | 0 | 0 | 0.083 | 0.008 | 0.118 | 0.027 | 0.134 | 0.051 | 0.170 | 0.084 | 0.227 | 0.099 |
| Mean | 0 | 0 | 0 | 0 | 0.082 | 0.010 | 0.115 | 0.024 | 0.129 | 0.076 | 0.160 | 0.116 | 0.202 | 0.129 |
| Minimum | 0 | 0 | 0 | 0 | 0.077 | 0.001 | 0.096 | 0.005 | 0.111 | 0.005 | 0.113 | 0.026 | 0.134 | 0.030 |
| Maximum | 0 | 0 | 0 | 0 | 0.087 | 0.023 | 0.144 | 0.038 | 0.154 | 0.416 | 0.219 | 0.551 | 0.245 | 0.566 |

Table 3.7: Data summary of Figure 3.9: Daily MAC-T glucose consumption

| | Day 0 | | Day 1 | | Day 5 | | Day 10 | | Day 14 | | Day 18 | | Day 21 | |
|---|---|---|---|---|---|---|---|---|---|---|---|---|---|---|
| | MI | CO-X | MI | CO-X | MI | CO-X | MI | CO-X | MI | CO-X | MI | CO-X | MI | CO-X |
| | g/L | g/L | g/L | g/L | g/L | g/L | g/L | g/L | g/L | g/L | g/L | g/L | g/L | g/L |
| 25th percentile | 0 | 0 | 0.40 | 0.16 | 0.39 | 0.19 | 0.39 | 0.19 | 0.39 | 0.21 | 0.39 | 0.19 | 0.39 | 0.19 |
| 50th percentile | 0 | 0 | 0.40 | 0.19 | 0.40 | 0.19 | 0.40 | 0.19 | 0.40 | 0.24 | 0.40 | 0.31 | 0.40 | 0.37 |
| 75th percentile | 0 | 0 | 0.40 | 0.19 | 0.40 | 0.19 | 0.40 | 0.20 | 0.40 | 0.36 | 0.40 | 0.55 | 0.40 | 0.66 |
| Interquartile range | 0 | 0 | 0 | 0.03 | 0.01 | 0 | 0.01 | 0.01 | 0.01 | 0.15 | 0.01 | 0.36 | 0.01 | 0.47 |
| Interquartile mean | 0 | 0 | 0.40 | 0.19 | 0.40 | 0.19 | 0.40 | 0.19 | 0.40 | 0.30 | 0.40 | 0.45 | 0.40 | 0.50 |
| Mean | 0 | 0 | 0.39 | 0.15 | 0.39 | 0.18 | 0.39 | 0.20 | 0.39 | 0.28 | 0.39 | 0.44 | 0.39 | 0.47 |
| Minimum | 0 | 0 | 0.36 | 0.00 | 0.36 | 0.15 | 0.36 | 0.19 | 0.36 | 0.19 | 0.36 | 0 | 0.36 | 0 |
| Maximum | 0 | 0 | 0.41 | 0.20 | 0.40 | 0.20 | 0.40 | 0.22 | 0.40 | 0.41 | 0.40 | 1.46 | 0.40 | 1.46 |

### 3.2.3 Alamar blue reduction

The C/A ratio of both fiber types appeared to fluctuate around a value of 1 during the 21 day study. A Two-Factor With Replication ANOVA test and Fisher's Least Significant Difference (LSD) protocol was employed to compare the average C/A ratio at Days 1, 7, 14, and 21 of each encapsulation method (Figure 3.12). A significant difference was observed within the MI type fibers for the C/A ratios between Days 1 and 5, 1 and 10, 1 and 14, 1 and 18, and 1 and 21. A significant difference was also observed within the CO-X study for the C/A ratios between Days 1 and 5, 1 and 14, 1 and 18, 1 and 21, 10 and 18, 10 and 21, 14 and 18, and 14 and 21. The p-value corresponding to the ANOVA test used to analyze the C/A ratio data was 0.0072 (n=3). The p-value associated with the interaction between the two encapsulation methods was 1.53E-07, suggesting that there was a significant change in the differences of the two encapsulation methods throughout the study. Therefore, no conclusion can be made about which method gives higher C/A results, and no implications can be made about the MAC-T's metabolism of glucose or viability using this study.

**Ratio of the Cellular (C) and Acellular (A) Fluorescence in Alginate Hollow Fibers**
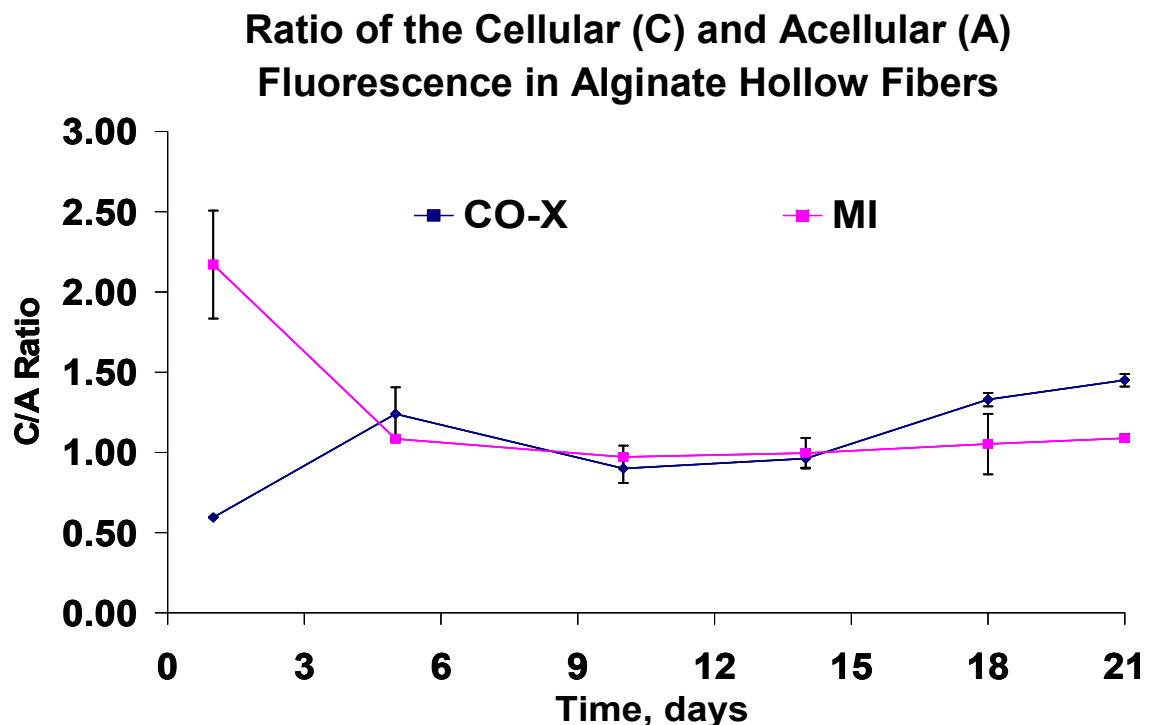


Figure 3.12: Ratio of the fluorescence in cellular ( C ) and acellular ( A ) alginate fibers for the MI and CO-X (n=9, cellular and n=3, acellular) for both encapsulation methods.  The error bars indicate standard deviation.

### 3.2.4 Cell number

A Two-Factor With Replication ANOVA test was employed to compare the average cell count performed on Days 1, 7, 14, and 21 of each encapsulation method (Figure 3.13).  It was noticed that there was no significant difference in the average cell number between time points for either the MI or the CO-X encapsulation study.  The lack of a significant difference was validated by a p-value of 0.2450 (n=2).  It was also observed that there was no significant difference between the cell numbers counted between encapsulation methods. The p-value associated with the interaction between the two encapsulation methods (p = 0.708) suggests that there is not a significant difference in the

change between the two encapsulation methods throughout the study, as shown in Figure 3.13. The uncontrolled error (MSE) was 1.68E+11, which suggests that a larger sample size should be used with a hemacytometer. Therefore, it can be concluded with a 95% confidence level that based on our sample size and procedure of measurement, there is no evidence to suggest that the average cell numbers found at Days 1, 7, 14, and 21 are different. However, one can observe that there is much higher variability in the measurements made on Day 21 than the measurements made on Day 1 of the study.
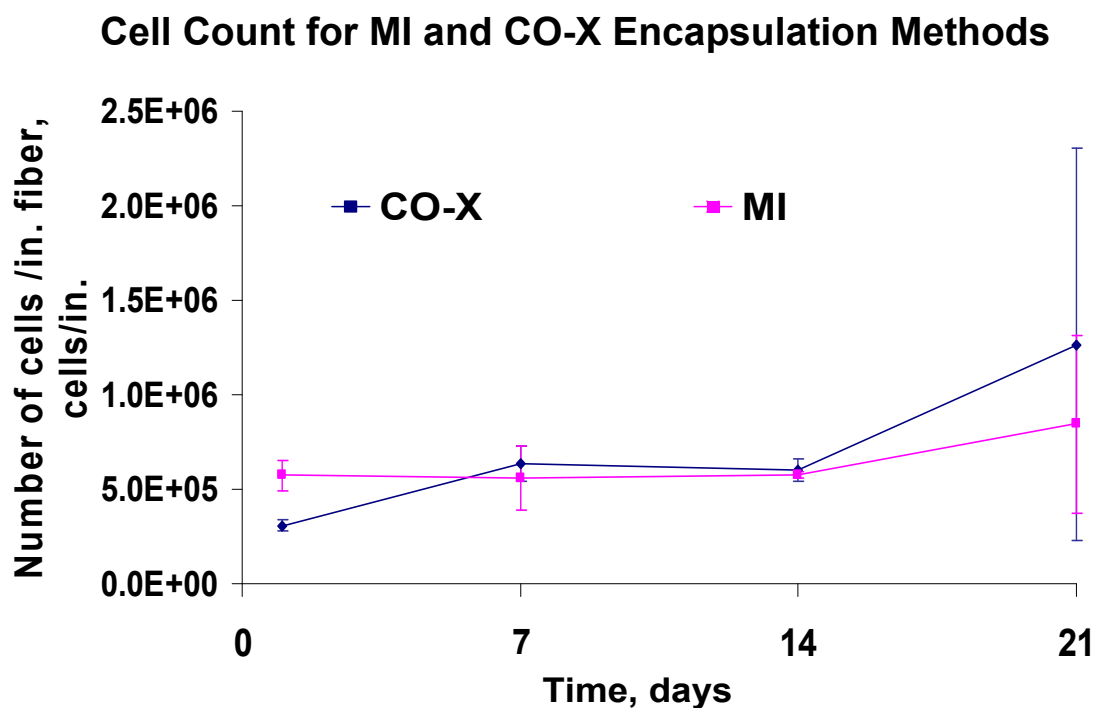


Figure 3.13: MAC-T cell count performed via hemacytometer. MAC-T cell count for MI (n=4) and CO-X (n=2) encapsulation methods over 21 days. The error bars denote the standard deviation.

### 3.2.5 The expression of green fluorescent protein (GFP)

Fluorescent microscopy was used to qualitatively analyze the expression of GFP for both fiber types on Days 1, 10, 14, and 21 (Figure 3.14). In the

analysis, the micrographs captured on Day 1 were used as the basis of comparison within each fiber type. No noticeable decrease in GFP expression by the MAC-Ts inside each type of fiber was observed. Also, it is important to note that the expression of GFP allowed one to observe the differences in the location and distribution of MAC-Ts between the two encapsulation methods. In the CO-X fiber type, the cells were distributed in the fiber wall; whereas, the MAC-Ts were located in the lumen of the MI type fibers.
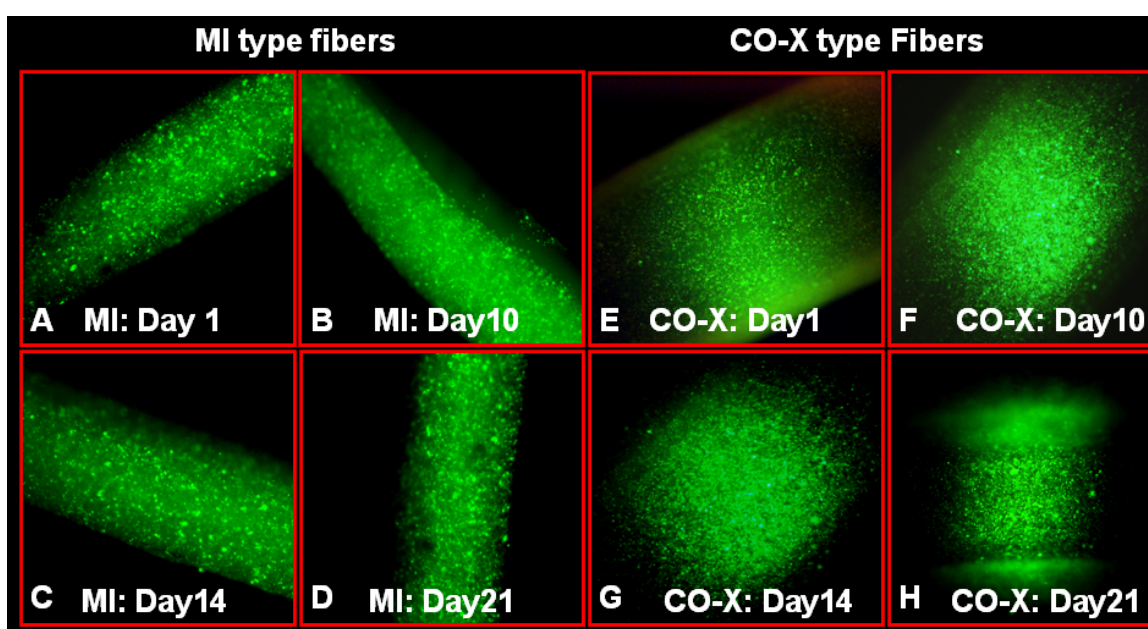


Figure 3.14: The expression of GFP for Days 1, 10, 14, and 21 of the MI (A-D) and CO-X (E-H) encapsulation studies. The total magnification is 25X for all pictures.

### 3.2.6 Histological processing

Histological processing was completed by subjecting 30 micron sections of GMA embedded hollow fibers of both the MI (Figures 3.15 – 3.17) and CO-X (Figures 3.18 – 3.21) encapsulation methods to toluidine blue staining. These fibers were removed from culture on Days 1, 7, 14, and 21. Cells could not be distinguished on a MI type fiber that had been removed from culture on Day 7

and no micrographs were made of its sections. In general, the staining process enabled the cells to be labeled blue and the alginate pink or dark purple, depending on the concentration of the alginate.

After one day in culture, the geometry of the MI type hollow fiber was been compromised, but the wall thickness has been maintained (Figure 3.15). Notice that little to no cell aggregates are present within the internal cell suspensions. The embedding matrix has not been maintained and appears to be stretched.



Figure 3.15: Day 1 toluidine blue staining pictures of MI encapsulated MAC-Ts. Total magnifications are indicated.

Relative to Day 1, less of the cell suspension is present within the lumen of the MI type fiber on Day 14 (Figure 3.16A). It is evident that the embedding method is not sufficient to maintain the in vitro morphology of the hollow fiber,

because the wall of the hollow fiber has been compromised (Figure 3.16B).  The cells that are present in the alginate matrix within the lumen of the hollow fiber conform to the cobblestone morphology present at various locations within the human body, such as the simple squamous epithelium on the surface of peritoneal mesothelium, the transitional epithelium of the contracted bladder, and the epithelial cells that surround the mammary gland (Figure 3.16B and Figure 3.16D).  An alginate "string" has left the lumen, but remains attached to the hollow fiber wall (Figure 3.16C), which suggests that during the embedding process, the fiber ends do not remain capped and allow part of the cell suspension to escape.  It appears that the cells have released an anchoring matrix (Figure 3.16D).
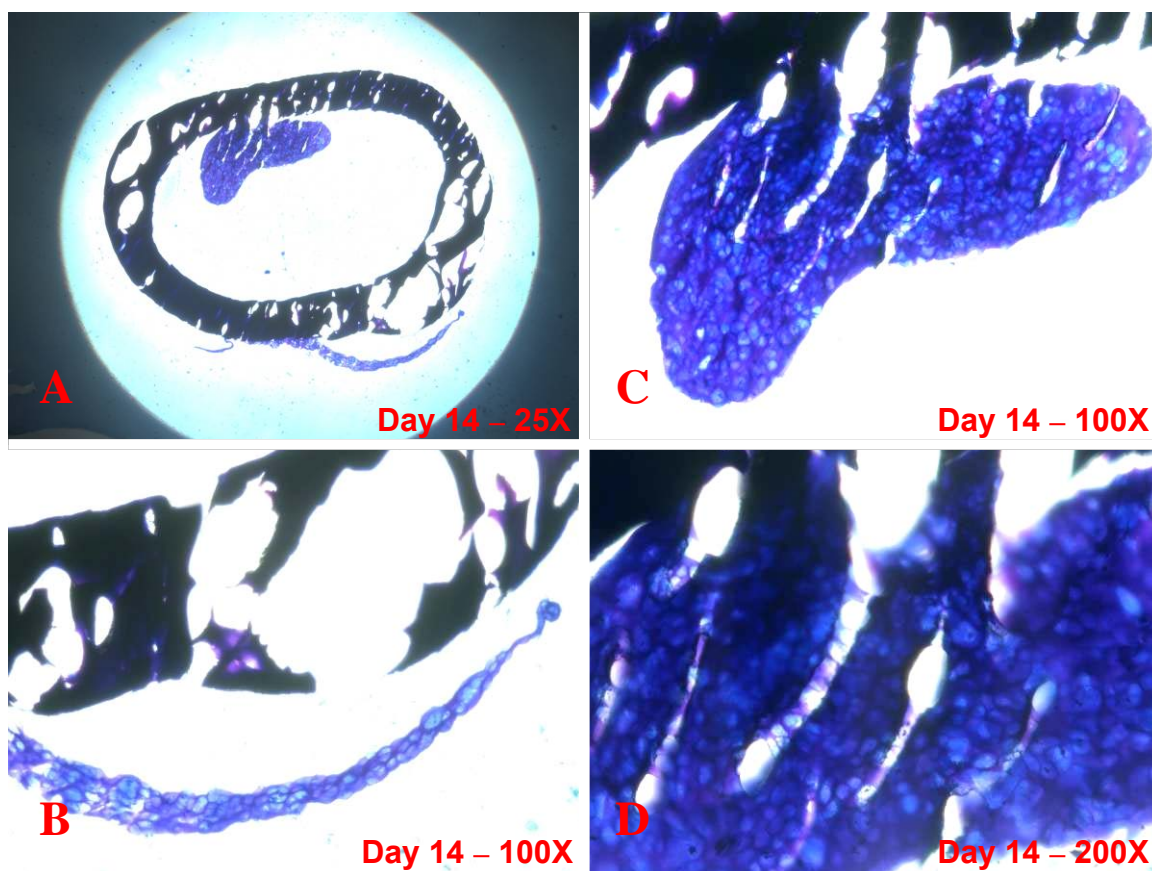
Figure 3.16: Day 14 toluidine blue micrographs of MAC-Ts (blue) encapsulated in a 0.74 wt% alginate suspension matrix (black and dark purple) and MI encapsulated MAC-Ts.  Total magnifications are indicated.

Micrographs were taken of the cell and fiber morphology of the MI type fiber on Day 21 (Figure 3.17).  These micrographs reveal that the same GMA embedding and histological processing techniques have a greater affect on the fiber morphology as time progresses (Figure 3.17A & Figure 3.17D).  The micrographs also reveal few cell aggregates and more dissolution of the internal suspension matrix (Figure 3.17B & Figure 3.17C).
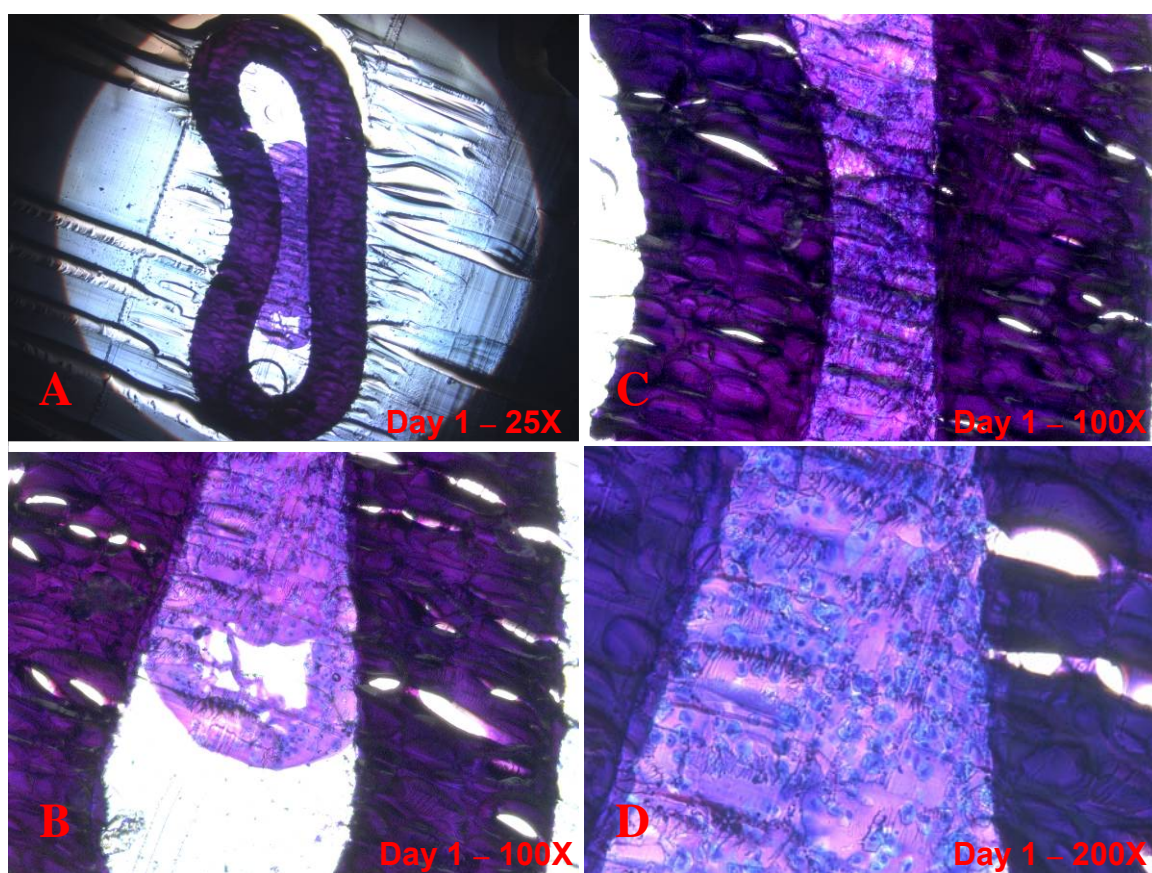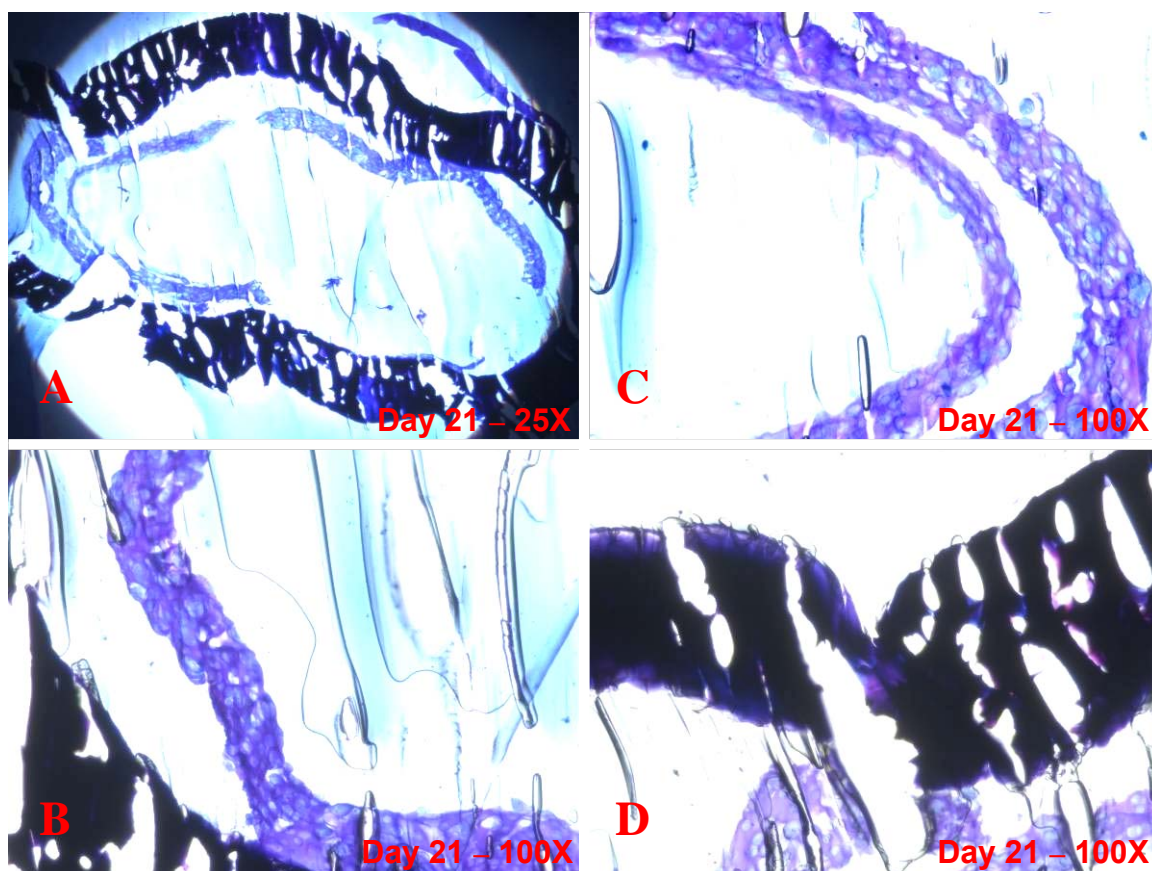
Figure 3.17: Day 21 toluidine blue staining pictures of MI encapsulated MAC-Ts. Total magnifications are indicated.

Histological processing of the CO-X type fibers also resulted in the staining of the MAC-Ts' nuclei (blue). The micrographs taken on Day 1 reveal striations that were caused by razor blade sectioning, as shown in Figure 3.18. The sections stained on Day 7 disclose the 3-D structure of the fiber as well as the distribution and morphology of the cells (Figure 3.19). Cells are located sporadically within the fiber wall. Most of the cells remain in the rounded morphology. After 14 days of culturing, the wall of the CO-X type fiber remained intact, as shown in Figure 3.20). However, it appears that cells had not been encapsulated from the 9 o'clock to the 12 o'clock position in this particular inch of

fiber (Figure 3.20A). Day 21 sectioning and staining reveals that the CO-X spinning trial did not encapsulate cells from the 9 o'clock to the 12 o'clock position (Figure 3.21). Notice that sections of the fiber walls appear to be on these pictures reveal that the hollow fiber appears to be twisted (Figure 3.21A-C). Finger-like voids appear in the hollow fiber wall (Figure 3.21D).
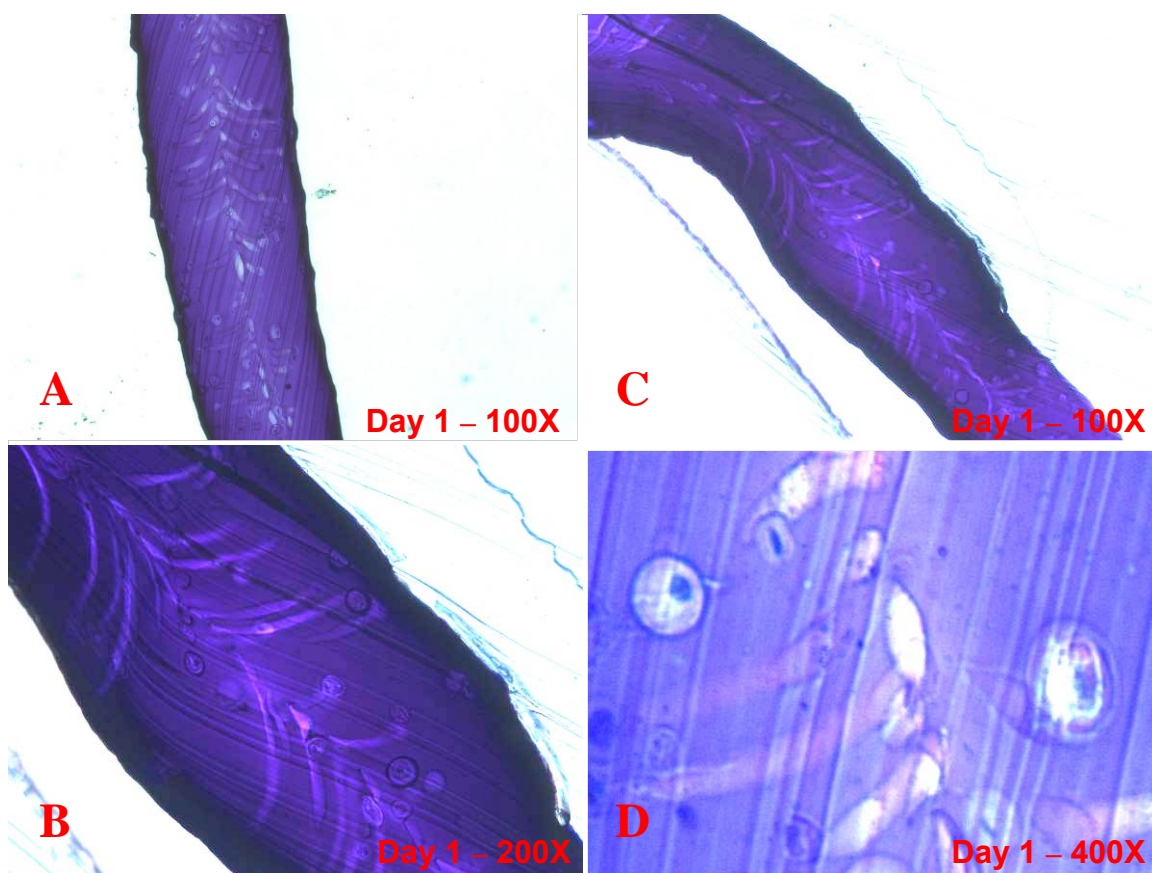


Figure 3.18: Day 1 toluidine blue staining pictures of CO-X encapsulated MAC-Ts. Total magnifications are indicated.
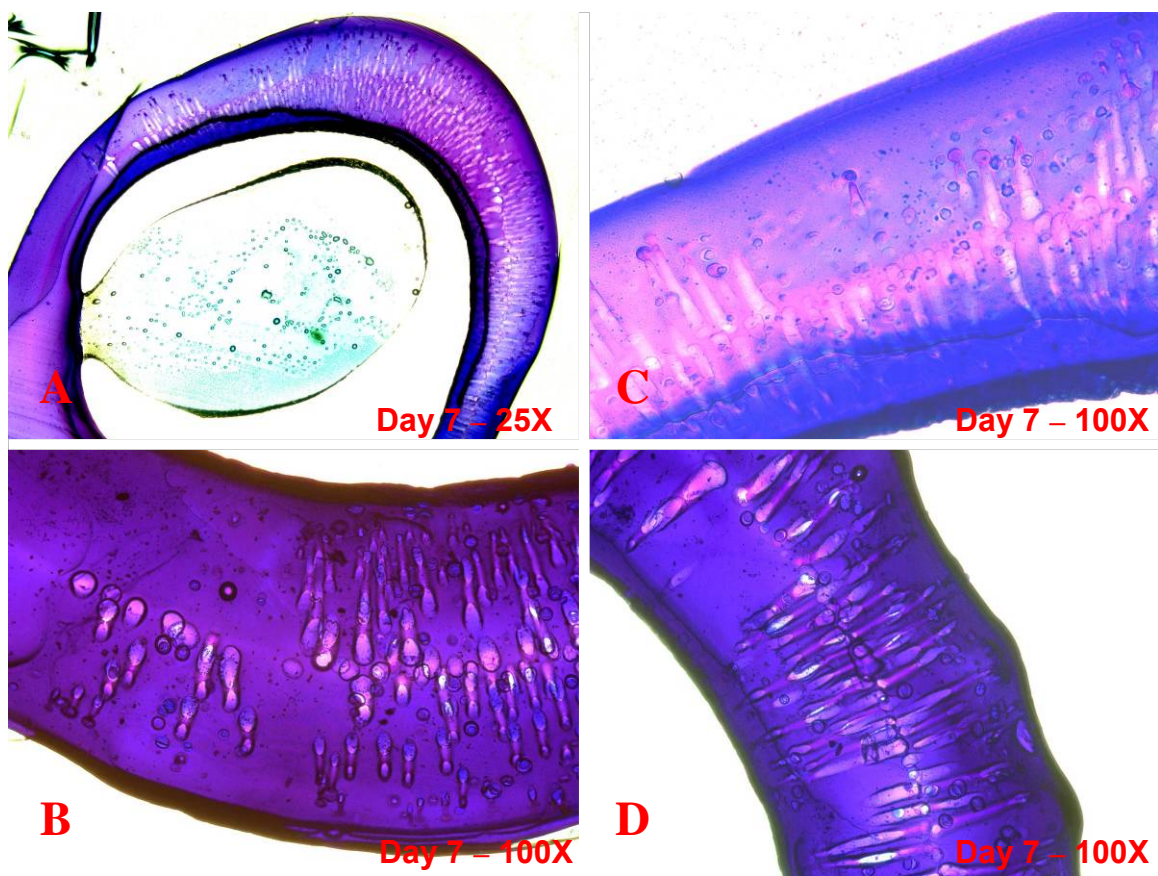
Figure 3.19: Day 7 toluidine blue staining pictures of CO-X encapsulated MAC-Ts.  Total magnifications are indicated.
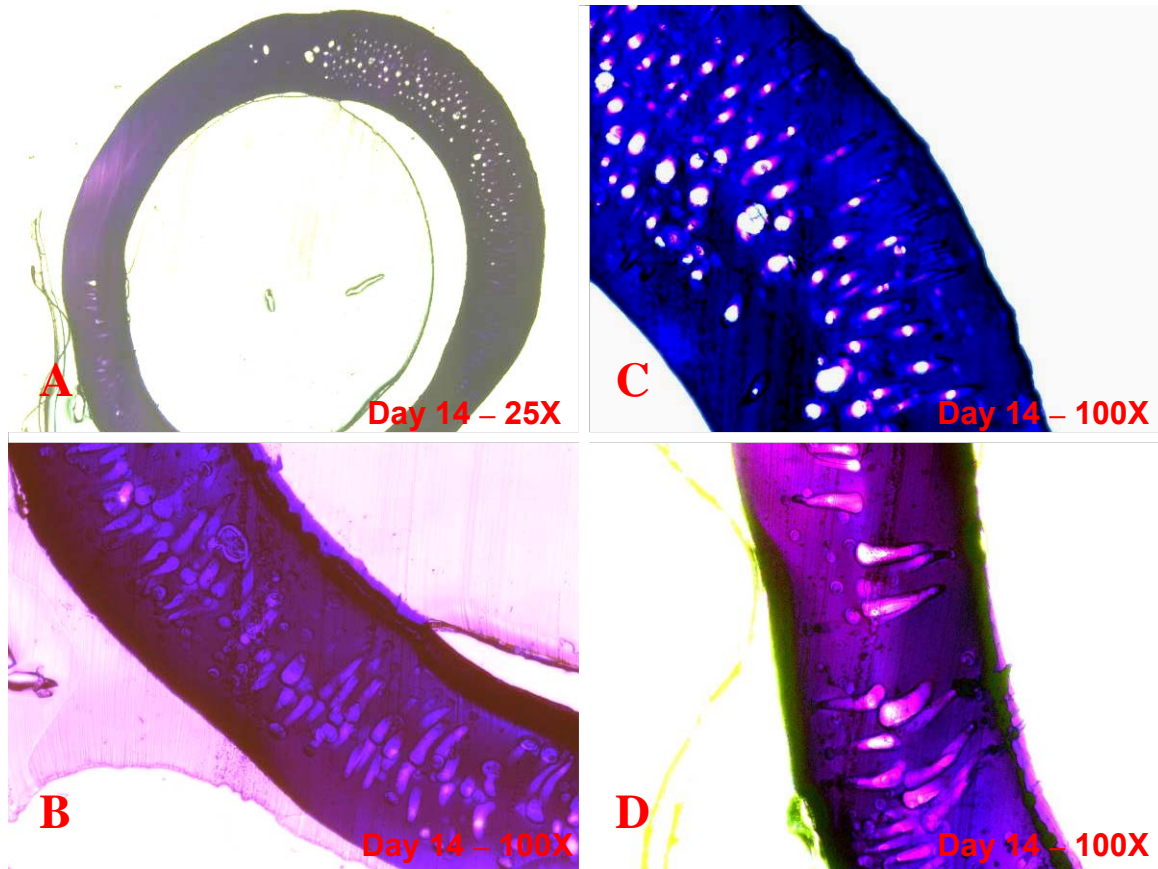
Figure 3.20: Day 14 toluidine blue staining pictures of CO-X encapsulated MAC-Ts.  Total magnifications are indicated.
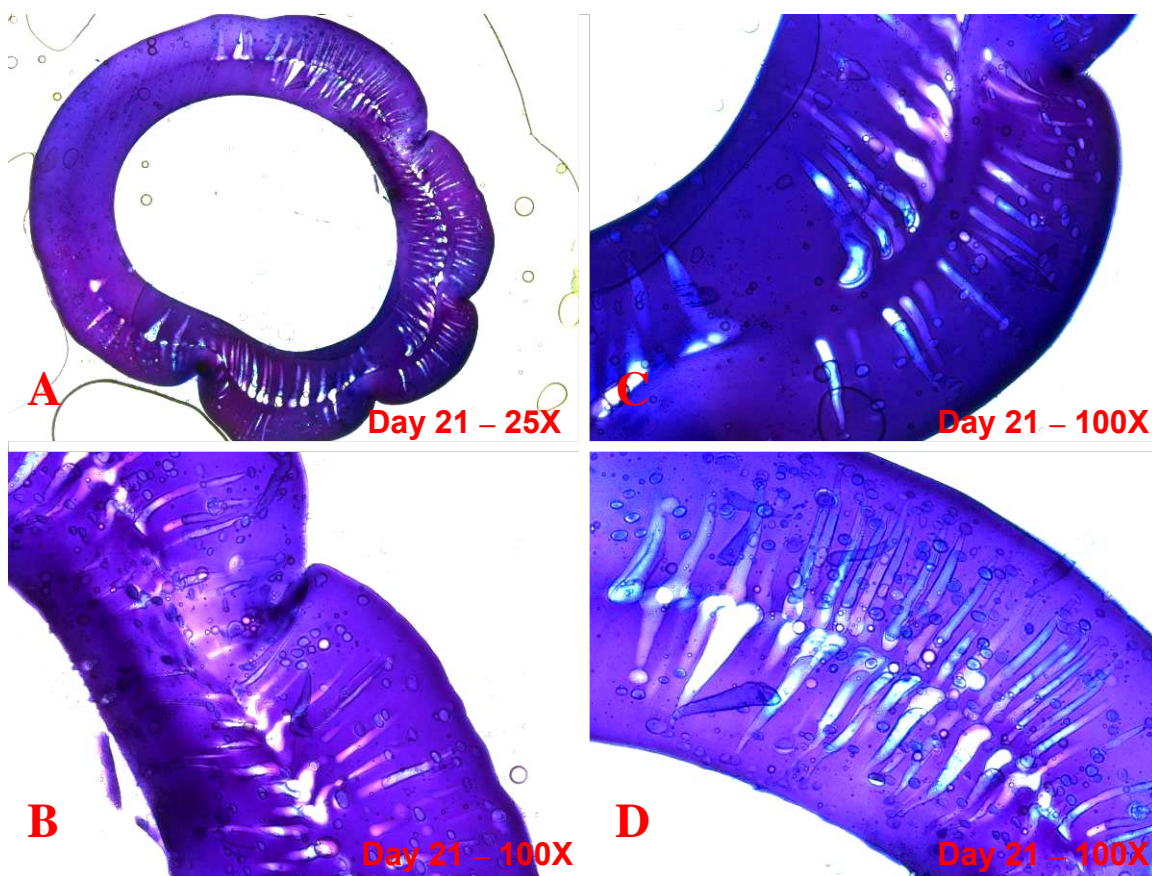
Figure 3.21: Day 21 toluidine blue staining pictures of CO-X encapsulated MAC-Ts.  Total magnifications are indicated.

### 3.2.7 Histomorphological analysis

One-factor ANOVA tests were performed on the Y/X ratio (Figure 3.22) and cell area (Figure 3.23) data, which were followed by calculations of Fisher's Least Significant Differences (LSDs) to compare the means of these two measurements from days 1, 7, 14, and 21 for each encapsulation method.  For the MI study, there was a significant difference in the Y/X ratios between Days 1 and 21, and 14 and 21.  For the CO-X study, there was a significant difference in the Y/X ratio between days 1 and 7, and 1 and 21.  There was also a significant difference in the cell area between Days 1 and 21 and Days 14 and 21.  For the CO-X study, there was a significant difference in the cell area between Days 1

and 7, and 7 and 14.  The p-values corresponding to the ANOVA tests employed

for the Y/X ratios and cell area were 3.09E-12 and 3.92E-04 (n=20), respectively.

**Y/X Ratio for MI and CO-X Encapsulation Methods**
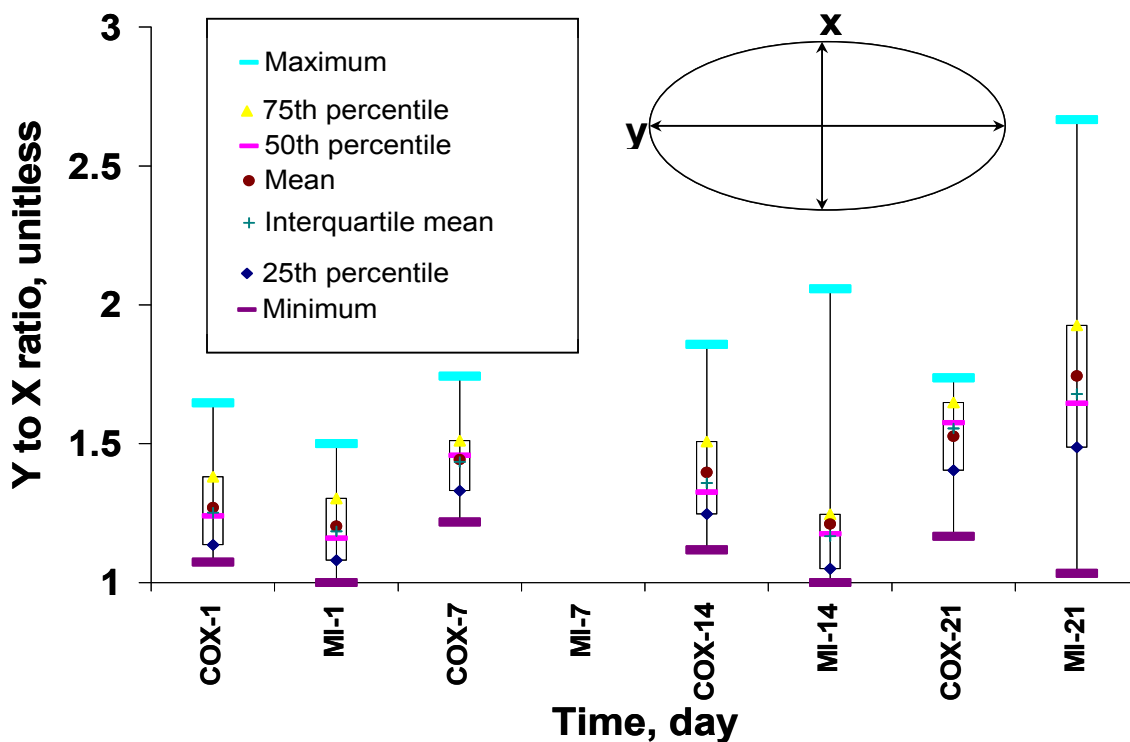


Figure 3.22: Box and whisker plot of the y to x ratio calculated as part of the histomorphological analysis of the MI and CO-X encapsulation methods over 21 days (n=20).    Notice that the distribution of the Y/X ratio for the CO-X encapsulation method does not vary greatly over the duration of the study.
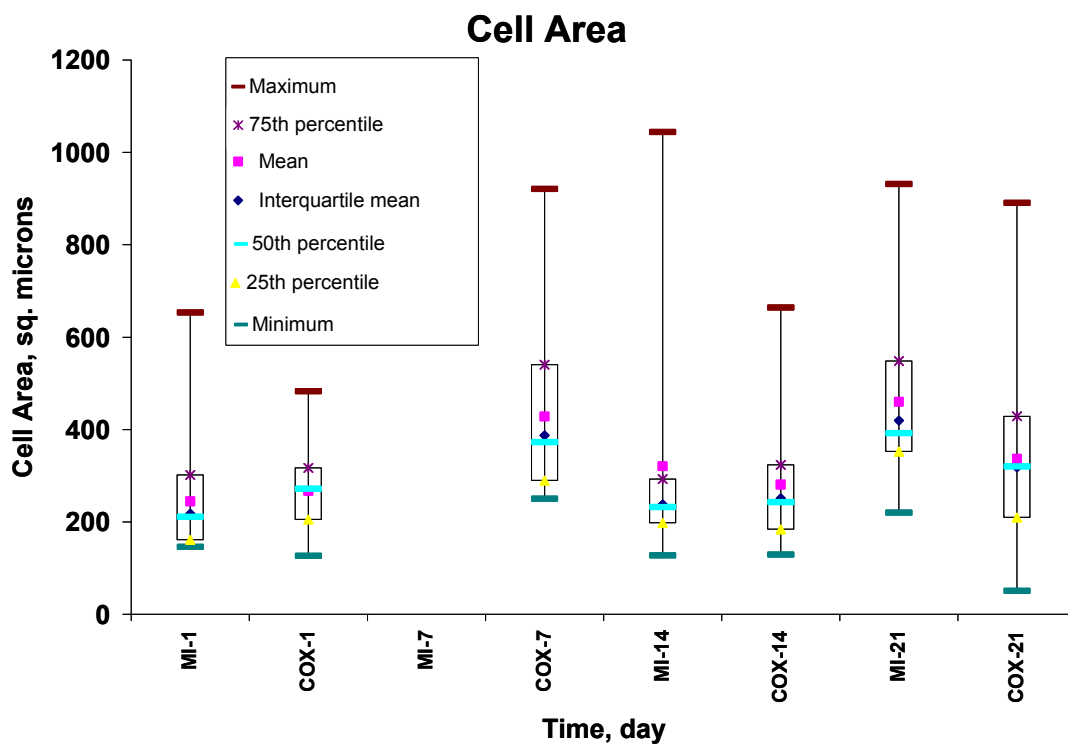
Figure 3.23: Box and whisker plot of the cell area calculated with the histomorphological analysis for the MI and CO-X encapsulation methods over 21 days (n=20).

References

1.    Pereira, L., Sousa, A., Coelho, H., Amado, A.M., and Ribeiro-Claro, P.J.A. Use of FTIR, FT-Raman, and 13C-NMR spectroscopy for identification of some seaweed phycocolloids. Biomolecular Engineering 2003;20(4-6):223-228.

2.    Sartori, C., Finch, D.S., Ralph, B., and Gilding, K. Determination of the cation content of alginate thin films by FTIR spectroscopy. Polymer 1997;38(1):43-51.

3.    Wasikiewicz, J.M., Yoshii, F., Nagasawa, N., Wach, R.A., and Mitomo, H. Degradation of chitosan and sodium alginate by gamma radiation, sonochemical and ultraviolet methods. Radiation Physics and Chemistry 2005;73(5):287-295.

# CHAPTER FOUR

# DISCUSSION

## 4.1 Sodium alginate solution properties

Sigma Aldrich and Fischer Scientific are the distributors of sodium alginates, which are manufactured targeting viscosity specifications rather than molecular weight or M/G ratio. Therefore the manufacturer only provides molecular weight ranges and a typical value for the M/G ratio for each lot number. The manufacturers do, however, provide values for the apparent viscosity of these alginates at 2 wt% and 25 °C. On the other hand, the standard operating procedures and specifications used to measure the viscosity, e.g., shear rate, type of rheometry, solvent ionic strength, are not disclosed; all of these factors have been found to affect the measurement of viscosity [1,2]. These possible differences in testing methods may explain the large differences in our assessment of the viscosity profile and the literature values[3-5] provided by the alginate distributors, as shown previously in Table 3.3.

Despite these potential differences in methodology, the main goals in our viscosity investigation were achieved. These goals were to estimate the viscosity for the three alginate types, determine the extent to which the apparent viscosity of alginate is affected by concentration and shear rate, and to establish an acceptable fiber spinning viscosity that would promote the fabrication of a hollow fiber.

Determining the properties of alginate using a cone and plate rheometer employs the use of shear force measurements.  Therefore, the accuracy of shear force dependent viscosity measurements is based on the expectation that once the cone is set in motion, the alginate will conform to its geometry.  However, alginate is a non-Newtonian, pseudo-plastic material and can be best categorized as a complex fluid because it exhibits a nonconforming, solid-like behavior.  Physical evidence that alginate is a non-Newtonian fluid is the development of the die swell (extrudate swell) phenomena as alginate emerges from the capillary tube of the fiber spinneret pack[6]. The solid-like viscosity behavior of alginate was also confirmed through preliminary studies, and the extent of the solid-like viscosity behavior was found to depend on concentration, as shown in Figures 4.1(A-B).
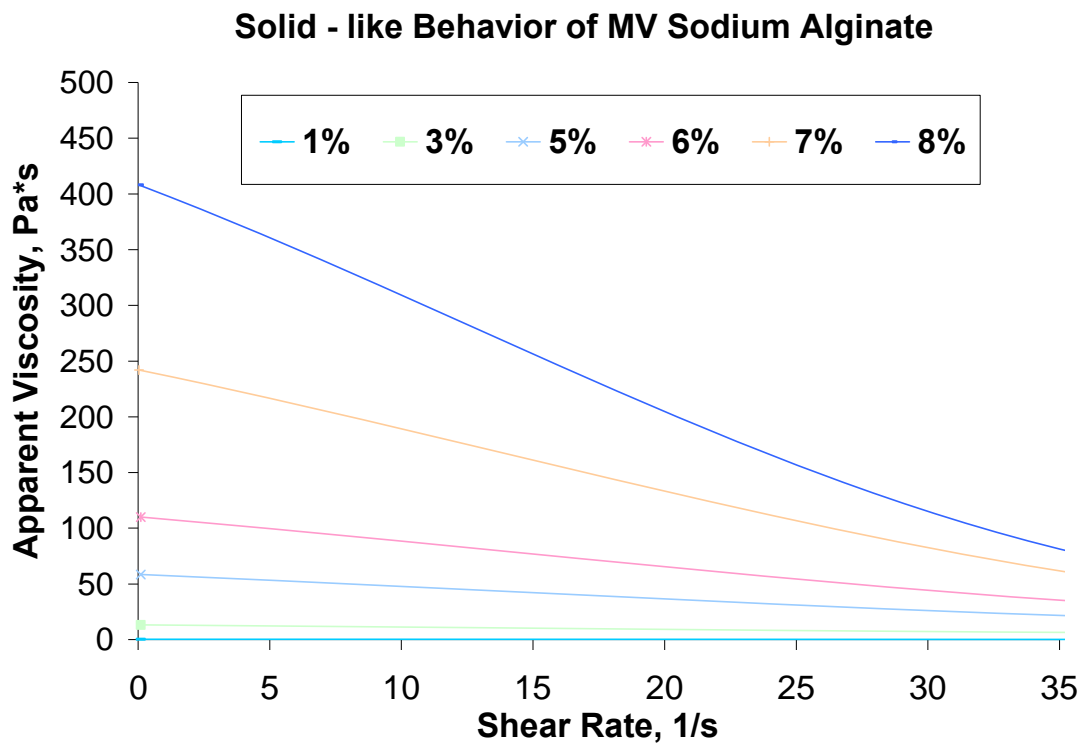
Figure 4.1A: The schematic curves of the apparent viscosity versus shear rate for alginate, a complex fluid. The apparent viscosity decreases linearly between 0.1 – 35 sec$^{-1}$. The decrease in apparent viscosity in response to an increasing shear rate is known as shear thinning[6,7].

**Solid - like Behavior of MV Sodium Alginate**
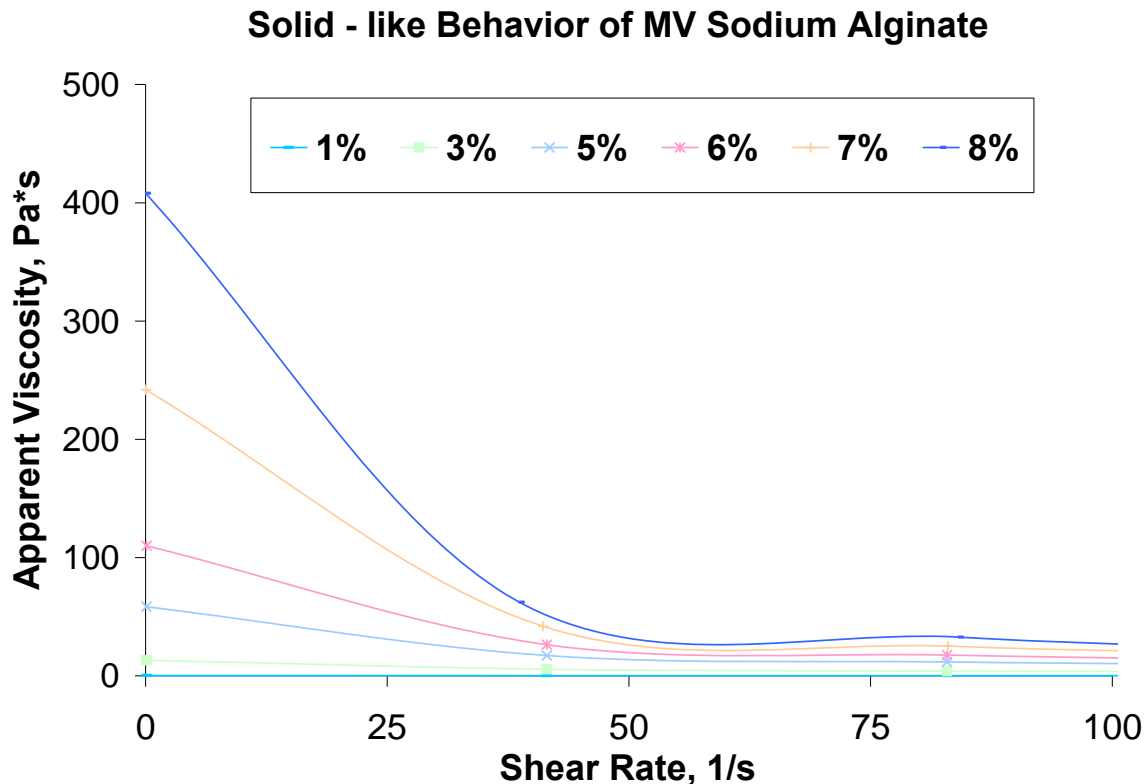


Figure 4.1B: The schematic curves of the apparent viscosity versus shear rate for alginate, a complex fluid. For a "solid-like" complex fluid, the viscosity decreases with increasing shear rate, which is known as shear thinning[6,7].

One may hypothesize that the differences between the literature and measured apparent viscosity values may be due to the Weissenberg effect. The Weissenberg effect occurs when non-Newtonian fluids (i.e sodium alginate powder and water solutions) do not flow outward, but climb up the shaft of the cone that induces the high shear rate[8]. Therefore, it is important to examine how the Weissenberg effect affects viscosity measurements with a plate and cone rheometer in order to understand how the accuracy of the molecular weight measurements may be limited by the chosen method of measurement.

Guion and Hood suggest that the difficulty of using rotational devices to measure viscosity is that the Weissenberg effect causes a material gap to form,

especially with "tacky" substances, that breaks the contact between the cone height and the alginate. They also suggest that in order to compensate for the Weissenberg effect, this material gap must be repacked between time points, and that the Weissenberg effect can be minimized by adding enough alginate to form a layer above the top of the cone[9]. Figure 3.4 is an illustration of the shear rate dependent shear stress of MV sodium alginate that was gathered during preliminary trials in which we were learning how to effectively use the rheometer. The slopes of the curves shown are equal to the apparent viscosity. From 0 to 100 $s^{-1}$, the apparent viscosity of the 6 wt% curve is increasing, and then decreases to nearly 0 at 600 $s^{-1}$. For shear rates higher than 600 $s^{-1}$, the viscosity is negative, which goes against Newton's first law, which says that there will always be an inertial force, or a resistance to flow, that must be overcome for movement to take place. There are no free flowing fluids. The curves for 6-8 wt% exhibit the Weissenburg effect, which causes a material gap to form and breaks the contact between the cone height and the alginate. This phenomenon is commonly referred to as "slip." Our contention is that when we established the viscosity profile of the three alginates types, a sufficient amount of alginate was added to the testing plate, thereby minimizing the Weissenberg effect.

Section 2.2.3 describes the methods that were employed to determine the intermediate behavior of the spinning solution preparation. Although the viscosity depends on temperature, it was believed that the relationship between the different types of alginates at 100 $s^{-1}$ would not vary greatly between the temperature range of 20 and 25 °C. Also, it is important to note that both of

these temperatures have been used in the literature for characterization purposes. In order to compare the apparent viscosities of the three types of sodium alginates, an average temperature of 22.5 °C was used. It was determined that the dependence of the apparent viscosity on alginate concentration was the greatest at a shear rate of 100 s$^{-1}$ when compared with shear rates of 1,000 and 10,000 s$^{-1}$. The shear rate is synonymous to the rate of polymer extrusion in the spinning process. The shear rate was estimated to be 125 s$^{-1}$ by using a shear rate equation specified for Newtonian fluids[10]. The approach was deemed appropriate because it was observed that a 6 wt% MV sodium alginate solution exhibits a Newtonian-like behavior above a shear rate of 65 s$^{-1}$, as shown in Figure 4.1B. The Newtonian-like behavior is one in which changes in the shear rate have minimal affects on the apparent viscosity.

Figure 3.5 shows that 6 wt% MV based blends have experienced a time-dependent viscosity. It is thought that the decrease in viscosity may be due to a flow-induced breakdown or alignment of the polymer chains[6].

Perhaps it is not mere coincidence that the apparent viscosity of 6 wt% MV decreases by 50 % after being autoclaved. The mechanism that would describe such an occurrence is called degradation. Degradation is different from dissolution. Alginate dissolution occurs because there is a lower concentration of a particular crosslinking agent outside the alginate matrix than there is within the alginate matrix. Dissolution in alginate can also occur because another molecule, such as lactic acid, binds the crosslinking agents. The ultimate result in dissolution is that the alginate monomers become water soluble.

In the literature, researchers have degraded alginate by using acid, enzymatic hydrolysis, and gamma irradiation techniques. When alginate is degraded, a double bond is formed at the C4 carbon of the alginate monomers, resulting in D-glucono-lactone molecules that contain ketone functional groups[11]. It is also known that autoclaving alginate induces depolymerization of the alginate chains[12]. Among the effects of degradation are a decrease in viscosity and molecular weight, and darker hue. The decrease in viscosity and molecular weight occur primarily because of main alginate chain scission, and the darker hue occurs because of the formation of the double bond, which changes the refractive index of the alginate chains[13].

We have observed that autoclaving alginate can cause a decrease in viscosity, as shown in Figure 3.5. We have also noticed that autoclaving changes the color of the sodium alginate solution from light brown to dark brown. The color change and the decrease in viscosity are both clues that lead us to infer that we may have changed the chemistry of our alginate precursor solution when autoclaving.

## 4.2 M/G block ratio

The statistical analysis revealed that there was a significant difference between the average %G block values calculated from Methods 1 and 2 and the average %G block values calculated using Method 3. One major caveat in determining the M/G block ratio and the %G block was the limitation of literature values for the alginate types employed in this study. In fact, the linear regressions employed in Methods 1 and 2 were fabricated using data from a

variety of brown seaweed species that included but were not limited to the brown seaweed species of macrocystis pyrifera. Method 3, however, was a more conceptual method that was based on characteristic guluronic and mannuronic acid FTIR-ATR peaks[14]. Nevertheless, the analysis was conducted for a sodium alginate that stemmed from the laminaria hyperborea species of sodium alginate. According to Smidrod and Brown, alginates derived from the macrocystis pyrifera species of brown seaweed have a M/G ratio and %G block in the range of 1.02-1.52 and 39-50 %, respectively[15].

Prior to the study, two pieces of information were given that pertained to the M/G block ratio and %G block characterization. It was known that the LV and MV alginate types from Sigma were from the Macrocystis pyrifera source of brown seaweed. Second, according to Acros Organics technical support representatives, the %G block contained in the AO alginate type was between 65-75 %[3], which suggested that either the alginate originated from the Macrocystis pyrifera source of brown seaweed and was chemically modified to change the conformation of its M block residues to G block residues, or the alginate originated from a source that typically has a higher %G block associated with its polymer chains. One example of the latter is laminaria hyperborea, which has a range of %G block between 44-70 % depending on whether the alginic acid is removed from the fronds or stipes of the brown seaweed plant[16]. The three types of alginates are from the Macrocystis pyrifera source of brown seaweed; and since it is likely that the methods that used circular dichroism spectrophotometry were dependent on the concentration and the ionic strength

of the solvent, the FTIR-ATR technique remains as the method of choice for determining the %G block for alginates.

## 4.3 Cell Response
### 4.3.1 Lactic acid production and glucose consumption

It was evident that lactic acid was produced and glucose was consumed by MAC-Ts under the MI and CO-X encapsulation methods (Figures 3.8 to 3.11). It is important to note that Figure 3.8 accumulates the glucose consumed by the encapsulated MAC-Ts. As shown in Figure 3.7 and 3.11, the distribution of the values recorded are heavily skewed to the right. When plotting the mean values plus or minus the standard deviation of all the samples collected on a particular day, the skew results in standard deviation bars that are less than zero. Therefore, the occurrence of these deviation bars that include negative values are not indicative of negatively measured values, but of a distribution that was heavily skewed to the right.

One can observe lag times in the MAC-Ts lactic acid production of one and five days, respectively. Why do these lag times occur? Can and should these lag times be minimized? Do the lag times exist only within the constraints of this experiment or do the lag times occur for all culture studies?

Relative to the other days that the cells were in culture, the occurrence of these lag times in the production of lactic acid and consumption of glucose suggest that the cells were not as metabolically active. One rationale for the lag time is that the cells were becoming acclimated to their encapsulation environment and that they were methodically leaving a state of inactivity after being exposed to nitrogen gas, sub-physiological temperatures, and a high

concentration of $CaCl_2$ solution. Statistically speaking, if we increased the number of fiber segments analyzed or the fibers were more porous over a greater range of the fiber length, would the results indicate that the lag time phenomenon does not exist? Material scientists may pose the question of whether there are differences in the diffusion/transport capabilities of the two fiber types. A shorter lag time may suggest that the fiber may have larger pore sizes (less selectivity) or a higher degree of pore connectivity. On the other hand, a longer lag time suggests that the fiber may have low lactic acid diffusion rates to the culture medium because of smaller pore sizes (higher selectivity) and less pore connectivity. The MI encapsulation method was a bi-component fiber, comprised of a 0.74 wt% low viscosity alginate base in the lumen and 6 wt% medium viscosity in the annular. The differences in diffusion properties may also suggest that the CO-X is advantageous because it naturally limits the diffusion of molecules. The dilute concentration of low viscosity used as the cell suspension matrix in the manual injection method had a lower density than the 10:1::autoclaved 6 wt% MV alginate:DMEM solution that was used to encapsulated the MAC-Ts under the CO-X method. It is intuitive that a lower density alginate has less inertial forces, prohibiting its movement with respect to a higher density alginate. Therefore, a lower density alginate has a lower matrix modulus and shear force of extrusion. A lower density alginate imposes less shear forces onto the cell membranes during co-extrusion or manual injection, since a smaller shear force is required to extrude or inject the cells, respectively. Frangos and coworkers provided a review on the effect of shear stress on cell

metabolism[17-19]. They found that shear stress can expedite metabolite production, increase the strength of attachment, and promote the viability of anchorage-dependent mammalian cells. They also propose that shear stress acts as an external stimuli to the cell cytoskeleton, causing signal transduction across the cell plasma membrane that stimulates cell metabolism.

Initially, a rat aorta fibroblast cell line was used as an adhesion dependent model to access the feasibility of cellular incorporation. However, we were unable to qualitatively distinguish these cells from the fiber matrix without employing destructive methods. Fortunately, a hardy GFP labeled MAC-T cell line was readily available, and the expression of GFP from the MAC-Ts offered a non-destructive alternative to making qualitative assessments of the MAC-Ts' viability, metabolism of glucose, and location within lumen or wall of the fiber. It is highly likely that these metabolic activity results are dependent upon cell type.

### 4.3.2 Alamar Blue

There was no significant differences in the alamar Blue reduction between Days 1 and 21 for either encapsulation type. One may hypothesize that alamar Blue reduction is not an effective method to determine the cellular respiration / glucose metabolism of encapsulation cells because the method that was employed in this study was based on a protocol developed within our lab to study the cellular respiration of cells seeded on the surface of scaffolds. Furthermore, the C/A ratio remained close to a value of 1. Nevertheless, a low C/A ratio was expected. In fact, it is our contention that this study should not be excluded; because, during preliminary studies, three 1-inch co-extrusion type fiber

segments were placed in a single well of a 6-well plate, and it was determined that increasing the cell number increased the validity of the alamarBlue study. Specifically, it was determined that the success of the alamarBlue assay is dependent upon controlling and maintaining a threshold cell density of 1.2 X10$^6$ cells/1-inch fiber. In addition to improving the effectiveness of the cell counting method, an attempt was made to reach the threshold cell density by increasing the targeted cell seeding density from 1.8 X 10$^6$ to 3.0 X 10$^6$ cells/mL (alginate + DMEM). These attempts to reach the threshold cell density resulted in an average cell count of approximately 5.7 and 3.1 X 10$^5$ cells/1-inch fiber for the MI and CO-X encapsulation methods on Day 1, respectively. These cell counts reveal an opportunity to overcome equipment design limitations by using a higher target cell density of 0.65 – 1.2 X 10$^7$ cells/mL (alginate + DMEM). Perhaps, a more suitable encapsulation material will require fewer cells to yield the desired alamar Blue reduction response that was given by 1.2 X10$^6$ encapsulated MAC-Ts.

### 4.3.3 Cell number

Two issues regarding the cell number must be addressed. First, the difference between the targeted cell seeding density and the actual cell seeding density must be minimized. The actual cell seeding density was less than the targeted cell seeding density in the co-extrusion method. The difference in seeding cell density can be attributed to the lack of an even cell distribution within the polymer chamber. Although the alginate-DMEM/cell mixture was well mixed when the chamber was loaded, an uneven distribution of cells may have been

promoted due to axial mixing. It was thought that that partially filling the polymer chamber with a green colored acellular alginate solution prior to loading the cellular alginate-DMEM mixture would enable an operator to establish the hollow fiber spinning conditions to spinning cellular fibers. However, it was determined that axial mixing occurs, because the initial and final segments of the hollow fibers contained traces of green dye and were cellular. The axial mixing can be attributed to the nitrogen pressure spike that occurs prior to spinning. The pressure spike effect is a design limitation. One may hypothesize that the pressure spike can be minimized by maintaining the extrusion lever in the ON position (vertical) after polymer loading, so that the alginate/DMEM cell suspension will be extruded initially by gravitational forces, and once the nitrogen flow begins, the extrusion will occur and the axial mixing will be minimized.

The second issue that must be addressed regarding the cell number is the high variability on Day 21 of the cell number measurements. It is important to reemphasize the method by which the cells were counted, namely, the dissolution of the alginate fiber in order to release the encapsulated cells. The cell population of a fiber could not be measured on different days using this destructive method. Therefore, the variability that occurs shows the lack of consistency in the population of cells within each fiber. For the co-extrusion method, an even distribution of cells was initially assumed and 6ft of cellular hollow fiber was spun, cut into 1-inch segments and cultured and analyzed in the same order in which they were spun. The first 12 fiber segments were used in the cell response analysis during Days 1-7, the next 12 fiber segments were

used during Days 8-14, and a third set of fiber segments were analyzed during Days 15-21. Therefore the high variability may be explained as the cell seeding density increasing along the length of fiber. The high variability for the MI method on Day 21 may be explained by limitations in the manual extrusion method. A 3mL syringe was used to add a suspended cell solution to the lumen of hollow fibers, and the ends of these filled fibers were gelled. The syringe was refilled from a stock solution of cells after all of the solution in the syringe had been added to fibers. It is possible that while the solution in the syringe was being added to the hollow fibers, the cells in the stock solution may have aggregated. If true, then the extent of the cell aggregation may have increased as more fibers were filled. This hypothesize would indicate that the syringe that was used to fill the fibers that were analyzed during Days 15-21 contained either a higher actual cell seeding density than the targeted cell seeding density, an even distribution of the cells within the suspended cell solution in the syringe, or possibly a combination of these two occurrences. Cell aggregation could be minimized and an even distribution of cells could have been promoted through the agitation of the stock solution of suspended cells[20].

### 4.3.4 Histology

Is it a coincidence that there are very few cell aggregates and that most of the cells are round (Fiber 3.18)? We may also see an effect from using a higher concentration of alginate. Perhaps less cell aggregates develop when encapsulation matrix consists of a higher concentration of sodium alginate. It can be hypothesized that MAC-Ts conform to the cobblestone morphology when

multiple cell-cell junctions are available and that cells have more mobility in less concentrated alginate gels.

Figure 3.19A suggests that the distribution of cells into the hollow fiber can vary during the duration of the process. Is there a coincidence that the fiber wall does not contain holes? There may be a link between MAC-T lactic acid production and the increased rate of fiber decalcification and alginate dissolution[21]. If lactic acid production contributes to fiber decalcification, then an expedited rate of alginate dissolution may explain the gaps shown in Figure 3.20.

Clinicians use hollow fibers containing membrane voids in selective permeability applications such as membrane oxygenation and hemodialysis[22]. The void structure of a fiber membrane depends on processing conditions, such as how the exchange rate of the solvent/coagulant during the wet phase inversion process is controlled[23]. These processing conditions can be used to produce sponge, cylinder, and finger voids. Finger voids can normally be formed during the phase inversion process, when demixing occurs between two immiscible liquids (i.e. polymer solvent and water) so that the membrane consists of the porous sheath that covers an internal finger-type structure. However, in our dry/wet spinning process, our polymer solvent (distilled water) is miscible with our coagulant solution (aqueous calcium chloride) and yields fibers with a five layer morphology (Figure 4.2). We hypothesize that the annular gap forms because as the hollow fiber membrane is crosslinked from the periphery and lumen side of the hollow fiber, it is pulled in the direction of the coagulant. The annular gap is not formed when glycerol is added to the alginate solution.

Perhaps, the rate and extent of alginate crosslinking is impeded by glycerol's hydroxyl (-OH) functional groups.

The lactic acid produced by the MAC-Ts, slowly decalcified the fiber wall. A two-way influx of medium into these interstitial sites of decalcified alginate further promotes dissolution and finger-type void formation, as shown in Figure 3.19D. The formation of these voids creates porous hollow alginate fibers. If the formation of these finger voids could be controlled could be advantageous for use in selective permeability applications.
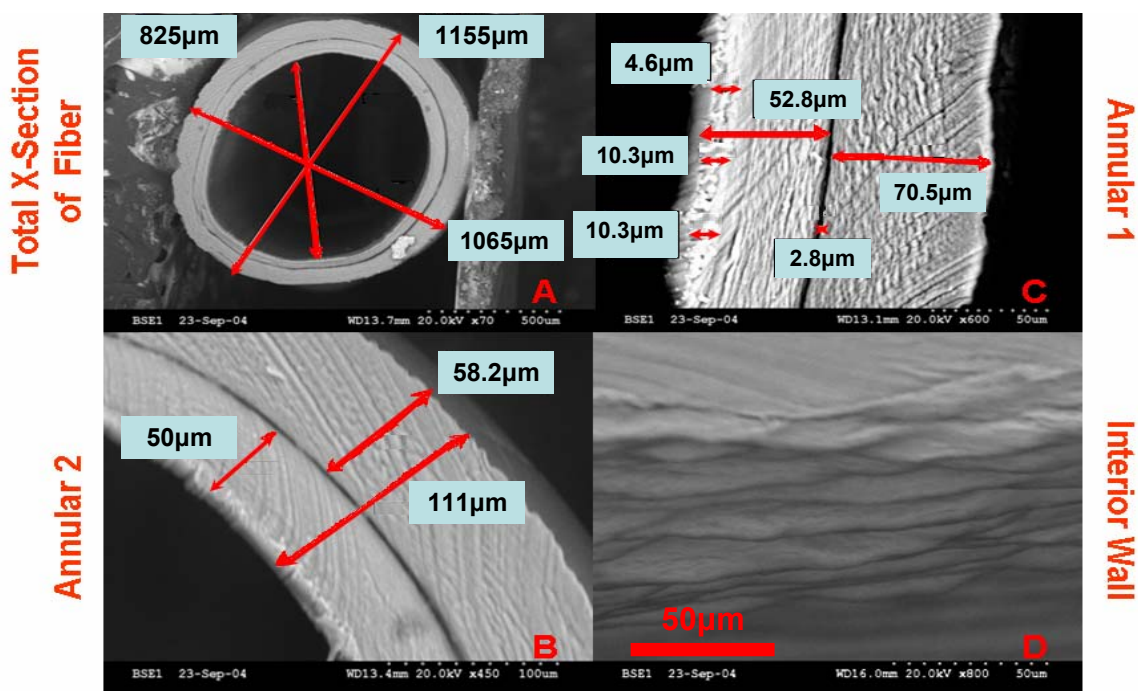


Figure 4.2: The five layer morphology consists of thin sheaths of highly crosslinked alginate on the periphery and the interior of the lumen. A spongy-like alginate support matrix which is concentrically divided by an annular gap is contained within these thin sheaths.

A modified GMA embedding technique was employed to minimize the effect of histological processing on the hollow fiber geometry for Day 1 for the CO-X type hollow fibers, since the gelation technique employed on the internal

cell suspension of the MI type hollow fibers significantly reduced the volume of their cell suspensions. The cell suspension volume reduction made the MI hollow fiber susceptible to concaving inward during the dehydration and polymerization steps of the 90 minute GMA embedding process.

Attention must be paid to the fixation method used to preserve the morphology of the MAC-Ts, and to the sectioning method that was employed to prepare the sections for staining. It was observed that if exposure time of the hollow fiber to 10% NBF extended beyond 2 minutes, the fiber would begin to swell. The formalin was diluted in PBS, and it is probable that the swelling occurred from contact with the PBS and not with the formalin itself. Perhaps a three step process involving cell fixation, re-gelation, and dehydration could be used to preserve both the MAC-T and fiber morphologies. Possible options for the fixation would be to increase the concentration of the NBF or use a fixative that is more potent than NBF, such as gluteraldehyde, in order to decrease swelling effect and exposure time[24]. A review of fixative diffusion rates has been thoroughly discussed in the literature and suggests that a fixation time of 2 minutes using 10% NBF is not adequate[25].

## 4.4 Limitations of the current design of the hollow fiber spinning technology

The experiment also reveals several limitations of the current design of the hollow fiber spinning technology for its use in cell encapsulation. The current design lacks the temperature control, chamber gas, and mixing devices that would be desired to maintain physiological conditions (i.e. 5 %$CO_2$ and 37 °C) and an even distribution of cells within a polymer matrix in the polymer chamber.

The cells are exposed to lower temperatures and a high nitrogenous environment during the co-extrusion encapsulation method, which may be the key contributing factor to the lag time, or period of adjustment observed in the MAC-Ts' lactic acid production and glucose consumption. Lower temperatures cause a decrease in the cell metabolic activity. Exposure to high nitrogenous environments may induce hypoxia, which has been known to induce a quiescent state in many cell types[26]. The variations in the cell count and assessment of the glucose metabolism studies may be attributed to the lack of an even distribution of cells within the polymer chamber, which directly affects the distribution of cells along the length of the extruded fiber. There was also a high variation in the cell count on Day 21 for both extrusion methods.

## References

1.    Vlachopoulos, J. and Strutt, D. The role of rheology in polymer extrusion. 2003.

2.    Zhang, H., Wang, H., Wang, J., Guo, R., and Zhang, Q. The effect of ionic strength on the viscosity of sodium alginate solution. Polymers for Advanced Technologies 2001;12(Nov/Dec):740-745.

3.    Osterwinter, U. Alginic acid, sodium salt. In: Jones W, editor. Clemson; 2005.

4.    Sigma-Aldrich. A2158: Alginic acid sodium salt from brown algae - low viscosity. 2006-2007.

5.    Sigma-Aldrich. A2033: Alginic acid sodium salt from brown algae - medium viscosity. 2006-2007.

6.    Larson, R.G. Constitutive equations for polymer melts and solutions. Boston: Butterworths Publishers; 1988.

7.    Subramanian, R.S. Fluid mechanics lecture notes: Non-newtonian flows. Clarkson University; 2003. p 1-5.

8.    Larson, R.G. The structure and rheology of complex fluids. New York: Oxford University Press; 1999.

9.    Guion, T.H. and Hood, J.R. Viscosity profiles of printing thickeners at high shear rates and their use in predicting paste flow in screen printing. Textile Research Journal 1985;55(8):498-508.

10.   Fournier, R.L. Basic transport phenomena in biomedical engineering. Lillington, NC: Taylor & Francis; 1999. 440 p.

11.   Nagasawa, N., Mitomo H., Yoshii F., Kume, T. Radiation-induced degradation of sodium alginate. Polymer Degradation and Stability 2000;69(3):279-285.

12.   Daigle, D.J., and Cotty, P.J. The effect of sterilization, pH, filler and spore inoculum concentration on the preparation of alginate pellets. Biocontrol Science and Technology 1997;7:3-10.

13.   Brown, P.J. The effect of double bond formation in polymers. In: Jones W, editor. Clemson, SC, USA: Clemson University; 2006.

14. Pereira, L., Sousa, A., Coelho, H., Amado, A.M., and Ribeiro-Claro, P.J.A. Use of FTIR, FT-Raman and 13C-NMR spectroscopy for identification of some seaweed phycocolloids. Biomolecular Engineering 2003;20(4-6):223-228.

15. Mchugh, D.J. Production and utilization of products from commercial seaweeds. FAO Fisheries Technical Papers:T288. 1987.

16. Morris, E.R., Rees,D. A., Sanderson G. R.  and Thom, D. Conformation and circular dichroism of uronic acid residues in glycosides and polysaccharides. Journal of the Chemical Society-Perkin Transactions 2. 1975:1418-1425.

17. Bhagyalakshmi, A. and Frangos, J.A. Mechanism of shear-stress induced prostacyclin production in human-endothelial cells. FASEB Journal 1988;2(4):A822-A822.

18. Frangos, J.A., Gupte, A., Berthiaume, F., and Oscilowski, V. Stimulation of endothelial protein-synthesis by shear-stress. FASEB Journal 1988;2(5):A1076-A1076.

19. Frangos, J.A., Mcintire, L.V., and Eskin, S.G. Shear-stress induced stimulation of mammalian-cell metabolism. Biotechnology and Bioengineering 1988;32(8):1053-1060.

20. Unsworth, J.M., Rose, F., Wright, E., Scotchford, C.A., and Shakesheff, K.M. Seeding cells into needled felt scaffolds for tissue engineering applications. Journal of Biomedical Materials Research Part A 2003;66A(2):425-431.

21. Yoo, I.K., Seong, G.H., Chang, H.N., and Park, J.K. Encapsulation of Lactobacillus casei cells in liquid-core alginate capsules for lactic acid production. Enzyme and Microbial Technology 1996;19(6):428-433.

22. Kawakami, H., Kanamori, T. and Kubota, S. Development of a fluorinated polyimide hollow fiber for medical devices. The Japanese Society for Artificial Organs 2003;6:124–129.

23. Taketani, Y., Nagaoka, S. and Kawakami, H. Fabrication of three-dimensionally ordered microporous membrane by wet phase separation. Journal of Applied Polymer Science 2004;92:3016-3021.

24. Tzeng, Y.L., Datta, A.K., Strole, C.A., Lobritz, M.A., Carlson, R.W., and Stephens, D.S. Translocation and surface expression of lipidated serogroup B capsular polysaccharide in neisseria meningitidis. Infect Immun 2005;73(3):1491-505.

25. Start, R.D., Layton, C.M., Cross, S.S., and Smith, J.H. Reassessment of the rate of fixative diffusion. J Clin Pathol 1992;45(12):1120-1.

26. Tucci, M., Hammerman, S.I., Furfaro, S., Saukonnen, J.J., Conca, T.J., and Farber, H.W. Distinct effect of hypoxia on endothelial cell proliferation and cycling. American Journal of Physiology-Cell Physiology 1997;41(5):C1700-C1708.

# CHAPTER FIVE

## CONCLUSIONS AND RECOMMENDATIONS

### 5.1 Conclusions
### 5.1.1 Material characterization

Based on our findings, we can conclude that the viscosity profiles of the three alginate types differ, and that the type of alginate selected for future encapsulation studies will depend upon the targeted clinical application. Of the three alginate types, the LV sodium alginate has the lowest molecular weight, a requirement for renal clearance, and would therefore be the ideal candidate for short-term *in vivo* applications. We can also conclude that there is no difference in the G block % among the three alginate types.

### 5.1.2 Cell response

Based on our findings, our novel in-house textile hollow fiber spinning process can be used to encapsulate cells in MV and LV alginate-based solutions. Over the duration of 21 days, MAC-Ts encapsulated under the CO-X method produced less lactic acid and consumed less glucose. Based on the staining techniques employed and histomorphological analysis performed, we can conclude that the formation of cell clusters were inhibited when the cells were encapsulated in a 6 wt% MV based alginate solution using the CO-X encapsulation method. However, cell spreading occurred more readily in the MI type fibers than in the CO-X type fibers because of a less concentrated alginate matrix. Second, we can conclude that by Day 21, the cell area of MAC-Ts that

were encapsulated using the MI method exhibited larger cell areas than MAC-Ts encapsulated by using the CO-X method. Third, we can conclude that the production of lactic acid contributed to alginate dissolution.

## 5.2 Recommendations

Future work should address four initiatives. The first initiative should involve increased characterization of the sodium alginate and study of the effect of the measured properties on the MAC-Ts' viability and metabolic activity. The arrangement of the M and G blocks for each type of alginate should be determined to correlate conformation with viscosity. In addition, the influence of each alginate type's molecular weight on the cell viability and metabolism should be studied.

Second, the physical properties of the hollow fiber and how these properties change over time *in vitro* should be characterized. Currently, the tensile strength of a hollow fiber is difficult to measure because a gap exists in the wall of the fiber. A method to measure the tensile properties of the alginate hollow fibers should be devised. Atomic force microscopy (AFM) should be used to study how different alginate molecular weights, coagulation concentrations, and culturing methods influence the fibers' surface topology on a nanometer scale. Perhaps AFM should be used as a method of determining membrane porosity. Improving the characterization of the hollow fiber should include improving the histological methods detailed in this thesis. Namely, a more adequate fixation method must be devised that will elucidate the *in vitro* cell and fiber morphology through the preservation of cells and hollow fiber.

Third, future work should include studying the effects of proposed changes in the hollow fiber spinning technology on cell viability, metabolism, distribution, and fiber spinnability. One proposed change is to replace the nitrogen gas, used in the spinning process, with oxygen. The effect of oxygen on the cell's susceptibility to shock should be investigated because it has been proposed that nitrogen may be causing a delay in the cell cycle. Normally, mechanical stimuli cause the compression of the cell's cytoskeleton, which transmits signals to the cell nucleus. However, this effect may be inhibited in cells that experience hypoxia, which is promoted in a highly nitrogenous environment. Therefore, the effect of oxygen on alginate gelling should be determined. Since alginate is ionotropic and oxygen is high reactive and negatively charged, alginate exposure to oxygen may have some inhibitory effects on the binding of calcium to the alginate carboxylic acid group's anion. Another proposed change is to maintain physiological temperature conditions (37°C). Therefore, the effect of increasing the temperature of the coagulation fluid and the alginate spinning solution to 37°C on fiber spinnability and cell viability should be investigated. Increasing the bath temperature would increase the rate of gelation, which may promote a larger mechanical stress on the cells. One of the limitations of the current spinning system is that the CO-X extrusion method does not maintain an even distribution of cells in the spinning matrix. Thus, it would be intuitive to determine the optimal operating conditions for a baffle/mixer system within the polymer chamber that will maintain an even cell distribution with minimal cell detriment.

Fourth, in order to validate the feasibility of using the spinning apparatus for encapsulating cells and define the limitations of the purposed encapsulation methods, other cell lines, including an adhesion dependent human cell line, should be encapsulated and undergo viability and metabolic activity evaluations.